The University Of Sheffield.

Operator functional state modelling and adaptive control of automation in human-machine systems

By:

Luis Alberto Torres Salomao

A thesis submitted in partial fulfilment of the requirements for the degree of Doctor of Philosophy

The University of Sheffield
Faculty of Engineering
Department of Automatic Control
and Systems Engineering

July 2016

Acknowledgements

Firstly, I would like to express my sincere gratitude to my advisor, Prof. Mahdi Mahfouf for his continuous support throughout the PhD process. I would like to thank him for all his advice and motivation that encouraged me to search deeper into my field of study, and for his high standards from which I have learned the meaning of quality research.

Besides my advisor, I would like to thank Dr. Adam Roberts for his availability with all my technical questions throughout my studies, Prof. Ching-Hua Ting for his advice and support with regards to my modelling framework, and to Dr Emad El-Samahy for our experimental collaborative work at The Human Performance Laboratory. Additionally, I would like to specially thank all my fellow PhD students with whom I continuously chatted about research. Many thanks to Olusayo Obajemu, Ali Baraka and Dr. Adrian Rubio for all our conversations regarding fuzzy logic.

Special thanks to all the friends that sacrificed their time to help me with the real-time experiments performed in this study, without your support this thesis would not have been possible. Finally, I would also like thank all the ACSE staff for all their support during these almost four years of study.

To God,

to my beautiful wife Sandy for believing in my dream of studying abroad and putting her own career on hold during these almost four years, and to my parents and sister for their unconditional love and support.

Abstract

In this study, a new modelling and control framework based on type 2 fuzzy logic and validated with real-time experiments on human participants experiencing stress via mental arithmetic cognitive tasks is presented. The ultimate aim of the proposed modelling and control framework is the management and ultimately the prevention of performance breakdown in a human-computer interaction system with a special focus on human performance.

This work starts with a literature-based study of previously successful experimental designs, selecting the mental arithmetic operations cognitive task for its ease of implementation and validated through a series of statistical tests on 12 participants as far as its influence on commonly used psychophysiological markers is concerned. Additionally, a new marker for mental stress identification is introduced, the pupil diameter marker; validated with the same series of statistical tests for all 12 participants in the study.

For the validation of the introduced modelling and control techniques, two designed experiments which consist of carrying-out arithmetic operations of varying difficulty levels were performed by 10 participants (operators) in the study. With this new technique, effective modelling is achieved through a new adaptive, self-organising and interpretable modelling framework based on General Type-2 Fuzzy sets. This framework is able to learn in real-time through the implementation of

a re-structured performance-learning algorithm that identifies important features in the data without the need for prior training. The information learnt by the model is later exploited via an Energy Model Based Controller that infers adequate control actions by changing the difficulty levels of the arithmetic operations in the human-computer-interaction system; these actions being based on the most current psycho-physiological state of the subject under study. The successful real-time implementation of the proposed adaptive modelling and control strategies within the framework of the human-machine-interaction under study shows superior performance as compared to other forms of modelling and control, with minimal intervention in terms of model re-training or parameter re-tuning to deal with uncertainties, disturbances and inter/intra-subject parameter variability.

Acronyms

A-GT2-FCM	Adaptive General Type-2 Fuzzy C-Means
aCAMS	automation-enhanced Cabin Air Management System
ANFIS	Adaptive Network-based Fuzzy Inference System
ANFIS-C	Adaptive Network-based Fuzzy Inference System Controller
ANS	Autonomic Nervous System
AP	Accuracy Performance
CWT	Stroop Colour Word Testing
DL	Difficulty Level
E-MBC	Energy Model-Based Controller
ECG	ElectroCardiography
EEG	ElectroEncephalography
EIASC	Enhanced Iterative Algorithm with Stop Condition
EMG	ElectroMyography
EOG	ElectroOculography
FCM	Fuzzy C-Means
FS	Fuzzy Sets
GA	Genetic Algorithms
GT2FLS	General Type-2 Fuzzy Logic System
GT2FS	General Type-2 Fuzzy Sets
GUI	Graphical User Interface
HMI	Human-Machine Interaction
HR	Heart Rate
HRV	Heart Rate Variability
HRV1	Heart Rate Variability 1
HRV2	Heart Rate Variability 2
IT2FS	Interval Type-2 Fuzzy Sets
KM	Karnik-Mendel
MA	Mental Arithmetic
MCE	Model-based Control Experiment

ME-1	Modelling Experiment 1
ME-2	Modelling Experiment 2
MF	Membership Function
MSE	Minimum Square Error
MSE-GUI	Mental Stress Evaluation Graphical User Interface software
N-RL	Negative Reinforcement Learning
NN	Neural Network
O	Output
P-learning	Performance learning
PAP	Predicted Accuracy Performance
PD	Pupil Diameter
PDM	Pupil Diameter Marker
PID	Proportional-Integrative-Derivative
PO	Predicted Output
PSNS	Parasympathetic Nervous System
Q-L	Q-Learning
RL	Reinforcement Learning
SNS	Sympathetic Nervous System
T1	Type-1
T1FS	Type-1 Fuzzy Sets
T2FS	Type-2 Fuzzy Sets
TIR	Time In Range
TLI	Task Load Index

Publications

Related to this work

- L. A. TORRES-SALOMAO, M. Mahfouf, E. Elsamahy and C.-H. Ting, "Psycho-Physiologically-Based Real Time Adaptive General Type 2 Fuzzy Modeling and Control of Operator's Performance Undertaking a Cognitive Task," *IEEE Transactions on Fuzzy Systems*, (early access) 2016.
- E. Elsamahy, M. Mahfouf, L. A. TORRES-SALOMAO and J. Anzurez-Marin, "A New Computer Control System for Mental Stress Management using Fuzzy Logic", in *2015 IEEE Conference on Evolving and Adaptive Intelligent Systems*, Douai, 1-3 Dec. 2015.
- L. A. TORRES-SALOMAO, M. Mahfouf and E. El-Samahy, "Pupil Diameter Size Marker for Incremental Mental Stress Detection" in *2015 IEEE 17th International Conference on e-Health Networking, Applications and Services*, Boston, 14-17 Oct. 2015.
- L. A. TORRES-SALOMAO, M. Mahfouf and O. Obajemu, "Interval Type-2 Fuzzy Logic Adaptive Modelling for Human Operators Undergoing Mental Stress", in *Proceedings of 19th World Congress of the International Federation of Automatic Control*, Cape Town, pp. 9880-9885, 2014.
- O Obajemu, M Mahfouf and L. A. TORRES-SALOMAO, "A New Interval Type-2 Fuzzy Clustering Algorithm for Interval Type-2 Fuzzy Modelling with Application to Heat Treatment of Steel", in *Proceedings of 19th World Congress of the International Federation of Automatic Control*, Cape Town, pp. 10658-10663, 2014.

Related to other work

- L. A. TORRES-SALOMAO, J. Anzurez-Marin, J. M. Orozco-Sixtos and S. Ramírez-Zavala, "ANFIS Data Driven Modeling and Real-Time Fuzzy Logic Controller Test for a Two Tanks Hydraulic System", in *2015 IEEE Conference on Evolving and Adaptive Intelligent Systems*, Douai, 1-3 Dec. 2015.
- L. A. TORRES-SALOMAO and J. Anzurez-Marin, "Adaptive Neuro-Fuzzy Inference System Control for a Two Tanks Hydraulic System Model", *2013 IEEE International Autumn Meeting on Power, Electronics and Computing*, Morelia, November 2013.
- L. A. TORRES-SALOMAO, H. Gámez-Cuatzin, J. Anzurez-Marín and I. I. Lázaro-Castillo, "Fuzzy- PI Control, PI Control and Fuzzy Logic Control Comparison Applied to a Fixed Speed Horizontal Axis 1.5 MW Wind Turbine", In H. K. Kim, S. Ao, M. A. Amouzegar and B. B. Rieger (Eds.), *IAENG Transactions on Engineering Technologies*, Springer Netherlands, pp.167-181, 2013.

Contents

List of Figures

List of Tables

Chapter 1

INTRODUCTION

1.1 Psychophysiology, human factors and automation

1.1.1 Psychophysiology

Psychophysiology first emerged as a separate discipline in the 1950s when a group of physiological psychologists began referring to themselves as psychophysiologists. The subject matter of psychophysiology is the interaction of mind and body, which has been studied for centuries by philosophers, physicians, physicists, and most recently, psychologists [14].

The relationship between the body and the mind is studied through psychophysiological measurements or recordings. Psychophysiological measurements originate in the human body through electrochemical changes in neurones, muscles and gland cells. These signals are transmitted through the body to the skin surface and can be recorded with the use of electrode transducers [14]. Psychophysiology can be defined as the study of physical and mental states that respond to stimulation (i.e.,

mental stress or mental workload; and physical stress). Recorded psychophysiological signals may help us understand these underlying physical and mental states [13].

1.1.2 Human Factors

The application of behavioural and biological sciences for the design of machines and human-machine systems is named Human Factors (e.g., also known as Human Engineering or Human Factors Engineering, and Ergonomics). This discipline was initiated during World War II with the application of direct engineering for the interactions of modern weapons and their human operators [2].

With regards to behavioural sciences, human factors apply knowledge from cognitive psychology and the broader field of experimental psychology, similarly, biological sciences for human factors are related to human physiology and the study of organ functions above the cellular level (i.e., cardiovascular, brain, eye responses, etc.). It is worth noting that human factors engineering is mostly an empirical activity and should be interpreted within a practical context [2]. Human Factors make use of psychophysiology to identify human processes in order to better describe the interactions between humans and machines.

1.1.3 Human-Machine Interaction Systems

The human observes the environment which produces an effect in his/her body which in turn affects the environment. Causality operates both ways in the human-environment relationship. For this reason, and in order to fully describe a human-environment relationship, it is important to take into consideration the constraints that operate in both directions, i.e., all the factors that constrain the human from fully observing the environment, and all the factors that constrain the human in

his/her influence in the environment exactly as he or she might wish [2]. The study of human-environment relationship in Human Factors is known as Human-Machine Interaction.

Suitable examples of Human Machine-Interaction (HMI) systems are automated systems where human operators play some role. In fact, for very complex and/or safety critical system such as nuclear plants, aircrafts, air traffic control, spacecrafts, medical surgery, etc., the adaptive capabilities, reasoning and judgement of humans is often required to play an intrinsic role. These types of systems cannot be fully automated and thus, the human in the HMI system must be taken into account [13]. The decision on which tasks to automate and which to leave for the human operator is indeed concomitantly important and challenging [4], and the mental and physical state of the operator (e.g., its psychophysiological state) should be given special consideration [3, 5, 61].

There have been some initiatives in providing rules to guide the allocation of functions between humans and machines. The Fitts list (see Table 1.1) also known as the MABA-MABA list, is an example of such an endeavour dating back to 1951 [2].

The rules provided by the 'Fitts list' of Table 1.1 do not apply to current HMI automation systems. Intelligent adaptive algorithms powered by advances in computational technology are, for example, capable of perceiving and learning patterns and storing and recalling information. Additionally, advances in transducer technology help in the detection of signals that could never been accessed before. Perhaps the most important difference today between humans and machines is the ability of the former to exercise judgement and to conduct reasoning inductively, this representing the 'holy grail' of artificial intelligence.

Men Are Better At:
Detecting small amounts of visual, auditory, or chemical energy
Perceiving patterns of light or sound
Improvising and using flexible procedures
Storing information for long periods of time and recalling appropriate parts
Reasoning inductively
Exercising judgement

Machines Are Better At:
Responding quickly to control signals
Applying great force smoothly and precisely
Storing information briefly, erasing it completely
Reasoning deductively

Table 1.1: Fitts list for function allocation in HMI systems [2]

1.1.4 Automation for Human-Machine Interaction

Automation refers to the application of mechanical, electronic or computational devices for the substitution of activities that humans used to perform. This term was first used in the manufacturing industry [2], but includes nowadays a much broader meaning.

Automatic systems are a growing feature for most of the previously manually performed operations in Human Machine Interaction (HMI) systems [61]. However, the technology behind automation is not fully grasped by the general public, and, as its sophistication grows, the less likely it is to be understood [2]. This has two main repercussions on people, some may not trust automatic systems while others may over-trust these systems by attributing to them intelligence they do not possess [2].

The machines in which automation is present is very broad. Most of the control techniques used are model-based, since they require some type of interpretation of the phenomenon they wish to control, and most employ 50-year-old techniques that are in fact very simple. These techniques (e.g., Proportional-Integral-Derivative control among others) are usually not adaptive and can only optimally work for restricted

bandwidths. Despite all these shortcomings, automatic systems quickly replaced manual labour in industry and many other human activities, although only a few systems are in actual fact considered to be fully automated. In fact, most systems have very critical human interactions [2], and here lies the importance of the study of Human Factors and HMI.

The use of a model for automation is true even for more advanced intelligent control techniques that are defined as 'model-free' (e.g., fuzzy logic control), since most of the time a simple or semi-accurate description of the process under investigation is needed in the design process. Predictions or anticipation of future outcomes and interactions with key variables of a system are the way model-based controllers work. This modelling and control process is not challenging for most systems since these perform in a mostly-exact way (i.e., for washing machines or electric motors). However, for biological systems, such as HMI systems, this task becomes very difficult since their variables and features are normally not fully understood and drift considerably away from their 'typical' operating regions under similar conditions because of their high level of complexity [61].

1.2 The importance of adequate psychophysiological markers

The objective in any endeavour towards the automation of a HMI system is to fully integrate human and machine by taking into account their interdependencies and interactions. In order to achieve this objective, the issue of adequate psychophysiological recordings (e.g., psychophysiological markers) is very important if we wish to understand the human part of the system. The search for new measurements that can help one understand the inner processes in the affective state of the human should

be perceived to stem from an incremental effort [61].

As the tasks humans perform inside HMI systems evolved from physical towards cognitive, the role of mental workload should be given a special attention [2]. To fully understand what mental workload is, it would be perhaps more useful to define what it is not [2]. Hence, mental workload:

- is not physical workload. Physical workload is understood to be the mechanical energy consumption in calories by operators during any given task.
- is not an objective measure of any task defined in terms of its complexity or the way it is done. To illustrate this idea it is convenient to think of an operator performing a mentally stressful task. An experienced operator may perform this task well without a high level of mental workload. However, an inexperienced operator may perform poorly given his/her high level of mental workload. It is important to point-out that even if related, task load is independent of mental workload.
- is not a human operator performance. Before high mental workload is experienced, operator performance may show little change. However, with a slight change in mental workload, operator performance could rapidly and precipitously decrease. It should be noted that changes in mental workload do not necessarily change with the same rate as operator performance. Mental workload identification is helpful in the prediction of precipitous decreases in operator performance before these occur.

The most commonly used and certified markers to identify mental workload are derived from cardiovascular signals. Heart Rate Variability (HRV) has been found to strongly correlate to mental stress (e.g., as mental workload is also known) in several experimental configurations in the literature such as in [18, 19, 20, 21, 22, 23,

24, 25, 26, 27, 28, 29, 30, 31, 32, 33, 34, 36]. Another source of previously successful markers is the encephalographic (brain) activity recording [42, 43]. In the literature, the prefrontal cortex activity of the brain through the "Task Load Index" (TLI) has been found to correlate to mental workload [44, 45, 46, 47]. The HRV and TLI markers have been linked to complex operator tasks in HMI systems in [7, 8, 13, 41].

In addition to these two sources of information regarding the mental affective state of operators, it is worth noting the rise of the pupil size for the assessment of mental workload. Pupil size has been used by researchers in different experimental classification configurations (e.g., they have been able to detect stress and no stress states) in [49, 50, 51, 52, 53, 54, 55, 56, 57, 58, 59]. However, the potential of pupil size to detect incremental levels of mental workload has not been explored sufficiently. A first approach into the incremental detection properties of this recording was undertaken in the Human Performance Laboratory at The University of Sheffield in [61, 62].

1.3 Modelling of biological systems

Advances in computational systems have changed the way we think and have opened up the path for many paradigm changes in diverse areas of technology and science. We nowadays, carry in our pockets a computational power that was unknown when the first computers were born. These electronic machines are now present in most of the devices we interact with (the definition of HMI system). We constantly rely on their operations and relegate to them many of the other activities we previously took responsibility for.

Automation systems are finding their way into all devices thinkable thanks to this revolutionary computational power. These automated devices range from consumer

friendly electronic devices to very specialised equipment breaking the barriers of science such as the hadron collider at CERN, or the electronic devices for space exploration [61].

This has meant a shift from traditional approaches to modelling and control for the community working with control systems. On the one hand, traditional approaches are mainly based in mathematics and laws of nature, on the other hand, new modelling and control data-driven approaches rely in simple 'mining' algorithms powered by very fast and intensive computations. Artificial neural networks and fuzzy logic systems are some of the many techniques that take advantage of this change in paradigms facilitated by the advancement in computational technologies. We are now capable of describing numerically, very complex systems that we have yet to understand ourselves. There are however many barriers yet to be broken and the exploration of Human Machine Interaction (HMI) systems is one of them.

Slowly but surely we find ourselves with ever more advanced and intelligent algorithms and techniques that are able to self-adapt and evolve as the system they are called upon to monitor itself is evolving. Data-driven automatic approaches are now able to begin to understand HMI systems by extracting meaningful features. However, most of these techniques (i.e., neural network approaches, support vector machines, clustering approaches, fuzzy logic systems), lack one or more of the following highly desirable features for HMI systems:

- Adaptation. Understood as the ability to restructure themselves in real-time in response to changes in the system they monitor.

- Handling of uncertainty. Their ability to handle ill-defined systems with unmodelled dynamics.

- Interpretability. To be able to easily translate what these models learn into

rules understandable by humans.

- Self-Organisation. Their ability to learn by themselves and in real-time without the need for a training phase.

As will be introduced in the development of this work, in order to close the loop for the HMI system (of operators performing mentally stressful arithmetic operations) under study it is necessary to address these desirable features to construct a fully functional system.

1.4 Objective and contributions

Overall objective

- To design a synergetic modelling and control framework to improve the performance of operators in a Human-Machine Interaction system.

Specific objectives

- To assess the mental stress incremental prediction power of the pupil size marker through a series of experimental sessions on a Human-Machine Interaction system.
- To design an experimental framework for the application of automation for Human-Machine Interactions, including an effective task for the inducement of mental stress and a graphical user interface software for the deployment of the task and the assessment of performance and computation of the algorithms for the automation system.

- To design an adaptive modelling an control algorithm capable of tackling inter and intra variability across human operators in a Human-Machine Interaction system.

- To perform a series of experimental sessions on human operators for the validation of the modelling/control algorithm in real-time and its comparison with a neural-network-based modelling/control system.

Main contributions

The main contribution of this work is the design and real-time experimental validation through comparison of a new adaptive and self-organising modelling and control algorithm. This algorithm was tested in real-time in a series of experiments for operators performing a mentally stressful task in a Human-Machine Interactive system, achieving superior modelling and control results as compared to participant-specific fixed ANFIS (neural network approach) models and controllers.

In the field of current research in fuzzy logic of type 2, this work contributes with a new inference process based in a restructured Fuzzy C-Means clustering algorithm. In this way, the computationally intensive issue of general type 2 fuzzy logic is solved, rendering an algorithm capable of being applied for real-time modelling and control problematics that require the full handling of uncertainty coupled with interpretability properties.

Additionally, this dissertation contributes to the area of Psychophysiology with the statistical and experimental validation of the pupil size as a marker for the incremental detection of mental stress. Validation was a achieved through a series of statistical two-sample t tests for the pupil marker and these results compared to similar tests applied to cardiovascular and brain commonly used markers.

1.5 Thesis organisation

This thesis is organised as follows: Chapter 2 presents the experiment design for the obtention of meaningful data of humans performing the mentally stressful Mental Arithmetic experiment. This Chapter describes the most commonly used psychophysiological markers (i.e., HRV and TLI) for the assessment of the human state as well as introducing the new pupil size marker. Additionally, an account of previously used experimental designs in the literature as well as a description of the designed computational interface for the deployment of the experimental sessions is presented. The Chapter concludes by analysing the prediction power of the selected psychophysiological markers under the Mental Arithmetic experiment design.

Chapter 3 deals with fuzzy logic of type 2 theory by addressing its diverse configurations as well as common problematics in its deployment. It introduces the use of a simplification known as interval type 2 fuzzy logic and presents its application to the modelling of operator performance in a HMI configuration. Following these results, this Chapter introduces the necessity for a new adaptive fuzzy-based algorithmic design that solves many of the current problematics in the field. An approach to an adaptive fuzzy-based modelling/control technique is presented in Chapter 4. Following this new algorithmic design, its application and validation is presented in Chapter 5 with modelling and control experiment sessions for ten participants in a HMI system configuration as described in Chapter 2. Chapter 6 finalises this work by presenting its concluding remarks and future research recommendations.

Chapter 2

DESIGN OF EXPERIMENT

2.1 Psychophysiological Markers

2.1.1 Introduction

Stress, mental or physical, is regulated by the sympathetic (SNS) and parasympathetic (PSNS) divisions of the Autonomic Nervous System (ANS). These systems work in opposition to automatically regulate stress-relaxation states in the human body. The SNS originates in the thoracic and lumbar regions of the spinal cord; the PSNS originates in the brain stem and the lower part of the spinal cord. Whenever the SNS is activated it regulates the body for a probable crisis (e.g., the "fight or flight" response) by dilating the pupil diameter, causing sweat glands to secrete sweat, increasing the heart rate, etc. In contrast, the PSNS generally causes relaxation of the body [55].

For the present work, a special interest was given to the psychophysiological recordings for the production of markers related to mental workload or stress. A thorough literature review was carried-out in order to identify the most prominent, successful and promising psychophysiological measures that could achieve and

quantify this state. Among such identified markers the most prominent and generally used is Heart Rate Variability (HRV). However, it is important to note that cardiovascular (e.g., HRV calculated from the ElectroCardiogram) as well as other bodily measurements are reactive to many more processes in the human body other that mental workload. For this reason, a pool of markers derived from recordings of different body systems (e.g., cardiovascular, brain, eye) is necessary to discriminate between real and false marker activations which are driven from biological processes other than mental workload.

With the carried-out literature review, recordings previously used for mental stress detection other that ElectroCardiography (ECG) included: ElectroMyography (EMG), ElectroEncephalography (EEG), ElectroOculography (EOG), skin conductance, respiration and Pupil Diameter (PD) measurement. Among these recordings, ECG and EEG were identified as the most powerful markers in the published results. PD has not been widely explored, however, it was quickly apparent from the few studies found that it had promising predictive powers. In the next sections of this Chapter, the used psychophysiological markers description will be reviewed in more detail. The last Section addresses a comparison among the selected markers, the Heart Rate Variability marker (HRV, derived from ECG), the Task Load Index marker (TLI, derived from EEG) and the Pupil Diameter Marker (PDM).

In addition to the use of a pool of successful psychophysiological markers, the problematic of false activation can also be tackled with an appropriate experiment design that blocks the effect of variables known to alter such psychophysiological recordings (e.g., respiration, temperature changes, lighting changes, drugs, arousal, mental state). In Section 2.2 a description of the laboratory experimental framework used will also be presented.

2.1.2 ElectroCardiography Heart Rate Variability marker

2.1.2.1 Introduction

ElectroCardiography (ECG) is the recording of the activity of the heart, which represents the main organ in the cardiovascular system. The cardiovascular system is a complex physiological system that regulates many subsystems subject to central and peripheral autonomic controls as well as humoral influences. This system is highly sensitive to neural and behavioural processes and its complexity is such that it is susceptible to many disorders driven from psychological factors such as stress [15].

In addition to the heart, the cardiovascular system is composed of a distribution system known as the vasculature. The heart functions as a pump, and together with the vasculature ensures that blood flows into all tissues of the body [15].

For ECG recordings one should be especially interested in the cardiac cycle, composed of all events occurring in the heart from one beat to the next. This cycle is composed of two main epochs, diastole and systole. During diastole the heart fills up with blood; systole corresponds to the period when the heart pumps this blood. The ECG depicts this cycle and can be simply described with the aid of the P wave and the QRS wave complex (see Figure 2.1). The cardiac cycle begins during the end of the diastole with a depolarisation wave passing through the atrial muscle (the P wave). The P wave is followed by atrial contraction, which is in fact the QRS complex that marks the start of the systole [15].

The heart, part of the cardiovascular system, is automatically controlled by the automatic nervous system through both the sympathetic and parasympathetic branches [12, 15]. Figure 2.2 depicts a model of the autonomic control of the heart period. In this model parasympathetic and sympathetic systems change independently, coactively and reciprocally [15].

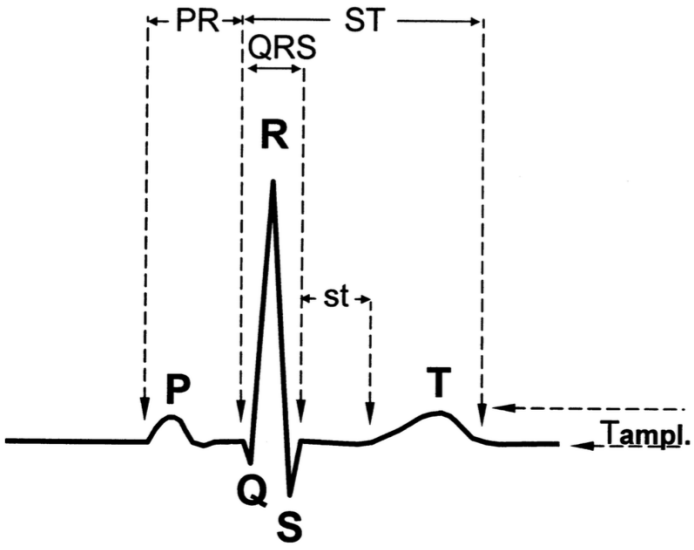

Figure 2.1: Electro-cardiogram (ECG) waves [15].

The heart period is an intrinsic metric in the calculation of Heart Rate Variability (HRV). It is the time in milliseconds between heart beats measured with the R spikes given by the ECG (see Figure 2.1). The R spike is used because of its sharper inflection that facilitates its automatic identification. Heart rate (beats/min or bpm) can be calculated from the heart period by dividing its value with a 60,000 constant. In fact, they are reciprocals, and the heart period (milliseconds) can be calculated by dividing heart rate by the same constant value [12, 15].

2.1.2.2 The Heart Rate Variability marker

Heart Rate Variability (HRV) has been used in psychophysiology for a long time now [15]. In fact, there exists an extensive literature on this topic and its applications to detection of mental stress like in: [18, 19, 20, 21, 22, 23, 24, 25, 26, 27, 29, 30, 31, 33, 36].

There are several frequency bands of heart period variability that have been used in the literature [15]:

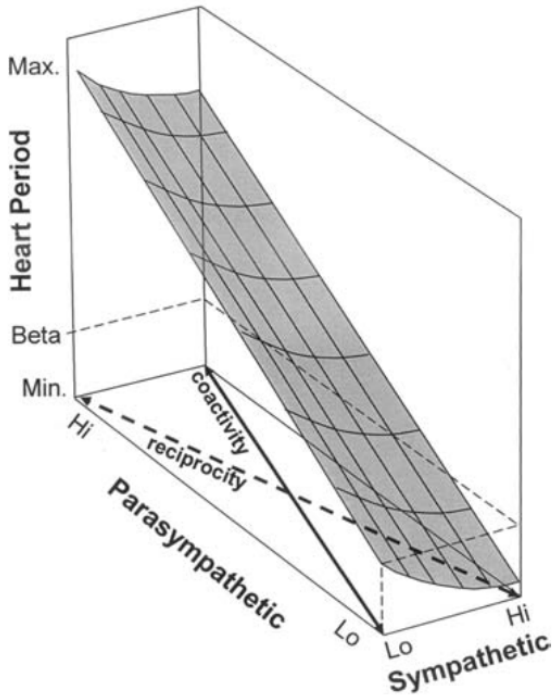

Figure 2.2: Model of Autonomic Control (Parasympathetic and Sympathetic branches) on heart period [15].

- The high-frequency band (0.12-0.15 to 0.4 Hz in adults). This band corresponds to respiratory sinus arrhythmia (RSA), which reflects respiratory gating of autonomic control.

- The mid-frequency band (0.05 to 0.15 or 0.8 to 0.12 Hz). This band is centred around 0.1 Hz as is sometimes referred as the Mayer wave. This band is useful in the quantification of mental workload.

- The low-frequency band (0.003 to 0.05 and even below 0.003). This band has been studied in physiology but has not received much attention in psycho-physiological studies.

The variation between beats of the heart (e.g., the normal sinus arrhythmia) used for the HRV was for a considerable time found to correlate with a healthy cardiovascular system [18]. The following studies identified a relationship between variations in the

heart rate with physical or mental workload: Stephen Porges (1995) in [22] explores the relationship of adult stressful events such as death, loss of job, etc., with HRV. The study highlighted the difference with other mammals and infants incapable of vocalising and introduced the importance of a non-invasive method for detecting stress based in cardiovascular signals such as HRV.

With regards to HMI systems, HRV has been used in studies in [7, 8, 9, 11, 12, 19] as a marker with an important role in the detection of operator's functional states. In [25] different experiments assess if talking or reacting (silently of aloud) affect HRV. This work also investigates the relationship between controlled breathing and its mimicking of sympathetic activation. Their results show that when sympathetic activity predominates (e.g., when on high degree of stress), the low frequency of the interval between adjacent EEG-R peaks (i.e., know as R-R interval) predominates regardless of the changes in respiration. It states that in the absence of stress, respiration alone is capable of completely altering the R-R interval spectrum by increasing the low frequency component. This represents an important result towards the avoidance of verbalisation in mental stress evaluation experiments.

In [23, 24] effects of mental and physical workloads on HRV are explored during computer work. In [23] the authors emphasise the necessity of standardisation of physical demands when the potential effect of mental stress is to be studied. Apart from HRV other taken indices in this research include: performance of task, heart rate (HR), mean arterial blood pressure and urinary concentrations of catecholamine. The work in [24] is a continuation of the work in [23] where Stoop Colour Word testing (see Section 2.2.2.1) is used as a means of inducing mental stress. In [24] Mental Arithmetic operations (see Section 2.2.3) are used for the induction of mental stress.

In [27] a study to evaluate the changes in HRV due to physical, mental and combined workload is presented. This study focuses on time-evolution using time

frequency analysis for 28 subjects as they perform 4 tasks that include postural load, mental task, mental and postural task as well as a resting phase. However, verbalisation during the experiment raises some questions about the results obtained. In [36] the idea of a practical means of measurement of mental stress is explored. The author emphasises the restrictions of measurements obtained via EEG, EOG and EMG when compared to ECG in the application of these measurement apparatus within a real-time commercial flight environment. In this study HRV together with the Bedford scale, are used as a means of detecting mental stress during flight conditions.

For the present work, two HRV marker indices were used following the results of previous experiments performed at The University of Sheffield [7, 8, 9, 11, 12], namely, Heart Rate Variability 1 (HRV1) and Heart Rate Variability 2 (HRV2). HRV1 is defined as the 0.1 Hz component of the heart rate (HR) signal and is calculated by averaging the power spectrum of the HR signal collected in periods of 30 s and in the frequency range from 0.07 Hz to 0.14 Hz. HRV2 is the ratio between the standard deviation over the mean value of the HR signal in the same period [12].

2.1.3 ElectroEncephalography Task Load Index marker

2.1.3.1 Introduction

The first performed ElectroEnchephalogarphic (EEG) recording in humans was carried-out in 1924 by the German psychiatrist Hans Berger. He recorded the measurement with one electrode placed over the forehead and the occipital cortex, obtaining rhythmic activity oscillating at 10 Hz during relaxed wakefulness without sensory stimulation or mental activity. This discovery marked what would be known as alpha waves. He was also the first to associate mental processes of arousal, memory

and consciousness with periodic fluctuations of the human EEG [15].

EEG measures assemblies of neuronal activity through their electrical response with millisecond temporal resolution, offering the possibility of studying brain function in real-time. However, EEG is constrained by distorting effects of the head volume conductor, low signal to noise ratios and limited spatial sampling due to practical limits on the numbers of electrodes that can be placed over the scalp. The oscillations recorded with the EEG are believed to be generated by the summation of excitatory and inhibitory potentials in cortical pyramidal neurones. Tens of thousands of these neurones are assumed to be involved [15].

2.1.3.2 Frequency bands in the EEG

Thanks to the millisecond temporal resolution of the EEG, not only fluctuations of its activity can be studied but also differentiations between functional inhibitory and excitatory activities. In general, low frequencies such as the delta and theta bands, show synchronised activity with large amplitudes. However, high frequencies like beta and gamma bands include small amplitudes due to desynchronisation in the neuronal activity [15]. The following sections briefly describe each of the most important EEG frequency bands and their application to diverse psychophysiological studies.

Delta band

Delta oscillations capture low frequency activity in the 1 Hz to 4 Hz range. This band is associated with sleep in healthy humans and with neurological pathology. It is the predominant activity in humans in their first two years of life. The slow-delta and theta activities diminish with age; in contrast, alpha and beta bands increase in a linear pattern across life. Delta activity can be described as mainly and inhibitory

rhythm [15].

Theta band

Theta activity is present in the 4 Hz to 8 Hz range mainly during sleep. During wakeful state, theta activity is present in two distinct types. The first has a widespread scalp distribution and is related to decreased alertness or drowsiness and impaired information processing. The second is called frontal midline theta activity, and is located as its name indicates in a frontal midline distribution. This activity has been linked with focused attention, with mental effort and stimulus processing. The frontal midline theta activity is thought to be related with the anterior cingulate cortex and is speculated that theta activity may be related to the gating of information processing flow in the limbic regions [15]. For the purpose of obtaining a cognition or mental workload index from EEG measurements, midline theta activity with alpha posterior activity recordings are used for the production of the Task Load Index (TLI) marker as will be introduced in Section 2.1.3.3.

Alpha band

The Alpha band is the EEG activity in the 8 Hz to 13 Hz range. Alpha activity can be easily recorded during relaxation and awake states and shows its greatest amplitude over posterior (i.e., in the occipital and temporal section of the brain) regions. It is best observed during resting periods when the subject with closed eyes. In fact, opening the eyes greatly diminishes the alpha rhythm. Drowsiness is also related to the attenuation of the alpha rhythm, which is generally accompanied with frequency lowering [15].

Beta band

The Beta band appears in the 13 Hz to 30 Hz frequency range. Beta activity is present in a symmetrical frontal and central distribution and generally replaces alpha rhythm during cognitive activity. Beta activity has been linked with attention and vigilance; suggesting increased excitatory activity during arousal or focused attention [15].

Gamma band

High frequency activity in the range of 36 Hz to 44 Hz is the Gamma rhythm. This rhythm is associated with attention, arousal, object recognition and the brain's ability to integrate various aspects of stimulators into a whole. This band is linked with brain activation [15].

2.1.3.3 The Task Load Index marker

The Task Load Index (TLI) marker is derived from EEG recordings of activity in the theta and alpha bands. This marker was explored by Gevins (1997) and his team in the works presented in [44, 45, 46, 47]. Studies performed in the Human Performance Laboratory at The University of Sheffield confirmed the predictive power of this marker in its relationship with mental stress in: [7, 8, 9, 11, 12].

The TLI is a neurophysiology-based marker and derives an index of task loading of participants in complex computer work. It refers to the degree in which neural resources are used. This monitoring method is useful since it is robust and reliable enough under structured (e.g., laboratory-based) task conditions. Additionally, it is sensitive and consistently varies according to the neural state of the participant, presenting a time resolution appropriate for the experiments performed [47].

The TLI is derived from the EEG theta and alpha power spectra. During a high task load, usually accompanied with a decrease in accuracy performance and eventual

breakdown, there is an increase in the theta power over the frontal regions of the scalp, and a decrease in the alpha power over widespread scalp regions [44, 45, 46, 47].

The TLI can be defined via the following two equations:

$$TLI_1 = \frac{P_{\theta,F_z}}{P_{\alpha,P_z}} \tag{2.1}$$

$$TLI_2 = \frac{P_{\theta,AF_z}}{P_{\alpha,CP_z,PO_z}} \tag{2.2}$$

where P_θ and P_α are the theta and alpha band power respectively in the F_z, P_z, AF_z, and the pool of CP_z and PO_z electrode locations according to the 10/20 system of Figure 2.9 in Section 2.2.4.2. The power spectrum of the theta (4 Hz to 7.5 Hz) and alpha (8 Hz to 12.5 Hz) activities was averaged [12].

2.1.4 Pupillometry Pupil Diameter marker

2.1.4.1 Introduction

Pupillometry refers to the measurement of the pupil size. The human pupil is an aperture at the centre of the iris of circular shape. Through this aperture light passes through to the retina; this aperture is actively controlled with the main purpose of adapting to light changes in the environment where the human interacts with the world.

Besides regulating the amount of light that passes to the retina, the human pupil responds to other processes such as mental and physical stress since the muscles that dilate or constrict its size are governed by the Autonomic Nervous System (ANS) though its Sympathetic (SNS) and Parasympathetic (PSNS) branches. The pupil diameter can vary between 1.5 mm to 9 mm and is controlled by opposing sets of

muscles in the iris, the sphincter and dilator pupillae, governed by the PSNS and SNS dilating and constricting the pupil aperture respectively [55].

The use of the pupil size as an indicator of the mental state of humans has not been widely explored. However, studies presented in [49, 50, 51, 52, 53, 54, 55, 56, 57, 58, 59, 60] explore its use for the assessment of the affective state in HMI configurations mainly with personal computers. These studies discuss the use of this new marker and compare it with other previously successful markers by addressing the classification of stress and no-stress states. In [55] the pupil diameter and the blink rate are experimentally explored in a computer HMI configuration as indicators of mental stress. The pupil diameter is shown to be a promising indicator of the affective state in humans in this study. The studies in [58, 59] explore the pupil size and the pupil size change acceleration as markers for the detection of mental stress in human-computer interactions. In these studies, pupil measurements are compared with EEG-based and Photoplethysmogram-based psychophysiological markers showing promise in the use of the pupil markers. The same authors explore techniques for the acquisition of pupil markers in [56, 57]. In [53, 54] Zhai and his team use galvanic skin response, blood volume pulse, skin temperature and pupil diameter as psychophysiological markers of emotional "stress" states in human participants interacting with a computer. These studies mainly focus in identifying stress and no-stress state classification. The study presented in [60] uses the pupil diameter to monitor changes of human reliability while operating HMI systems in an experimental configuration. This study compares the pupil size as an indicator of ANS regulation by comparing it with commonly used cardiovascular markers. In all these studies, the pupil diameter shows promise as a mental stress state indicator. However, for the purpose of the present research, its predictive power was explored for incremental mental stress level detection contrasting with the simple classification

of stress and no-stress problematic. The Pupil Diameter Marker (PDM) showed excellent results comparable to the predictive power of HRV. The results of this study are presented in Section 2.3.

2.1.4.2 The Pupil Diameter Marker

The Pupil Diameter Marker (PDM) corresponds to a relative measurement of the pupil size. For the present research study, an Eye Tracker from Gazepoint was used as is described in Section 2.2.4.2. A study relating to its use as a marker for mental stress detection in an incremental configuration is presented in [61].

The Eye Tracker hardware provides a pupil diameter measurement based in pixels of the acquired image. The image captured by the Eye Tracker is relative to the distance of the participant. However, the Gazepoint Eye Tracker provides a scale factor to account for head movements as well as a valid flag for blinking and invalid measurements. The PDM is calculated as follows:

$$PDM_L = (LPD)\,(LPSF)\,(LVF) \tag{2.3}$$

$$PDM_R = (RPD)\,(RPSF)\,(RVF) \tag{2.4}$$

$$PDM = \sum_{i=1}^{N} \frac{PDM_{L_i} + PDM_{R_i}}{2N} \tag{2.5}$$

where PDM_L and PDM_R stand for left pupil diameter marker and right pupil diameter marker respectively. LPD and RPD stand for left and right pupil diameter in pixels; $LPSF$ and $RPSF$ for left and right pupil scale factors;LVF and RVF stand for left and right pupil valid flags respectively. N is the number of acquired samples.

2.2 Design of Mental Stress Induction Experiment

2.2.1 Introduction

As discussed in Section 1.3, when automating a HMI system, an experiment design to gather data for modelling is required. The modelling of biological systems is heavily influenced by the acquisition of good quality data, the latter being understood to be data with hidden (significant) information that truly captures all the relevant operation dynamics of the system under investigation. In order to achieve this goal, the HMI system must be thoroughly analysed in order to identify all important variables that influence its operation. For the assessment of mental stress states in human operators many psychophysiological signals and markers have been found to correlate with stress in previous studies. In Section 2.1 a thorough explanation of the most commonly used markers based in cardiovascular (ElectroCardiographic ECG) and brain (ElectroEncephalographic EEG) signals can be found. Additionally, the use of a new eye marker based in the pupil size was introduced. For the validation of this new eye marker, a study evaluating its prediction power is presented in Section 2.3.

It is worth noting that psychophysiological (e.g., ECG, EOG, EMG, EEG) signals correlate with many more processes in the human body other than mental stress. Uncertainty when dealing with these signals is an important issue. Additionally, as introduced in Section 1.2, one is only able to measure the effect of mental stress in the human operator through the close scrutiny of his/her performance in a certain task (i.e., mental stress is acknowledged indirectly), a fact that adds into the uncertainty from the markers. With all these issues taken into account, the experiment design should consider the following desirable features with regards to the task to induce mental stress:

- The performed task should be demanding enough to effectively impair the operators ability to cognitively cope with its dynamics.
- It should be able to increment its difficulty in a way that can be easily described, reproduced and automatically controlled.
- It should address tasks similar to the ones found in current HMI systems and be comparable to them as well as to current research in the subject.
- It should be designed in a way that blocks the effects of other variables that may influence the dynamic properties of the psychophysiological signals.

Other desirable features include: intuitiveness and simplicity so there is no need for time-consuming training and to avoid unexperienced operators, and the ability to perform the task in a controlled environment (e.g. in a laboratory). With these features in mind, a literature review search for experimental setup frameworks that followed these guidelines was performed. Its results are presented in Section 2.2.2.

In addition to the selection of salient input-output variables (e.g., psychophysiological markers as inputs and operator's task performance as output), the experiment must be designed in a way that facilitates its reproduction as well as the blocking of variables with known undesirable effects (e.g., temperature changes, illumination changes, verbalisation, arousal, digestive processes, etc.) that may affect the observed physiological reactions of the operator's body. With this objective in mind, an experimental framework designed for a laboratory environment may prove to be useful. For the present work, a Graphical User Interface (GUI) was designed in MATLAB® for the experiment deployment. The designed characteristics and structure of this GUI are detailed in Section 2.2.4.

2.2.2 Literature review of mentally stressful tasks

2.2.2.1 Stroop Colour Word Testing

The Stroop Colour Word Testing (CWT) is an experiment commonly used in the Cognitive Psychology field. CWT was developed by Stroop in 1935 [16]. Current CWT-based experiments consist of two basic configurations called 'non-conflict' phase and 'conflict' phase. The subjects performing CWT tasks commonly interact with a computational system were they are responsible for linking written words of colour names with coloured buttons in a Graphical User Interface (GUI) configuration. The 'non-conflict' phase is based on written colour names where the colour of the letters is congruent to the spelled colour name (e.g., colour spelling: 'black' where the subject would have to select the black coloured button). The 'conflict' phase will have a colour written name coloured in an incongruent colour (e.g., colour spelling: 'white' and the subject would have to select the black button). As expected, researchers have found the non-congruent phase to be cognitively harder that the congruent phase [35].

Many works, such as those described in [23, 24, 35, 38, 53, 58, 59], use CWT as a mental stress stimulator. However, Garde in [23] reported no statistical changes in Heart Rate Variability (HRV) (i.e., the most commonly used cardiovascular marker for mental stress assessment) during CWT experiments. In [24, 38] CWT was compared to Mental Arithmetic operations and the later was found to generate more statistical significant mental stress effects. From the provided evidences in the literature, a CWT experiment should not be regarded as an appropriate mental stressor and should be avoided given the contrasting results. Following the desirable features of the mental stress induction experiments presented in Section 2.2.1, it should be noted that CWT does not satisfy the first and most important feature, i.e., a

cognitively demanding task. Additionally, as explained in the same Section, psychophysiological markers are highly responsive to other variables such as respiration rate changes provoked by verbalisation [25], physical demands, changes in temperature, etc. [14], and observed effects can be mistakenly regarded as arising from mental demands. Appropriate experimental tasks should take into account these well-known corruptive effects and seek to avoid them through a more careful design.

2.2.2.2 Mental Arithmetic

Experiments based on Mental Arithmetic (MA) operations relate to mental calculations of simple arithmetic operations such as summations or subtractions. As the number of digits of the operands increase, so does the difficulty in their mental calculation. Time countdown timers also increase this difficulty by providing just enough time to provide an answer. This type of experiment is very simple to implement computationally and is intuitive for subjects in the experiment. No training is required for the elementary level educated individuals and its simplicity makes it an easily reproducible experiment task.

Regarding the desirable experiment characteristics presented in Section 2.2.1, MA is deficient in the sense that it is not a close match to HMI systems found in real-life (e.g., control rooms of nuclear plants, operation of transport vehicles, etc.). However, the effects in the induction of mental stress with MA have been acknowledged by studies such as [17, 23, 24, 35, 38] were it has been compared with other cognitive stressors. Bernardi *et al.* (2000) [25] conducted a thorough analysis of MA by comparing it with silent and loud reading, controlled breathing and verbalisation. Their findings suggest that verbalisation and controlled breathing could markedly alter the assessment of cognitive workload with cardiovascular signals. They also concluded that MA may be regarded as an effective mental stressor.

Because of the evidence found in the literature, its intuitiveness, simplicity and reproducibility, Mental Arithmetic (MA) operations were chosen as the mental stress stimulation experiment for this work. More information regarding the experiment design with MA can be found in Section 2.2.3.

2.2.2.3 Operation of transport vehicles

The real or simulated operation of transport vehicles is an ideal environment for inducing mental stress in a configuration very similar to what may be found in real-life HMI systems. Operation of transport vehicles includes automobiles, airplanes (e.g., commercial and fighter planes) or even space shuttles. This area of research represents an ideal candidate for a HMI system where the pilot plays an intrinsic role (i.e., a human centric system).

However, despite having several advantages, the use of transport vehicles as mental stressors for research presents several complications mainly introduced by their complex reproducibility and/or their high cost. In the current literature one may find examples of such experiments in [19, 36, 37] where real-life scenarios were performed. In [19], a HMI system was modelled with an automobile driving experiment relating the Heart Rate Variability (HRV) cardiovascular marker where the driving performance was measured with the automobile sideslip angle, yawing acceleration and rolling velocity. Similarly, in [37], stress detection is explored with cardiovascular signals, skin conductance, respiration and ElectroMyographic (EMG) recordings during real-life driving in residential and highway roads. In both cases, the reproducibility of the experiment was of big concern since many of the variables cannot be fully controlled (e.g., variables such as weather, other cars and drivers, and many others). It is worth noting that reproducibility is a key aspect for obtaining statistically significant results. Additionally, the inability to control some variables may

clearly affect some of the results.

The issues regarding these types of experiments relate mainly to the difficulty in their reproducibility that may only be overcome with a simulation-based experiment. However, the complexity in the programming of a real-life simulation, the high running-costs associated (i.e., physical space, electricity consumption, equipment for its construction) as well as the training requirement (with associated expenses in the shape of training hours) for participants in the experiment are a big deterrent for their adoption.

2.2.2.4 Automation-enhanced Cabin Air Management System

The automation-enhanced Cabin Air Management System (aCAMS) is a computer software that simulates the remote monitoring and operation of an air quality system in a space cabin. This simulator was successfully used in the past in the Human Performance Laboratory at The University of Sheffield in [7, 8, 9, 10, 11, 12]. Given its laboratory-based configuration, the variables that may contribute to contaminated results can be handled and the experiment can be reproduced as many times as necessary. The only issue with this simulator relates to the many hours of training required for experienced operators (i.e., participants in the study) since it is not intuitive and a clear understanding of the functioning of some key variables is needed.

Participants in an aCAMS experiment are required to interact with a Graphical User Interface with information on variables corresponding to air quality of breathable air. They are entrusted with monitoring the performance of automatic controllers responsible for maintaining the air quality inside certain ranges. A number of failures can occur and the operators need to acknowledge these failures and take corrective measures to ensure appropriate air quality levels to remain inside the safe ranges. A simplified version of the system, requires operators to manually control

an increasing and decreasing number of variables that are left without automatic control in a cyclic-loading manner. An increase in variables for manual control was correlated with mental stress and operator's performance. Achieving a mental stress induction similar to what may be found in real-life systems of similar characteristics, such as a nuclear power plant control room.

The aCAMS simulator is a useful tool for providing a repeatable and trustworthy mental workload experiment. However, the necessity for extensive training and experienced operators make it time-consuming and costly to implement.

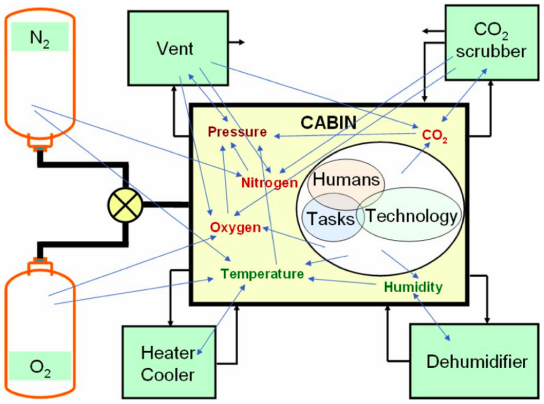

Figure 2.3: aCAMS model with interacting subsystems [7, 8].

2.2.2.5 Other experimental tasks

Many experiment designs have been reported in the literature and tested with the objective of providing necessary mental stress stimulation. Among those one can find the "cold pressor test" in [38], the "coin stacking task" in [37], "time pressure and verbal provocation" in [23, 24], "digit span recall test" in [51] and other less successful tasks such as "speech preparation task", "anger and appreciation recalling" and "student study time" in [31, 32, 33] respectively.

These experimental tasks are considered inadequate because for many of them, measures of experienced mental stress is subjective (i.e., qualitatively defined by

the participant or the experimenter) or cannot be reproduced since they are direct observations of human tasks within their daily experience. For the obtention of valuable results, a more quantitative and controlled approach is necessary in order to design a formal modelling and control framework that relates operator performance (i.e., as an indirect measure of mental workload) with the difficulty of the performed task in incremental (e.g., cyclic-loading) configurations.

2.2.3 The Mental Arithmetic operations experiment

The Mental Arithmetic (MA) operations experiment was selected as the task to induce mental stress in the participants of this study. This task was selected following extensive research presented in Section 2.2.2. The selected task in an experiment to induce mental stress is as important as the measured psychophysiological markers themselves [61]. For this specific reason, it is very important to analyse the task effectiveness in producing a cognitive load in the participant. Additionally, it is important to consider the aspects presented in Section 2.2.1 (i.e., reproducibility, representativeness of real-life HMI, simplicity, etc).

For the production of psychophysiological markers, three main measurements were taken: Electro-Encephalogram (EEG), Electro-Cardiogram (ECG) and pupil size. EEG and ECG were acquired using the ActiveTwo System by BioSemi [48]. ElectroOculogram measurements were also taken for future experiments on EEG noise recovery. The experimental framework utilised for the acquisition of these signals was the same as the one presented in [7, 8, 13]. With regards to the pupil size acquisition, a Gazepoint GP3 Eye Tracker was used [63, 64, 65] similarly as in [61, 62]. Figure 2.4 shows a participant in the study while connected to the data acquisition system.

Figure 2.4: Picture of a participant in the study while connected to the ActiveTwo Biosemi box for acquisition of EEG, ECG and EOG. The measures relating to the pupil size was acquired with the Gazepoint GP3 Eye Tracker

The experimental hardware structure was based on two computers (i.e., with Windows OS) communicating with each other. The 'participant' computer deployed a Mental Stress Evaluation Graphical-User-Interface (MSE-GUI) software that handled all processes needed for the MA experiment. The 'experimenter' computer ran the software correspondent to the acquisition hardware. For the ActiveTwo System, the ActiView LabVIEW™-based software from Biosemi was used. For the Gazepoint GP3 Eye Tracker, the Gazepoint Control software was used. This two-computer configuration [7, 8, 11, 12] allowed for the experimenter to supervise in real-time the signal acquisition without interrupting the participant's concentration. Figure 2.5 presents a diagram illustrating this hardware configuration.

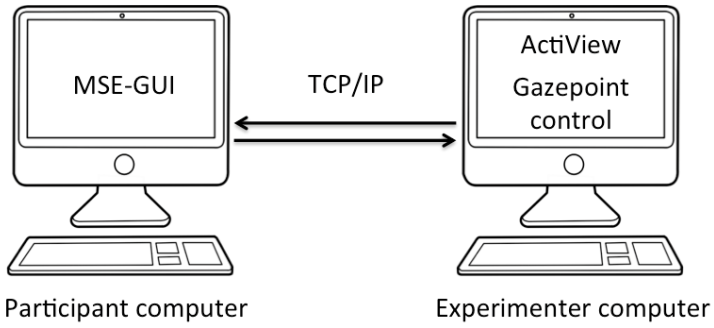

Figure 2.5: Diagram of the two-computer hardware configuration for the MA operations experimental framework.

2.2.4 Mental Stress Evaluation Graphical-User-Interface

2.2.4.1 Introduction

For the MA experiment, a Mental Stress Evaluation GUI (MSE-GUI) was designed in MATLAB®. Acquired data transmission was carried-out for EEG, ECG and EOG with this software over TCP/IP protocol, communicating with the ActiView software using the ActiveTwo System provided by BioSemi (see Figure 2.6) and the Gazepoint Control software for the GP3 Eye Tracker (see Figure 2.7). The signals handled by the ActiView software were acquired in a decimated 256 Hz frequency (i.e., from a native 2048 Hz acquisition frequency). For the Gazepoint Control software, acquisition was performed on a 60 Hz native frequency [61]. The GUI also supported, in addition to the acquisition of these signals, the experimental deployment of arithmetic operations at controlled intervals and with varying difficulty levels, the psycho-physiological markers real-time computation, the adaptive real-time model algorithm and the model-based controllers. Figure 2.8 shows an image of the user-end GUI designed in MATLAB® for the MA experiment.

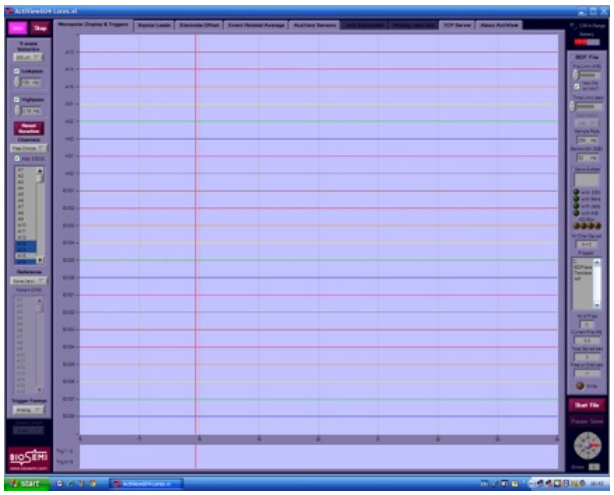

(a)

(b)

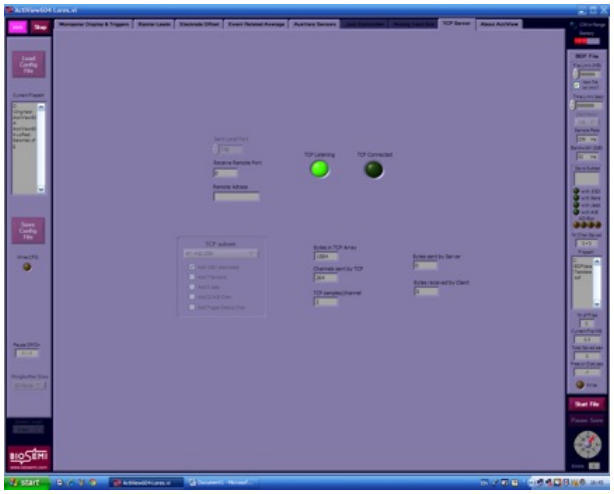

(c)

Figure 2.6: Image of the ActiView software by BioSemi [48]. (a) Main software window with all acquired signals plotted in real-time. (b) Electrode offset voltage amplitude check window. (c) TCP/IP connection window.

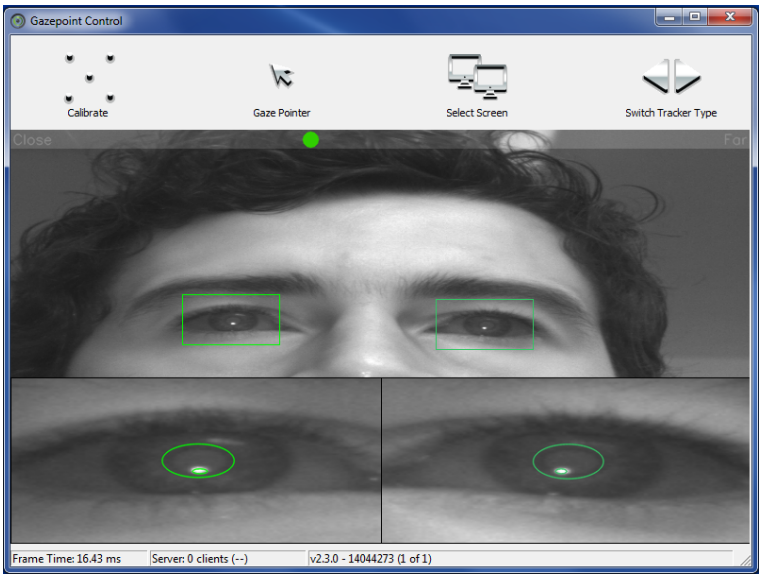

Figure 2.7: Image of the Gazepoint Control software [63, 64, 65].

The basic structure of MSE-GUI consisted on an initialisation of all global variables, TCP/IP hardware objects, and a timer object with one-second loops that performed the following main operations:

- Buffer read of EEG, ECG, EOG and Pupil data;
- Calling of functions for processing of TCP/IP packets for psychophysiological recordings;
- Storing on file of RAW processed data;
- Detection and switching of experiment phases (i.e., Phase 1 through 4) with the appropriate changes in MA operations difficulty levels;
- Handling of timers for remaining operation time and total experiment time;
- Calling of functions for marker processing (i.e., HRV, TLI, PDM);
- Calling of function for the evaluation of the participant's input (i.e., accuracy performance on the MA experiment);

- Calling of functions for real-time modelling and control;
- Storing on file of the input-output markers, real and predicted performance data, and controller action.

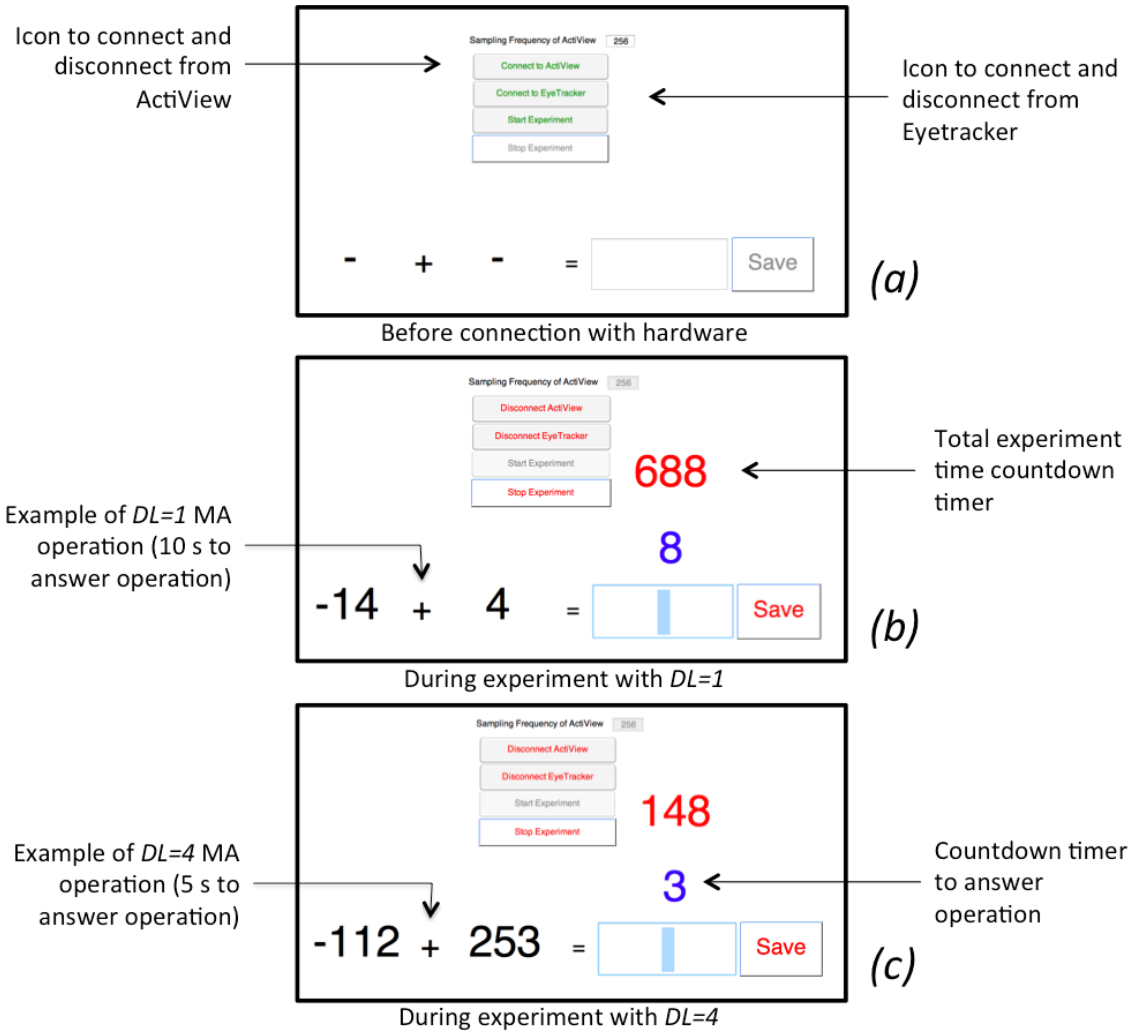

Figure 2.8: Graphical User Interface (GUI) software designed in MATLAB® for the MA experiment. (a) Shows the GUI before the hardware is connected (ActiView box and eye-tracker). (b) Shows the GUI during the experiment on DL=1. (c) Shows the GUI during the experiment on DL=4..

Additionally, GUI-MSE includes the standalone functions for the processing of the TCP/IP received packets, marker production, handling of GUI buttons (i.e., Experiment start, Save, Stop, Connect hardware, etc.), as well as other 'user defined' functions for the handling of timer-variables, MA experiment phases, MA operations, communication with hardware servers and processing of modelling and control frameworks in real-time. This basic structure was slightly modified for the different experimental sessions performed for modelling and control with respect to the activation or deactivation of the control action.

2.2.4.2 Communication with hardware

Communication with the acquisition hardware was achieved with the use of two TCP/IP MATLAB® objects that corresponded to the ActiView LabVIEW™-server and the Gazepoint Control-server. The system structure was based on two computers, with one handling the MSE-GUI software and being operated by the participant, and the second handling the acquisition servers being monitored by the experimenter (see Figure 2.5).

Acquisition of EEG, ECG and EOG

As outlined in Section 2.1, for the acquisition of the EEG markers, recordings were taken from the Pz, POz, CPz, Fz and AFz locations as defined by the international 10-20 system and as depicted in Figure 2.9. DRL and CMS in Figure 2.9 correspond to the reference electrodes for the EEG recordings.

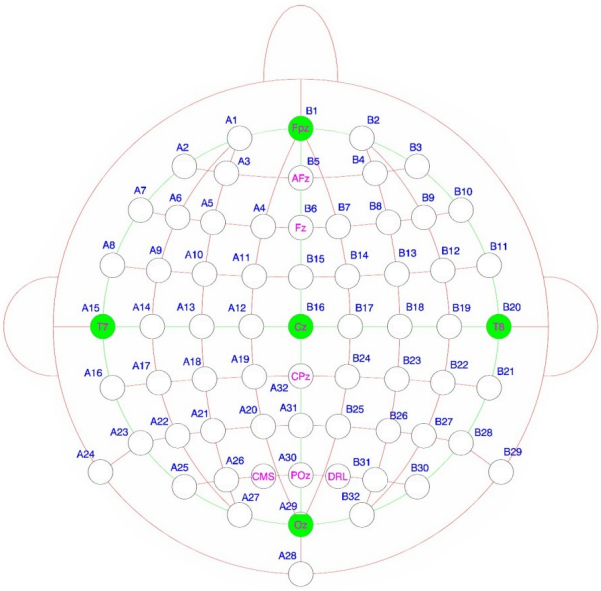

Figure 2.9: EEG electrode sites as defined by the international 10-20 system [48]

Figure 2.10 shows the ECG electrode locations of LA, RA and LL; and Figure 2.11 shows the EOG electrode locations of HR, VR, HL and VL. The reference electrodes MR and ML where located behind the ears above the area with less fat tissue above the bone as shown in Figure 2.12 [48].

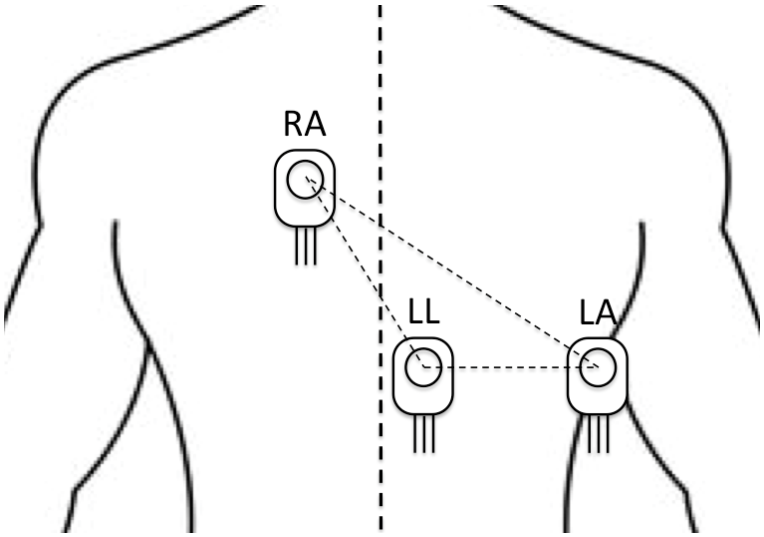

Figure 2.10: ECG electrode sites

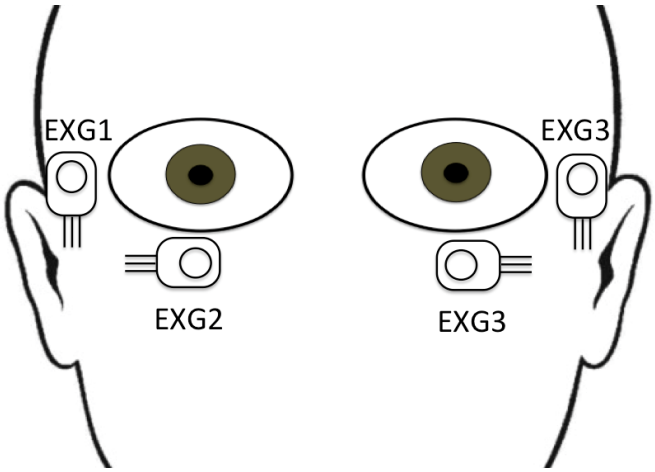

Figure 2.11: EOG electrode sites

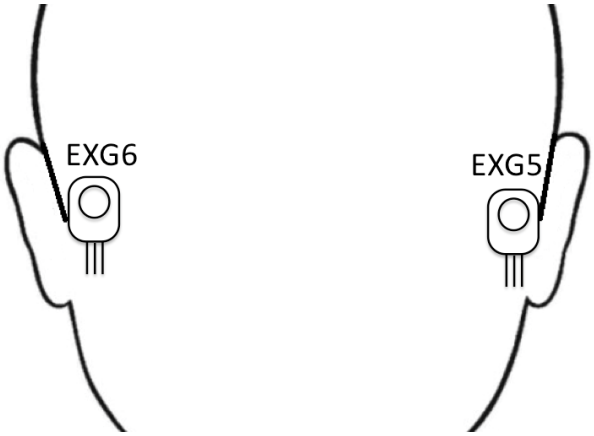

Figure 2.12: Reference electrode sites

The EEG, ECG and EOG RAW data were acquired in a decimated 256 Hz frequency (i.e., with a native 2048 Hz acquisition frequency). Every sample sent via TCP/IP was of 3 bytes size, with an additional byte of 'zero' value added by the MSE-GUI as the first byte for endianess (Windows 7® OS). These four bytes were integrated and converted into a 32 bit format in MSE-GUI. Table 2.1 shows the configuration parameters for the ActiView LabVIEW™ software.

Monopolar Display & Triggers	
Y-scale (Volts/div)	200 V
Lowpass	100 Hz
Highpass	0.16 Hz
Channels	Free Choice*, Add 8 EXG
Reference	None (raw)
Trigger Format	Analog
Screen Length	8 sec
File Limit	999999 MB
Time Limit	999999 sec
Decimation	1/8
Sample Rate	0 Hz
Bandwidth (3 dB)	0 Hz

Electrode Offset	
Displayed Range	20 mV
Channel Selection	All 256 Chan

TCP Server	
Sent Local Port	778
TCP subset	A1-H32 (256), Add 8 EX electrodes

*Selecting: A13, A14, A16, A31, A32, H30, H31, H32

Table 2.1: Configuration parameters for the ActiView LabVIEW™software

Converted data samples for the acquired EEG, ECG and EOG recordings were ordered and stored in real-time in a *'Acquisition-EEG_ECG_Data_*.txt'* file with 'Tab' as the separator for the matrix with the format shown in Table 2.2.

	1	2	3	4	5	6	7	8	9	10	11	12	13	14	15
		EEG					ECG			EOG				Reference	
		A13	A14	A16	A31	A32	H30	H31	H32	EXG1	EXG2	EXG3	EXG4	EXG5	EXG6
	Time	Pz	POz	CPz	Fz	AFz	LA	RA	LL	HR	VR	HL	VL	MR	ML
1	0.0039	*	*	*	*	*	*	*	*	*	*	*	*	*	*
2	0.0078	*	*	*	*	*	*	*	*	*	*	*	*	*	*
3	0.0117	*	*	*	*	*	*	*	*	*	*	*	*	*	*
...	...	...	...	...	...	...	...	...	...	...	...	...	...	...	...
256	1	*	*	*	*	*	*	*	*	*	*	*	*	*	*

Table 2.2: Format for storing RAW data for EEG, ECG and EOG

Acquisition of the pupil size

For the current experimental framework, the Eye Tracker was only used for the measurement of the pupil size. This hardware is capable of communicating via TCP/IP using extensible markup language (XML). This way, when communication is initiated, MSE-GUI instructs the server on which data to send. The data sent correspond to: time, data from the left eye and data from the right eye. For the calculation of the PDM marker GUI-MSE uses the diameter size in pixels of the image of the right and left pupils. The calculation takes into account the server-sent scaling factors and validation flags. The eye RAW data is stored in *'Acquisition-Eye_Data_*.txt'* files with 'Tab' separating the matrix; with the format shown in Table 2.3.

	1	2	3	4	5	6	7	8	9	10	11
	Time	LPCX	LPCY	LPD	LPS	LPV	RPCX	RPCY	RPD	RPS	RPV
1	0.0167	*	*	*	*	*	*	*	*	*	*
2	0.0334	*	*	*	*	*	*	*	*	*	*
3	0.0500	*	*	*	*	*	*	*	*	*	*
...	...	...	...	...	...	...	...	...	...	...	...
60	1	*	*	*	*	*	*	*	*	*	*

Table 2.3: Format for storing RAW for Eye data

For Table 2.3, the 'Time' column corresponds to the time in seconds since the last server initialisation or calibration; LPCX, RPCX, LPCY and RPCY correspond to the left and right x and y coordinates for the pupil positions. LPD and RPD provide the left and right pupil diameter in pixels. LPS and RPS provide the left and right pupil scaling factors; LPV and RPV are validation flags for both pupils taking binary values of 0 or 1.

2.2.4.3 Real-time modelling software

Two basic real-time modelling experiment configurations were performed. For the first configuration, Modelling Experiment 1 (ME-1), the psychophysiological markers were computed and used as inputs to the Adaptive General Type-2 Fuzzy C-Means (A-GT2-FCM) modelling framework of Section 4.3 for the production of Predicted Accuracy Performance (PAP) in an incremental difficulty configuration. The Modelling Experiment 2 (ME-2) was of similar characteristics but with scrambled difficulty phases. Figure 2.13 shows the difficulty configurations plotted against time for ME-1 and ME-2.

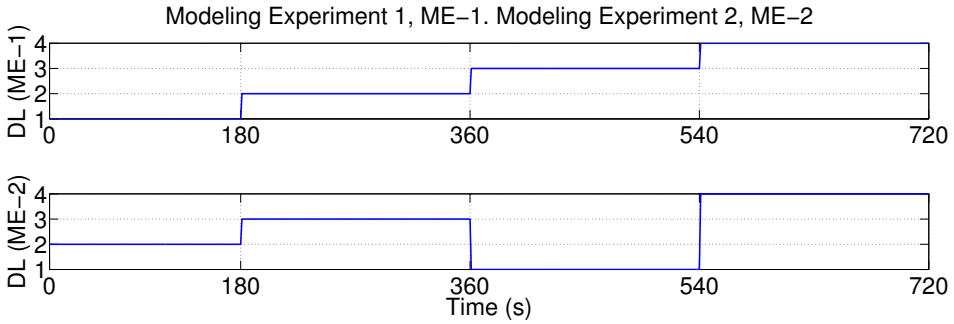

Figure 2.13: Difficulty level for Modelling Experiment 1 (increasing difficulty), top plot. Modelling Experiment 2 (scrambled difficulty), bottom plot.

Modelling Experiments 1 (ME-1) and 2 (ME-2) consisted of four (4) phases of 180 s each and were performed one after the other in the same session. For ME-1 these 4 consecutive phases were of incremental Difficulty Levels (DL), evolving from $DL = 1$ (relatively easy) to $DL = 4$ (most difficult). $DL = 1$ consisted of the summations of two random numbers of 1 to 2 digits with participants given 10 s to provide an answer (see Figure 2.8(b)), $DL = 2$ was similar to $DL = 1$ with the difference that participants had only 5 s to provide an answer. $DL = 3$ and $DL = 4$ followed this same pattern but with numbers of 2 to 3 digits and with participants having

10 s and 5 s to provide an answer respectively (see Fig. 2.8(c)). All participants experienced a decreased performance at $DL = 4$. For ME-2 the difficulty level phases were 'scrambled'. The order of the difficulty levels in ME-2 was changed to block the effect of fatigue and to evaluate the order change effect in the psychophysiological markers.

The computed psycho-physiological markers were obtained with acquired recordings with windows of 30 s of duration. The windows were shifted every second, hence obtaining a total of 690 samples for every modelling phase (i.e., ME-1 and ME-2) with 150 samples for Phase 1 and 180 samples for the remaining phases (Phase 2 through 4).

2.2.4.4 Real-time modelling and control software

Two real-time model-based control experiments of the same configuration (MCE) were performed for every participant in the study, their difference relating to the model-based controller used. This control experimental configuration used the same structure present in the ME-1 and ME-2, adding a controller that acted upon the difficulty profiles of Figure 2.13. The controller was designed with the objective of achieving a better performance and avoiding operator breakdown. Both difficulty profiles were implemented with the use of forced DL (i.e., the control variable) disturbances that followed the profiles of Figure 2.13.

2.2.5 Procedure for experiment

This study received ethical approval from The University of Sheffield. The participants were informed on the aims and objectives of the study including its full details and on the safety of the experiment. Both acquisition devices used (ActiveTwo box and GP3 Eye Tracker) were isolated from the electrical current. The only

concern was with respect to hygiene in the care of the reusable electrodes, which were washed after every experiment. All data collected were anonymised following the recommendations of the University when dealing with personal data. The participant names were kept in a secure file for future experiments and this file will be erased following the conclusion of the study. All participants in the study were informed that they may leave the experiment at any point if they do wish. They were also asked to avoid consuming drinks or food (i.e., digestive processes alter physiological responses) that may alter their physiological response such as coffee or alcohol at least two hours prior to the start of the experimental session. They were asked to relax and not to exercise before the experiment. During the experiment they were asked to avoid speaking, clenching their jaws or moving excessively to avoid contaminating the psychophysiological signals with undesirable disconnections.

The basic experimental procedure to be followed was:

1. Informing the participant of all experiment details and giving the appropriate recommendations for obtaining good quality data.

2. Connecting all hardware and electrodes for the acquisition.

3. Running the MSE-GUI and performing the actual experiment.

2.3 Prediction power of psychophysiological markers

2.3.1 Introduction

In this Section, a series of experimental sessions to evaluate the prediction power of the Pupil Diameter Marker (PDM) are presented. Additionally, these results are

compared to the previously used HRV and TLI markers for their validation in the Mental Arithmetic operations configuration of Section 2.2.3.

2.3.2 Evaluation of the PDM

Since the Pupil Diameter Marker (PDM) of Section 2.1.4 had never been used before in the experimental configuration proposed for this work, a series of preliminary experimental sessions on four participants (e.g., P01, P02, P03 and P04) were performed with the ME-1 and ME-2 Difficulty Level (DL) configurations of Figure 2.13, but with an added baseline phase where no operations were performed. For the baseline phase, the participant was asked to relax and try not to think on any stressful event.

A visual inspection of the PDM evolution together with the task performance was performed to evaluate if the MA experiment was in fact, producing the sought decrement in accuracy correlated with cognitive load. Figure 2.14 shows plots for Participant 3 (P03) and Participant 4 (P04) in the preliminary visualisation experiments.

From Figure 2.14 it can be observed that, as expected, $DL = 4$ is effective in producing a reduced task performance accuracy. This can be acknowledged by observing the last phase (e.g., from $Time = 720$ s to $Time = 900$ s). It is also clear that as difficulty levels increase there is a decrease in accuracy and that PDM changes its mean value as difficulty in the phases changes. The effect of the experiment in producing mental stress and a pupil size response is more visually apparent in P04. For P04 the PDM changes greatly with correlation to the DL of the operations. The task Accuracy Performance (AP) of the participant also decreases as the difficulty increases.

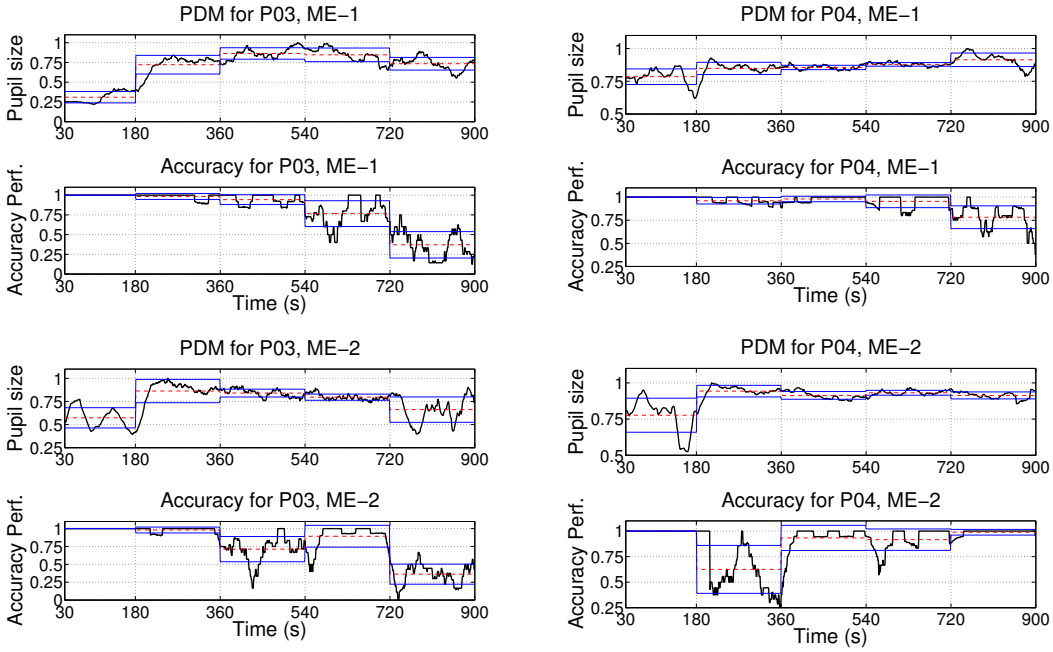

Figure 2.14: Plots showing the evolution of the PDM and the Accuracy Performance for P03 and P04 for ME-1 (e.g., Baseline, DL =1, 2, 3 and 4) and ME-2 (e.g., Baseline, DL =2, 3, 1 and 4) in the MA preliminary experiment. The plots show the mean and standard deviations for the PDM and the Accuracy Performance acquired signals.

From these preliminary results it was clear there was a clear pattern in the PDM across all four participants. To further evidence the results of Figure 2.14, acquisition of markers and evaluation of accuracy task performance was performed for all 4 participants in order to validate with a statistical two sample T-test the use of the PDM. Tables 2.4 to 2.7 show the results for the T-test that evaluated the incremental detection property of the PDM. For this test, the PDM marker vectors for each phase were compared against vectors of all other phases in each Modelling Experiment (e.g., ME-1 and ME-2) to investigate the ability of the marker of distinguishing between different DL. The Tables for P01, P02, P03 and P04 show the test decision H that decides if the marker data vectors come from a normal distribution of equal mean and variance. If $H = 0$, this means no significant difference is identified (e.g., with

a 5% confidence level). When $H = 1$, a significant difference in the data vectors is observed. Below the H test decision outcome, the p-values for the same tests are presented in the Tables.

From the results of Tables 2.4 to 2.7, a consistent PDM performance is observed for the detection of incremental levels of mental stress. This marker is able to differentiate in most cases the different DL in the MA experiment.

Further into this statistical two sample T-test, a few cases where the PDM does not correctly differentiate between phases can also be observed. This can be due to the fact that the participant is not incrementally mentally stressed whenever this effect is present in adjacent DL phases (i.e., the inability to differentiate between Phase 1 and Phase 2). Other cases can be explained by the fact that perhaps, the participant was not fully engaged with the experiment. The fact that the pupil constricts and dilates for many reasons such as level of available light or arousal should also be considered.

After this preliminary study it was concluded that the PDM would be effective in predicting the level of mental stress given its high correlation with the diverse DL in the MA experiment. Further results were obtained from the data collected from the ME-1 and ME-2 on all remaining participants in the study. Tables 2.8 through 2.15 present these additional evidences. From these Tables, similar results to the preliminary study can be observed throughout.

P01 - ME-1 - PDM

H	Baseline	Phase 1	Phase 2	Phase 3	Phase 4
Baseline	0				
Phase 1	0	0			
Phase 2	1	1	0		
Phase 3	1	1	1	0	
Phase 4	1	1	1	1	0

p values	Baseline	Phase 1	Phase 2	Phase 3	Phase 4
Baseline	1.0000				
Phase 1	0.5187	1.0000			
Phase 2	0.0000	0.0000	1.0000		
Phase 3	0.0000	0.0000	0.0000	1.0000	
Phase 4	0.0000	0.0000	0.0000	0.0000	1.0000

P01 - ME-2 - PDM

H	Baseline	Phase 2	Phase 3	Phase 1	Phase 4
Baseline	0				
Phase 2	1	0			
Phase 3	1	1	0		
Phase 1	1	0	1	0	
Phase 4	1	1	1	1	0

p values	Baseline	Phase 2	Phase 3	Phase 1	Phase 4
Baseline	1.0000				
Phase 2	0.0000	1.0000			
Phase 3	0.0000	0.0003	1.0000		
Phase 1	0.0000	0.1370	0.0001	1.0000	
Phase 4	0.0000	0.0000	0.0000	0.0000	1.0000

Table 2.4: PDM Statistical T-test results for ME-1 and ME-2 with Baseline for P01

P02 - ME-1 - PDM

H	Baseline	Phase 1	Phase 2	Phase 3	Phase 4
Baseline	0				
Phase 1	1	0			
Phase 2	1	1	0		
Phase 3	1	1	1	0	
Phase 4	1	1	1	1	0

p values	Baseline	Phase 1	Phase 2	Phase 3	Phase 4
Baseline	1.0000				
Phase 1	0.0000	1.0000			
Phase 2	0.0000	0.0012	1.0000		
Phase 3	0.0000	0.0000	0.0000	1.0000	
Phase 4	0.0000	0.0000	0.0000	0.0081	1.0000

P02 - ME-2 - PDM

H	Baseline	Phase 2	Phase 3	Phase 1	Phase 4
Baseline	0				
Phase 2	1	0			
Phase 3	1	1	0		
Phase 1	1	1	0	0	
Phase 4	1	1	1	1	0

p values	Baseline	Phase 2	Phase 3	Phase 1	Phase 4
Baseline	1.0000				
Phase 2	0.0000	1.0000			
Phase 3	0.0000	0.0000	1.0000		
Phase 1	0.0000	0.0000	0.4145	1.0000	
Phase 4	0.0000	0.0000	0.0000	0.0000	1.0000

Table 2.5: PDM Statistical T-test results for ME-1 and ME-2 with Baseline for P02

P03 - ME-1 - PDM

H	Baseline	Phase 1	Phase 2	Phase 3	Phase 4
Baseline	0				
Phase 1	1	0			
Phase 2	0	1	0		
Phase 3	1	1	1	0	
Phase 4	1	1	1	1	0

p values	Baseline	Phase 1	Phase 2	Phase 3	Phase 4
Baseline	1.0000				
Phase 1	0.0043	1.0000			
Phase 2	0.0591	0.0005	1.0000		
Phase 3	0.0003	0.0410	0.0000	1.0000	
Phase 4	0.0000	0.0000	0.0000	0.0000	1.0000

P03 - ME-2 - PDM

H	Baseline	Phase 2	Phase 3	Phase 1	Phase 4
Baseline	0				
Phase 2	1	0			
Phase 3	1	1	0		
Phase 1	1	1	1	0	
Phase 4	1	1	1	1	0

p values	Baseline	Phase 2	Phase 3	Phase 1	Phase 4
Baseline	1.0000				
Phase 2	0.0000	1.0000			
Phase 3	0.0000	0.0003	1.0000		
Phase 1	0.0000	0.0000	0.0000	1.0000	
Phase 4	0.0000	0.0000	0.0000	0.0000	1.0000

Table 2.6: PDM Statistical T-test results for ME-1 and ME-2 with Baseline for P03

P04 - ME-1 - PDM

H	Baseline	Phase 1	Phase 2	Phase 3	Phase 4
Baseline	0				
Phase 1	1	0			
Phase 2	1	1	0		
Phase 3	1	1	1	0	
Phase 4	1	1	1	1	0

p values	Baseline	Phase 1	Phase 2	Phase 3	Phase 4
Baseline	1.0000				
Phase 1	0.0000	1.0000			
Phase 2	0.0000	0.0322	1.0000		
Phase 3	0.0000	0.0000	0.0000	1.0000	
Phase 4	0.0000	0.0000	0.0000	0.0000	1.0000

P04 - ME-2 - PDM

H	Baseline	Phase 2	Phase 3	Phase 1	Phase 4
Baseline	0				
Phase 2	1	0			
Phase 3	1	1	0		
Phase 1	1	1	1	0	
Phase 4	1	1	1	1	0

p values	Baseline	Phase 2	Phase 3	Phase 1	Phase 4
Baseline	1.0000				
Phase 2	0.0000	1.0000			
Phase 3	0.0000	0.0000	1.0000		
Phase 1	0.0000	0.0000	0.0000	1.0000	
Phase 4	0.0000	0.0000	0.0000	0.0000	1.0000

Table 2.7: PDM Statistical T-test results for ME-1 and ME-2 with Baseline for P04

P05 - ME-1 - PDM					
H	Baseline	Phase 1	Phase 2	Phase 3	Phase 4
Baseline	0				
Phase 1	1	0			
Phase 2	1	1	0		
Phase 3	1	1	1	0	
Phase 4	1	1	1	1	0
p values	Baseline	Phase 1	Phase 2	Phase 3	Phase 4
Baseline	1.0000				
Phase 1	0.0000	1.0000			
Phase 2	0.0000	0.0000	1.0000		
Phase 3	0.0000	0.0000	0.0000	1.0000	
Phase 4	0.0000	0.0000	0.0000	0.0000	1.0000

P05 - ME-2 - PDM					
H	Baseline	Phase 2	Phase 3	Phase 1	Phase 4
Baseline	0				
Phase 2	1	0			
Phase 3	0	1	0		
Phase 1	0	0	0	0	
Phase 4	1	1	1	1	0
p values	Baseline	Phase 2	Phase 3	Phase 1	Phase 4
Baseline	1.0000				
Phase 2	0.0299	1.0000			
Phase 3	0.5886	0.0000	1.0000		
Phase 1	0.5919	0.2783	0.0905	1.0000	
Phase 4	0.0000	0.0000	0.0000	0.0000	1.0000

Table 2.8: PDM Statistical T-test results for ME-1 and ME-2 with Baseline for P05

P06 - ME-1 - PDM					
H	Baseline	Phase 1	Phase 2	Phase 3	Phase 4
Baseline	0				
Phase 1	1	0			
Phase 2	1	1	0		
Phase 3	1	1	1	0	
Phase 4	1	1	1	1	0
p values	Baseline	Phase 1	Phase 2	Phase 3	Phase 4
Baseline	1.0000				
Phase 1	0.0000	1.0000			
Phase 2	0.0003	0.0000	1.0000		
Phase 3	0.0000	0.0000	0.0000	1.0000	
Phase 4	0.0000	0.0000	0.0000	0.0000	1.0000

P06 - ME-2 - PDM					
H	Baseline	Phase 2	Phase 3	Phase 1	Phase 4
Baseline	0				
Phase 2	1	0			
Phase 3	1	1	0		
Phase 1	1	1	1	0	
Phase 4	1	1	1	1	0
p values	Baseline	Phase 2	Phase 3	Phase 1	Phase 4
Baseline	1.0000				
Phase 2	0.0000	1.0000			
Phase 3	0.0000	0.0000	1.0000		
Phase 1	0.0000	0.0000	0.0000	1.0000	
Phase 4	0.0000	0.0000	0.0000	0.0000	1.0000

Table 2.9: PDM Statistical T-test results for ME-1 and ME-2 with Baseline for P06

P07 - ME-1 - PDM					
H	Baseline	Phase 1	Phase 2	Phase 3	Phase 4
Baseline	0				
Phase 1	1	0			
Phase 2	1	1	0		
Phase 3	1	1	1	0	
Phase 4	1	1	1	1	0
p values	Baseline	Phase 1	Phase 2	Phase 3	Phase 4
Baseline	1.0000				
Phase 1	0.0000	1.0000			
Phase 2	0.0000	0.0006	1.0000		
Phase 3	0.0000	0.0000	0.0000	1.0000	
Phase 4	0.0000	0.0000	0.0000	0.0000	1.0000

P07 - ME-2 - PDM					
H	Baseline	Phase 2	Phase 3	Phase 1	Phase 4
Baseline	0				
Phase 2	1	0			
Phase 3	1	1	0		
Phase 1	1	1	1	0	
Phase 4	1	1	1	1	0
p values	Baseline	Phase 2	Phase 3	Phase 1	Phase 4
Baseline	1.0000				
Phase 2	0.0000	1.0000			
Phase 3	0.0000	0.0000	1.0000		
Phase 1	0.0000	0.0000	0.0000	1.0000	
Phase 4	0.0200	0.0000	0.0000	0.0000	1.0000

Table 2.10: PDM Statistical T-test results for ME-1 and ME-2 with Baseline for P07

P08 - ME-1 - PDM					
H	Baseline	Phase 1	Phase 2	Phase 3	Phase 4
Baseline	0				
Phase 1	1	0			
Phase 2	1	1	0		
Phase 3	1	1	1	0	
Phase 4	1	0	0	1	0
p values	Baseline	Phase 1	Phase 2	Phase 3	Phase 4
Baseline	1.0000				
Phase 1	0.0000	1.0000			
Phase 2	0.0000	0.0000	1.0000		
Phase 3	0.0000	0.0000	0.0000	1.0000	
Phase 4	0.0017	0.1252	0.8405	0.0000	1.0000

P08 - ME-1 (2)* - PDM					
H	Baseline	Phase 1	Phase 2	Phase 3	Phase 4
Baseline	0				
Phase 1	1	0			
Phase 2	1	1	0		
Phase 3	1	1	1	0	
Phase 4	0	0	1	1	0
p values	Baseline	Phase 1	Phase 2	Phase 3	Phase 4
Baseline	1.0000				
Phase 1	0.0006	1.0000			
Phase 2	0.0000	0.0000	1.0000		
Phase 3	0.0012	0.0000	0.0000	1.0000	
Phase 4	0.0542	0.4768	0.0000	0.0004	1.0000

Table 2.11: PDM Statistical T-test results for ME-1 with Baseline for P08. *only ME-1 was performed for this participant.

P09 - ME-1 - PDM

H	Baseline	Phase 1	Phase 2	Phase 3	Phase 4
Baseline	0				
Phase 1	1	0			
Phase 2	1	1	0		
Phase 3	1	1	1	0	
Phase 4	1	1	0	1	0

p values	Baseline	Phase 1	Phase 2	Phase 3	Phase 4
Baseline	1.0000				
Phase 1	0.0000	1.0000			
Phase 2	0.0000	0.0000	1.0000		
Phase 3	0.0000	0.0001	0.0000	1.0000	
Phase 4	0.0000	0.0000	0.3101	0.0000	1.0000

P09 - ME-2 - PDM

H	Baseline	Phase 2	Phase 3	Phase 1	Phase 4
Baseline	0				
Phase 2	1	0			
Phase 3	1	0	0		
Phase 1	1	1	1	0	
Phase 4	1	1	1	1	0

p values	Baseline	Phase 2	Phase 3	Phase 1	Phase 4
Baseline	1.0000				
Phase 2	0.0000	1.0000			
Phase 3	0.0000	0.1696	1.0000		
Phase 1	0.0000	0.0000	0.0000	1.0000	
Phase 4	0.0000	0.0000	0.0000	0.0148	1.0000

Table 2.12: PDM Statistical T-test results for ME-1 and ME-2 with Baseline for P09

P10 - ME-1 - PDM

H	Baseline	Phase 1	Phase 2	Phase 3	Phase 4
Baseline	0				
Phase 1	1	0			
Phase 2	1	1	0		
Phase 3	1	1	0	0	
Phase 4	1	1	1	1	0

p values	Baseline	Phase 1	Phase 2	Phase 3	Phase 4
Baseline	1.0000				
Phase 1	0.0000	1.0000			
Phase 2	0.0000	0.0000	1.0000		
Phase 3	0.0000	0.0000	0.3501	1.0000	
Phase 4	0.0000	0.0000	0.0065	0.0000	1.0000

P10 - ME-2 - PDM

H	Baseline	Phase 2	Phase 3	Phase 1	Phase 4
Baseline	0				
Phase 2	1	0			
Phase 3	1	1	0		
Phase 1	1	1	1	0	
Phase 4	1	1	1	0	0

p values	Baseline	Phase 2	Phase 3	Phase 1	Phase 4
Baseline	1.0000				
Phase 2	0.0000	1.0000			
Phase 3	0.0000	0.0000	1.0000		
Phase 1	0.0000	0.0000	0.0003	1.0000	
Phase 4	0.0000	0.0000	0.0001	0.1871	1.0000

Table 2.13: PDM Statistical T-test results for ME-1 and ME-2 with Baseline for P10

P11 - ME-1 - PDM

H	Baseline	Phase 1	Phase 2	Phase 3	Phase 4
Baseline	0				
Phase 1	1	0			
Phase 2	1	0	0		
Phase 3	1	1	1	0	
Phase 4	1	1	1	1	0

p values	Baseline	Phase 1	Phase 2	Phase 3	Phase 4
Baseline	1.0000				
Phase 1	0.0000	1.0000			
Phase 2	0.0000	0.3034	1.0000		
Phase 3	0.0000	0.0000	0.0000	1.0000	
Phase 4	0.0000	0.0000	0.0000	0.0000	1.0000

P11 - ME-2 - PDM

H	Baseline	Phase 2	Phase 3	Phase 1	Phase 4
Baseline	0				
Phase 2	1	0			
Phase 3	1	0	0		
Phase 1	1	1	1	0	
Phase 4	1	1	1	1	0

p values	Baseline	Phase 2	Phase 3	Phase 1	Phase 4
Baseline	1.0000				
Phase 2	0.0000	1.0000			
Phase 3	0.0000	0.3591	1.0000		
Phase 1	0.0000	0.0000	0.0000	1.0000	
Phase 4	0.0000	0.0000	0.0001	0.0000	1.0000

Table 2.14: PDM Statistical T-test results for ME-1 and ME-2 with Baseline for P11

P12 - ME-1 - PDM

H	Baseline	Phase 1	Phase 2	Phase 3	Phase 4
Baseline	0				
Phase 1	1	0			
Phase 2	1	1	0		
Phase 3	1	1	1	0	
Phase 4	1	1	1	1	0

p values	Baseline	Phase 1	Phase 2	Phase 3	Phase 4
Baseline	1.0000				
Phase 1	0.0000	1.0000			
Phase 2	0.0000	0.0000	1.0000		
Phase 3	0.0000	0.0000	0.0000	1.0000	
Phase 4	0.0000	0.0000	0.0000	0.0316	1.0000

P12 - ME-2 - PDM

H	Baseline	Phase 2	Phase 3	Phase 1	Phase 4
Baseline	0				
Phase 2	1	0			
Phase 3	1	1	0		
Phase 1	1	1	1	0	
Phase 4	1	1	1	1	0

p values	Baseline	Phase 2	Phase 3	Phase 1	Phase 4
Baseline	1.0000				
Phase 2	0.0000	1.0000			
Phase 3	0.0000	0.0000	1.0000		
Phase 1	0.0000	0.0088	0.0000	1.0000	
Phase 4	0.0000	0.0000	0.0000	0.0289	1.0000

Table 2.15: PDM Statistical T-test results for ME-1 and ME-2 with Baseline for P12

In order to further visualise the ability of the PDM in differentiating between DL phases, Table 2.16 presents the average test decision H for all 12 participants for ME-1 and ME-2 configurations with added Baseline. Since P08 only performed ME-1, this Table presents an average of 12 results for ME-1 and an average of 11 results for ME-2.

All Participants Average - ME-1					
H	Baseline	Phase 1	Phase 2	Phase 3	Phase 4
Baseline	0.0000				
Phase 1	0.9167	0.0000			
Phase 2	0.9167	0.9167	0.0000		
Phase 3	1.0000	1.0000	0.9167	0.0000	
Phase 4	1.0000	0.9167	0.8333	1.0000	0.0000

All Participants Average - ME-2					
H	Baseline	Phase 2	Phase 3	Phase 1	Phase 4
Baseline	0.0000				
Phase 2	1.0000	0.0000			
Phase 3	0.9091	0.8182	0.0000		
Phase 1	0.9091	0.8182	0.8182	0.0000	
Phase 4	1.0000	1.0000	1.0000	0.9091	0.0000

Table 2.16: Average PDM Statistical T-test results for ME-1 and ME-2 with Baseline for all participants (12 participants for ME-1 and 11 participants for ME-2).

As is evidenced with values close to 1 in Table 2.27, in most cases, the PDM is able to differentiate between DL phases. Additionally to the statistical two sample T-test, it is helpful to investigate the activation trend in the PDM as it follows the different DL of all experiment phases. Figure 2.15 presents the trends obtained for all 12 participants in the study.

From the activation patterns of Figure 2.15 it is clear how for the ME-1 as DL increases, so does the mean of the PDM. For the ME-2, the mean PDM increases or decreases in a participant-dependent fashion. As can be observed, there is no clear pattern even if the PDM responds to the the changes in DL. These participant-dependent activation patterns evidence the importance of a modelling algorithm capable of adapting to the changes in cognitive workload.

In this Section the prediction power of the PDM was shown. It was also clear from the activation patterns how the PDM responds in a participant-dependent fashion. The evidences presented seek to illustrate the problematic in dealing with psychophysiological markers with the objective of predicting cognitive workload as well as the outstanding prediction power of the PDM. However, in order to fully

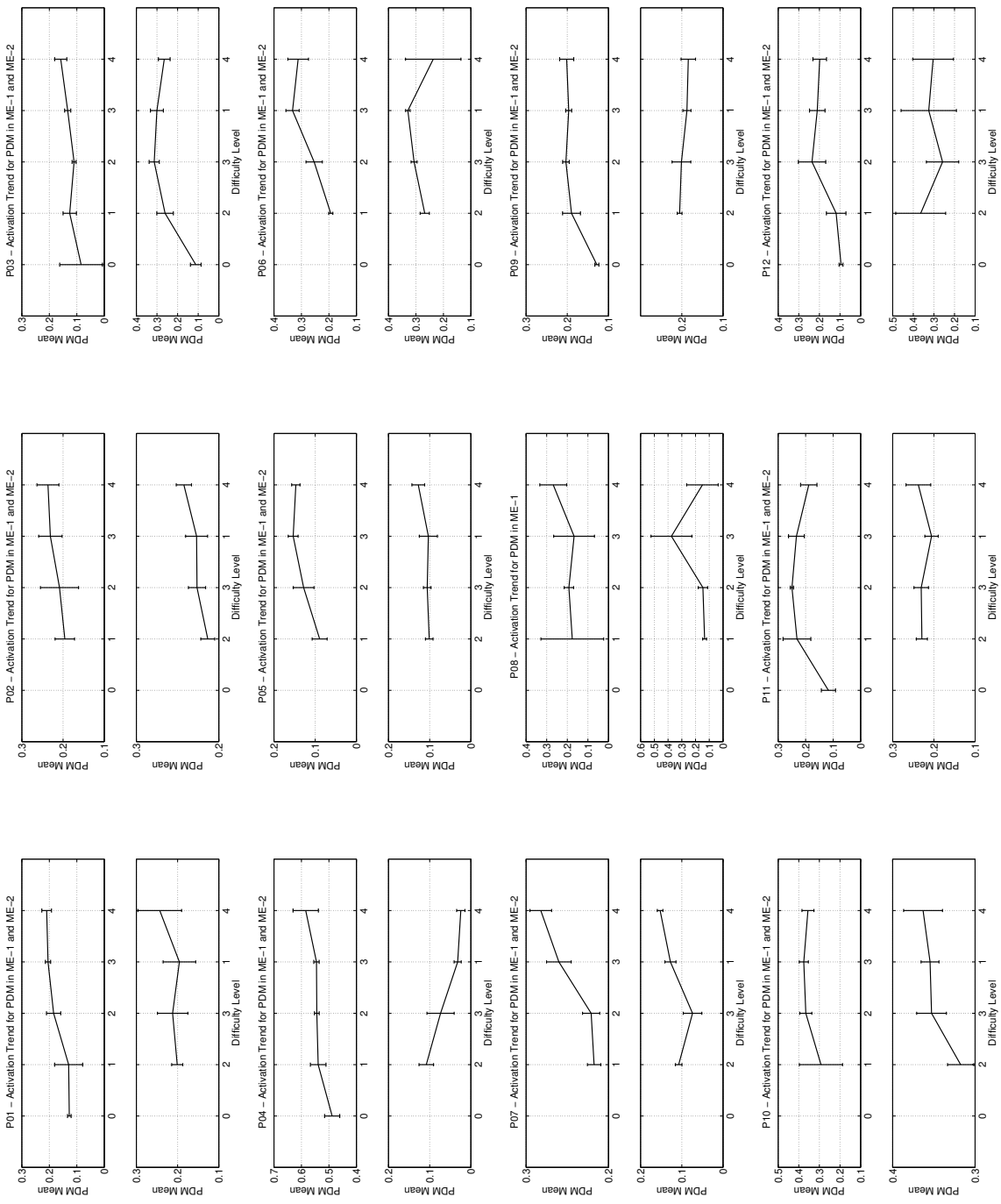

Figure 2.15: Plots showing the activation trend of the PDM for all participants in the study. Trends are presented for ME-1 (e.g., Baseline, DL =1, 2, 3 and 4) and ME-2 (e.g., Baseline, DL =2, 3, 1 and 4) for the MA experiment. The plots show the mean and standard deviations for the PDM.

validate PDM as a new mental stress marker, a comparison with previously successful markers may be useful. The next Section deals with this necessary comparison.

2.3.3 Comparison of the PDM with HRV and TLI

In order to evaluate the prediction power of the PDM as compared with the previously tested HRV and TLI markers, a study comparing their ability to discriminate between phases in the MA operations experiment was performed. Two participants (P04 and P05) were not able to continue with these tests due to personal circumstances, however, participant indices remained the same to avoid confusion throughout this document. A total of ten participant datasets were used for this comparison test. Additionally, baseline studies were not performed for this study since the statistical difference between baseline and the DL phases in the MA experiment configurations was established for PDM and previously for HRV and TLI markers as in [7, 8, 11, 12]. In this study, importance was given to the ability of the markers in distinguishing between different DL phases and in comparing their prediction power to the newly introduced PDM.

The following pages present Tables showing statistical two-sampled T-tests for HRV (i.e., HRV1 and HRV2) and TLI (i.e., TLI1 and TLI2) markers with the same configuration as for PDM. The difference in these Tables resides in the fact that a baseline phase is not introduced. Additionally, a statistical two-sampled T-test was also performed for the accuracy task performance (AP) to show that the MA operations experiment was successful in cognitively impacting the participants with its different DL phases. An accuracy decrement for phase 4 was observed among all participants even if with accuracy levels of diverse pattern for each participant.

Tables 2.17 through 2.26 show the T-tests for HRV1, Tables 2.27 through 2.36 show the T-tests for HRV2, Tables 2.37 through 2.46 show these tests for TLI1 and

Tables 2.47 through 2.56 for the TLI2 marker. The statistical two-sampled T-tests for AP are presented in Tables 2.57 through 2.66.

In Tables 2.17 through 2.26 the ability of the HRV1 marker in distinguishing between DL in the MA operations of ME-1 and ME-2 configuration is observed. For the majority of the participants in the study this marker has significant statistical differences between most DL phases. However, for some participants, two or more phases cannot be statistically distinguished (e.g., P01, P03, P09 and P11). For the case of the HRV2 marker (Tables 2.27 through 2.36), its ability of distinguishing between phases presents a few problems for some participants in the study. However, for most cases, this marker is able to differentiate between phases. This trend is observed throughout the Tables correspondent to TLI1 and TLI2.

P01 - ME-1 - HRV1				
H	Phase 1	Phase 2	Phase 3	Phase 4
Phase 1	0			
Phase 2	1	0		
Phase 3	0	1	0	
Phase 4	1	1	1	0
p values	Phase 1	Phase 2	Phase 3	Phase 4
Phase 1	1.0000			
Phase 2	0.0000	1.0000		
Phase 3	0.1475	0.0000	1.0000	
Phase 4	0.0000	0.0000	0.0005	1.0000

P01 - ME-2 - HRV1				
H	Phase 2	Phase 3	Phase 1	Phase 4
Phase 2	0			
Phase 3	1	0		
Phase 1	1	0	0	
Phase 4	1	0	1	0
p values	Phase 2	Phase 3	Phase 1	Phase 4
Phase 2	1.0000			
Phase 3	0.0000	1.0000		
Phase 1	0.0000	0.1181	1.0000	
Phase 4	0.0000	0.3019	0.0046	1.0000

Table 2.17: HRV1 Statistical T-test results for ME-1 and ME-2 for P01

P02 - ME-1 - HRV1				
H	Phase 1	Phase 2	Phase 3	Phase 4
Phase 1	0			
Phase 2	1	0		
Phase 3	1	1	0	
Phase 4	1	1	1	0
p values	Phase 1	Phase 2	Phase 3	Phase 4
Phase 1	1.0000			
Phase 2	0.0000	1.0000		
Phase 3	0.0000	0.0000	1.0000	
Phase 4	0.0000	0.0000	0.0000	1.0000

P02 - ME-2 - HRV1				
H	Phase 2	Phase 3	Phase 1	Phase 4
Phase 2	0			
Phase 3	1	0		
Phase 1	1	1	0	
Phase 4	1	1	1	0
p values	Phase 2	Phase 3	Phase 1	Phase 4
Phase 2	1.0000			
Phase 3	0.0000	1.0000		
Phase 1	0.0000	0.0000	1.0000	
Phase 4	0.0000	0.0000	0.0000	1.0000

Table 2.18: HRV1 Statistical T-test results for ME-1 and ME-2 for P02

P03 - ME-1 - HRV1				
H	Phase 1	Phase 2	Phase 3	Phase 4
Phase 1	0			
Phase 2	1	0		
Phase 3	0	1	0	
Phase 4	1	0	1	0
p values	Phase 1	Phase 2	Phase 3	Phase 4
Phase 1	1.0000			
Phase 2	0.0001	1.0000		
Phase 3	0.0691	0.0000	1.0000	
Phase 4	0.0000	0.7554	0.0000	1.0000

P03 - ME-2 - HRV1				
H	Phase 2	Phase 3	Phase 1	Phase 4
Phase 2	0			
Phase 3	1	0		
Phase 1	1	0	0	
Phase 4	0	1	1	0
p values	Phase 2	Phase 3	Phase 1	Phase 4
Phase 2	1.0000			
Phase 3	0.0005	1.0000		
Phase 1	0.0001	0.1334	1.0000	
Phase 4	0.3164	0.0251	0.0067	1.0000

Table 2.19: HRV1 Statistical T-test results for ME-1 and ME-2for P03

P06 - ME-1 - HRV1				
H	Phase 1	Phase 2	Phase 3	Phase 4
Phase 1	0			
Phase 2	1	0		
Phase 3	1	1	0	
Phase 4	1	0	1	0
p values	Phase 1	Phase 2	Phase 3	Phase 4
Phase 1	1.0000			
Phase 2	0.0000	1.0000		
Phase 3	0.0000	0.0000	1.0000	
Phase 4	0.0000	0.9308	0.0000	1.0000

P06 - ME-1 - HRV1				
H	Phase 2	Phase 3	Phase 1	Phase 4
Phase 2	0			
Phase 3	1	0		
Phase 1	1	1	0	
Phase 4	1	1	1	0
p values	Phase 2	Phase 3	Phase 1	Phase 4
Phase 2	1.0000			
Phase 3	0.0000	1.0000		
Phase 1	0.0000	0.0000	1.0000	
Phase 4	0.0000	0.0000	0.0029	1.0000

Table 2.20: HRV1 Statistical T-test results for ME-1 and ME-2 for P06

P07 - ME-1 - HRV1				
H	Phase 1	Phase 2	Phase 3	Phase 4
Phase 1	0			
Phase 2	1	0		
Phase 3	1	1	0	
Phase 4	1	1	0	0
p values	Phase 1	Phase 2	Phase 3	Phase 4
Phase 1	1.0000			
Phase 2	0.0000	1.0000		
Phase 3	0.0000	0.0000	1.0000	
Phase 4	0.0000	0.0000	0.8875	1.0000

P07 - ME-2 - HRV1				
H	Phase 2	Phase 3	Phase 1	Phase 4
Phase 2	0			
Phase 3	1	0		
Phase 1	1	1	0	
Phase 4	1	1	1	0
p values	Phase 2	Phase 3	Phase 1	Phase 4
Phase 2	1.0000			
Phase 3	0.0000	1.0000		
Phase 1	0.0000	0.0000	1.0000	
Phase 4	0.0000	0.0000	0.0000	1.0000

Table 2.21: HRV1 Statistical T-test results for ME-1 and ME-2 for P07

P08 - ME-1 - HRV1				
H	Phase 1	Phase 2	Phase 3	Phase 4
Phase 1	0			
Phase 2	1	0		
Phase 3	1	1	0	
Phase 4	1	1	0	0
p values	Phase 1	Phase 2	Phase 3	Phase 4
Phase 1	1.0000			
Phase 2	0.0000	1.0000		
Phase 3	0.0000	0.0000	1.0000	
Phase 4	0.0000	0.0000	0.1477	1.0000

P08 - ME-1(2) - HRV1				
H	Phase 1	Phase 2	Phase 3	Phase 4
Phase 1	0			
Phase 2	1	0		
Phase 3	1	1	0	
Phase 4	1	0	1	0
p values	Phase 1	Phase 2	Phase 3	Phase 4
Phase 1	1.0000			
Phase 2	0.0000	1.0000		
Phase 3	0.0000	0.0000	1.0000	
Phase 4	0.0000	0.3241	0.0000	1.0000

Table 2.22: HRV1 Statistical T-test results for ME-1 for P08. *only ME-1 was performed for this participant.

P09 - ME-1 - HRV1				
H	Phase 1	Phase 2	Phase 3	Phase 4
Phase 1	0			
Phase 2	1	0		
Phase 3	1	1	0	
Phase 4	1	0	1	0
p values	Phase 1	Phase 2	Phase 3	Phase 4
Phase 1	1.0000			
Phase 2	0.0009	1.0000		
Phase 3	0.0000	0.0031	1.0000	
Phase 4	0.0026	0.6608	0.0007	1.0000

P09 - ME-2 - HRV1				
H	Phase 2	Phase 3	Phase 1	Phase 4
Phase 2	0			
Phase 3	0	0		
Phase 1	1	1	0	
Phase 4	1	1	0	0
p values	Phase 2	Phase 3	Phase 1	Phase 4
Phase 2	1.0000			
Phase 3	0.6838	1.0000		
Phase 1	0.0000	0.0000	1.0000	
Phase 4	0.0000	0.0000	0.3728	1.0000

Table 2.23: HRV1 Statistical T-test results for ME-1 and ME-2for P09

P10 - ME-1 - HRV1				
H	Phase 1	Phase 2	Phase 3	Phase 4
Phase 1	0			
Phase 2	1	0		
Phase 3	1	1	0	
Phase 4	1	1	0	0
p values	Phase 1	Phase 2	Phase 3	Phase 4
Phase 1	1.0000			
Phase 2	0.0001	1.0000		
Phase 3	0.0000	0.0000	1.0000	
Phase 4	0.0000	0.0000	0.7044	1.0000

P10 - ME-2 - HRV1				
H	Phase 2	Phase 3	Phase 1	Phase 4
Phase 2	0			
Phase 3	1	0		
Phase 1	1	1	0	
Phase 4	1	1	1	0
p values	Phase 2	Phase 3	Phase 1	Phase 4
Phase 2	1.0000			
Phase 3	0.0000	1.0000		
Phase 1	0.0000	0.0000	1.0000	
Phase 4	0.0000	0.0318	0.0000	1.0000

Table 2.24: HRV1 Statistical T-test results for ME-1 and ME-2 for P10

P11 - ME-1 - HRV1				
H	Phase 1	Phase 2	Phase 3	Phase 4
Phase 1	0			
Phase 2	1	0		
Phase 3	1	1	0	
Phase 4	1	1	1	0
p values	Phase 1	Phase 2	Phase 3	Phase 4
Phase 1	1.0000			
Phase 2	0.0000	1.0000		
Phase 3	0.0000	0.0005	1.0000	
Phase 4	0.0000	0.0000	0.0000	1.0000

P11 - ME-2 - HRV1				
H	Phase 2	Phase 3	Phase 1	Phase 4
Phase 2	0			
Phase 3	1	0		
Phase 1	1	0	0	
Phase 4	1	0	0	0
p values	Phase 2	Phase 3	Phase 1	Phase 4
Phase 2	1.0000			
Phase 3	0.0000	1.0000		
Phase 1	0.0000	0.5781	1.0000	
Phase 4	0.0000	0.9598	0.5799	1.0000

Table 2.25: HRV1 Statistical T-test results for ME-1 and ME-2for P11

P12 - ME-1 - HRV1				
H	Phase 1	Phase 2	Phase 3	Phase 4
Phase 1	0			
Phase 2	1	0		
Phase 3	1	1	0	
Phase 4	1	1	1	0
p values	Phase 1	Phase 2	Phase 3	Phase 4
Phase 1	1.0000			
Phase 2	0.0000	1.0000		
Phase 3	0.0317	0.0000	1.0000	
Phase 4	0.0000	0.0000	0.0000	1.0000

P12 - ME-2 - HRV1				
H	Phase 2	Phase 3	Phase 1	Phase 4
Phase 2	0			
Phase 3	1	0		
Phase 1	0	1	0	
Phase 4	1	1	1	0
p values	Phase 2	Phase 3	Phase 1	Phase 4
Phase 2	1.0000			
Phase 3	0.0000	1.0000		
Phase 1	0.5957	0.0000	1.0000	
Phase 4	0.0000	0.0000	0.0000	1.0000

Table 2.26: HRV1 Statistical T-test results for ME-1 and ME-2 for P12

P01 - ME-1 - HRV2				
H	Phase 1	Phase 2	Phase 3	Phase 4
Phase 1	0			
Phase 2	1	0		
Phase 3	1	1	0	
Phase 4	1	1	1	0
p values	Phase 1	Phase 2	Phase 3	Phase 4
Phase 1	1.0000			
Phase 2	0.0000	1.0000		
Phase 3	0.0001	0.0000	1.0000	
Phase 4	0.0073	0.0000	0.0000	1.0000

P01 - ME-2 - HRV2				
H	Phase 2	Phase 3	Phase 1	Phase 4
Phase 2	0			
Phase 3	1	0		
Phase 1	0	1	0	
Phase 4	0	1	0	0
p values	Phase 2	Phase 3	Phase 1	Phase 4
Phase 2	1.0000			
Phase 3	0.0006	1.0000		
Phase 1	0.3746	0.0050	1.0000	
Phase 4	0.9587	0.0002	0.3643	1.0000

Table 2.27: HRV2 Statistical T-test results for ME-1 and ME-2 for P01

P02 - ME-1 - HRV2				
H	Phase 1	Phase 2	Phase 3	Phase 4
Phase 1	0			
Phase 2	1	0		
Phase 3	1	1	0	
Phase 4	1	1	1	0
p values	Phase 1	Phase 2	Phase 3	Phase 4
Phase 1	1.0000			
Phase 2	0.0000	1.0000		
Phase 3	0.0000	0.0000	1.0000	
Phase 4	0.0000	0.0000	0.0000	1.0000

P02 - ME-2 - HRV2				
H	Phase 2	Phase 3	Phase 1	Phase 4
Phase 2	0			
Phase 3	1	0		
Phase 1	1	0	0	
Phase 4	1	1	1	0
p values	Phase 2	Phase 3	Phase 1	Phase 4
Phase 2	1.0000			
Phase 3	0.0000	1.0000		
Phase 1	0.0000	0.1528	1.0000	
Phase 4	0.0000	0.0000	0.0000	1.0000

Table 2.28: HRV2 Statistical T-test results for ME-1 and ME-2 for P02

P03 - ME-1 - HRV2				
H	Phase 1	Phase 2	Phase 3	Phase 4
Phase 1	0			
Phase 2	1	0		
Phase 3	1	0	0	
Phase 4	1	1	1	0
p values	Phase 1	Phase 2	Phase 3	Phase 4
Phase 1	1.0000			
Phase 2	0.0008	1.0000		
Phase 3	0.0000	0.1601	1.0000	
Phase 4	0.0000	0.0026	0.0411	1.0000

P03 - ME-2 - HRV2				
H	Phase 2	Phase 3	Phase 1	Phase 4
Phase 2	0			
Phase 3	1	0		
Phase 1	1	1	0	
Phase 4	0	1	1	0
p values	Phase 2	Phase 3	Phase 1	Phase 4
Phase 2	1.0000			
Phase 3	0.0000	1.0000		
Phase 1	0.0001	0.0015	1.0000	
Phase 4	0.6571	0.0000	0.0000	1.0000

Table 2.29: HRV2 Statistical T-test results for ME-1 and ME-2for P03

P06 - ME-1 - HRV2				
H	Phase 1	Phase 2	Phase 3	Phase 4
Phase 1	0			
Phase 2	1	0		
Phase 3	1	0	0	
Phase 4	0	1	1	0
p values	Phase 1	Phase 2	Phase 3	Phase 4
Phase 1	1.0000			
Phase 2	0.0000	1.0000		
Phase 3	0.0120	0.0744	1.0000	
Phase 4	0.0571	0.0000	0.0000	1.0000

P06 - ME-2 - HRV2				
H	Phase 2	Phase 3	Phase 1	Phase 4
Phase 2	0			
Phase 3	1	0		
Phase 1	1	1	0	
Phase 4	1	0	1	0
p values	Phase 2	Phase 3	Phase 1	Phase 4
Phase 2	1.0000			
Phase 3	0.0327	1.0000		
Phase 1	0.0000	0.0000	1.0000	
Phase 4	0.0097	0.8798	0.0000	1.0000

Table 2.30: HRV2 Statistical T-test results for ME-1 and ME-2 for P06

P07 - ME-1 - HRV2				
H	Phase 1	Phase 2	Phase 3	Phase 4
Phase 1	0			
Phase 2	0	0		
Phase 3	1	1	0	
Phase 4	1	1	1	0
p values	Phase 1	Phase 2	Phase 3	Phase 4
Phase 1	1.0000			
Phase 2	0.7909	1.0000		
Phase 3	0.0000	0.0000	1.0000	
Phase 4	0.0413	0.0007	0.0000	1.0000

P07 - ME-2 - HRV2				
H	Phase 2	Phase 3	Phase 1	Phase 4
Phase 2	0			
Phase 3	0	0		
Phase 1	1	1	0	
Phase 4	1	1	1	0
p values	Phase 2	Phase 3	Phase 1	Phase 4
Phase 2	1.0000			
Phase 3	0.6001	1.0000		
Phase 1	0.0000	0.0000	1.0000	
Phase 4	0.0000	0.0000	0.0000	1.0000

Table 2.31: HRV2 Statistical T-test results for ME-1 and ME-2 for P07

P08 - ME-1 - HRV2				
H	Phase 1	Phase 2	Phase 3	Phase 4
Phase 1	0			
Phase 2	1	0		
Phase 3	1	1	0	
Phase 4	1	1	0	0
p values	Phase 1	Phase 2	Phase 3	Phase 4
Phase 1	1.0000			
Phase 2	0.0065	1.0000		
Phase 3	0.0000	0.0126	1.0000	
Phase 4	0.0000	0.0005	0.0659	1.0000

P08 - ME-1(2) - HRV2				
H	Phase 1	Phase 2	Phase 3	Phase 4
Phase 1	0			
Phase 2	1	0		
Phase 3	1	1	0	
Phase 4	0	1	1	0
p values	Phase 1	Phase 2	Phase 3	Phase 4
Phase 1	1.0000			
Phase 2	0.0000	1.0000		
Phase 3	0.0135	0.0000	1.0000	
Phase 4	0.4379	0.0000	0.0027	1.0000

Table 2.32: HRV2 Statistical T-test results for ME-1 for P08. *only ME-1 was performed for this participant.

P09 - ME-1 - HRV2				
H	Phase 1	Phase 2	Phase 3	Phase 4
Phase 1	0			
Phase 2	1	0		
Phase 3	1	1	0	
Phase 4	1	1	1	0
p values	Phase 1	Phase 2	Phase 3	Phase 4
Phase 1	1.0000			
Phase 2	0.0000	1.0000		
Phase 3	0.0000	0.0043	1.0000	
Phase 4	0.0000	0.0000	0.0001	1.0000

P09 - ME-2 - HRV2				
H	Phase 2	Phase 3	Phase 1	Phase 4
Phase 2	0			
Phase 3	0	0		
Phase 1	1	1	0	
Phase 4	1	1	0	0
p values	Phase 2	Phase 3	Phase 1	Phase 4
Phase 2	1.0000			
Phase 3	0.7705	1.0000		
Phase 1	0.0000	0.0000	1.0000	
Phase 4	0.0038	0.0147	0.0741	1.0000

Table 2.33: HRV2 Statistical T-test results for ME-1 and ME-2for P09

P10 - ME-1 - HRV2				
H	Phase 1	Phase 2	Phase 3	Phase 4
Phase 1	0			
Phase 2	1	0		
Phase 3	0	1	0	
Phase 4	1	1	1	0
p values	Phase 1	Phase 2	Phase 3	Phase 4
Phase 1	1.0000			
Phase 2	0.0002	1.0000		
Phase 3	0.9783	0.0131	1.0000	
Phase 4	0.0000	0.0000	0.0023	1.0000

P10 - ME-2 - HRV2				
H	Phase 2	Phase 3	Phase 1	Phase 4
Phase 2	0			
Phase 3	1	0		
Phase 1	1	1	0	
Phase 4	1	1	0	0
p values	Phase 2	Phase 3	Phase 1	Phase 4
Phase 2	1.0000			
Phase 3	0.0000	1.0000		
Phase 1	0.0000	0.0000	1.0000	
Phase 4	0.0000	0.0000	0.2374	1.0000

Table 2.34: HRV2 Statistical T-test results for ME-1 and ME-2 for P10

P11 - ME-1 - HRV2				
H	Phase 1	Phase 2	Phase 3	Phase 4
Phase 1	0			
Phase 2	1	0		
Phase 3	1	1	0	
Phase 4	1	1	0	0
p values	Phase 1	Phase 2	Phase 3	Phase 4
Phase 1	1.0000			
Phase 2	0.0000	1.0000		
Phase 3	0.0000	0.0004	1.0000	
Phase 4	0.0000	0.0284	0.2343	1.0000

P11 - ME-2 - HRV2				
H	Phase 2	Phase 3	Phase 1	Phase 4
Phase 2	0			
Phase 3	1	0		
Phase 1	1	0	0	
Phase 4	1	0	0	0
p values	Phase 2	Phase 3	Phase 1	Phase 4
Phase 2	1.0000			
Phase 3	0.0000	1.0000		
Phase 1	0.0000	0.5319	1.0000	
Phase 4	0.0000	0.6844	0.8009	1.0000

Table 2.35: HRV2 Statistical T-test results for ME-1 and ME-2for P11

P12 - ME-1 - HRV2				
H	Phase 1	Phase 2	Phase 3	Phase 4
Phase 1	0			
Phase 2	1	0		
Phase 3	1	1	0	
Phase 4	1	1	1	0
p values	Phase 1	Phase 2	Phase 3	Phase 4
Phase 1	1.0000			
Phase 2	0.0000	1.0000		
Phase 3	0.0165	0.0000	1.0000	
Phase 4	0.0000	0.0111	0.0000	1.0000

P12 - ME-2 - HRV2				
H	Phase 2	Phase 3	Phase 1	Phase 4
Phase 2	0			
Phase 3	1	0		
Phase 1	1	1	0	
Phase 4	1	1	1	0
p values	Phase 2	Phase 3	Phase 1	Phase 4
Phase 2	1.0000			
Phase 3	0.0045	1.0000		
Phase 1	0.0000	0.0000	1.0000	
Phase 4	0.0000	0.0000	0.0001	1.0000

Table 2.36: HRV2 Statistical T-test results for ME-1 and ME-2 for P12

P01 - ME-1 - TLI1				
H	Phase 1	Phase 2	Phase 3	Phase 4
Phase 1	0			
Phase 2	0	0		
Phase 3	1	0	0	
Phase 4	1	1	1	0
p values	Phase 1	Phase 2	Phase 3	Phase 4
Phase 1	1.0000			
Phase 2	0.1542	1.0000		
Phase 3	0.0023	0.0762	1.0000	
Phase 4	0.0000	0.0000	0.0000	1.0000

P01 - ME-2 - TLI1				
H	Phase 2	Phase 3	Phase 1	Phase 4
Phase 2	0			
Phase 3	1	0		
Phase 1	1	1	0	
Phase 4	1	1	1	0
p values	Phase 2	Phase 3	Phase 1	Phase 4
Phase 2	1.0000			
Phase 3	0.0000	1.0000		
Phase 1	0.0000	0.0000	1.0000	
Phase 4	0.0000	0.0000	0.0000	1.0000

Table 2.37: TLI1 Statistical T-test results for ME-1 and ME-2 for P01

P02 - ME-1 - TLI1				
H	Phase 1	Phase 2	Phase 3	Phase 4
Phase 1	0			
Phase 2	1	0		
Phase 3	1	1	0	
Phase 4	1	1	0	0
p values	Phase 1	Phase 2	Phase 3	Phase 4
Phase 1	1.0000			
Phase 2	0.0000	1.0000		
Phase 3	0.0000	0.0065	1.0000	
Phase 4	0.0000	0.0411	0.5524	1.0000

P02 - ME-2 - TLI1				
H	Phase 2	Phase 3	Phase 1	Phase 4
Phase 2	0			
Phase 3	0	0		
Phase 1	0	0	0	
Phase 4	1	1	1	0
p values	Phase 2	Phase 3	Phase 1	Phase 4
Phase 2	1.0000			
Phase 3	0.2831	1.0000		
Phase 1	0.3727	0.1042	1.0000	
Phase 4	0.0000	0.0000	0.0000	1.0000

Table 2.38: TLI1 Statistical T-test results for ME-1 and ME-2 for P02

P03 - ME-1 - TLI1				
H	Phase 1	Phase 2	Phase 3	Phase 4
Phase 1	0			
Phase 2	1	0		
Phase 3	1	1	0	
Phase 4	1	0	1	0
p values	Phase 1	Phase 2	Phase 3	Phase 4
Phase 1	1.0000			
Phase 2	0.0000	1.0000		
Phase 3	0.0000	0.0000	1.0000	
Phase 4	0.0000	0.6849	0.0000	1.0000

P03 - ME-2 - TLI1				
H	Phase 2	Phase 3	Phase 1	Phase 4
Phase 2	0			
Phase 3	1	0		
Phase 1	1	1	0	
Phase 4	1	1	1	0
p values	Phase 2	Phase 3	Phase 1	Phase 4
Phase 2	1.0000			
Phase 3	0.0000	1.0000		
Phase 1	0.0000	0.0000	1.0000	
Phase 4	0.0000	0.0000	0.0000	1.0000

Table 2.39: TLI1 Statistical T-test results for ME-1 and ME-2 for P03

P06 - ME-1 - TLI1				
H	Phase 1	Phase 2	Phase 3	Phase 4
Phase 1	0			
Phase 2	1	0		
Phase 3	0	1	0	
Phase 4	1	1	1	0
p values	Phase 1	Phase 2	Phase 3	Phase 4
Phase 1	1.0000			
Phase 2	0.0000	1.0000		
Phase 3	0.2474	0.0000	1.0000	
Phase 4	0.0000	0.0000	0.0000	1.0000

P06 - ME-2 - TLI1				
H	Phase 2	Phase 3	Phase 1	Phase 4
Phase 2	0			
Phase 3	1	0		
Phase 1	1	1	0	
Phase 4	1	1	1	0
p values	Phase 2	Phase 3	Phase 1	Phase 4
Phase 2	1.0000			
Phase 3	0.0000	1.0000		
Phase 1	0.0000	0.0000	1.0000	
Phase 4	0.0348	0.0000	0.0087	1.0000

Table 2.40: TLI1 Statistical T-test results for ME-1 and ME-2 for P06

P07 - ME-1 - TLI1				
H	Phase 1	Phase 2	Phase 3	Phase 4
Phase 1	0			
Phase 2	1	0		
Phase 3	0	1	0	
Phase 4	1	1	1	0
p values	Phase 1	Phase 2	Phase 3	Phase 4
Phase 1	1.0000			
Phase 2	0.0000	1.0000		
Phase 3	0.1846	0.0000	1.0000	
Phase 4	0.0278	0.0000	0.4529	1.0000

P07 - ME-2 - TLI1				
H	Phase 2	Phase 3	Phase 1	Phase 4
Phase 2	0			
Phase 3	1	0		
Phase 1	1	0	0	
Phase 4	1	1	1	0
p values	Phase 2	Phase 3	Phase 1	Phase 4
Phase 2	1.0000			
Phase 3	0.0000	1.0000		
Phase 1	0.0000	0.9421	1.0000	
Phase 4	0.0017	0.0000	0.0000	1.0000

Table 2.41: TLI1 Statistical T-test results for ME-1 and ME-2 for P07

P08 - ME-1 - TLI1				
H	Phase 1	Phase 2	Phase 3	Phase 4
Phase 1	0			
Phase 2	1	0		
Phase 3	1	1	0	
Phase 4	0	1	1	0
p values	Phase 1	Phase 2	Phase 3	Phase 4
Phase 1	1.0000			
Phase 2	0.0000	1.0000		
Phase 3	0.0000	0.0054	1.0000	
Phase 4	0.3296	0.0000	0.0000	1.0000

P08 - ME-1(2) - TLI1				
H	Phase 1	Phase 2	Phase 3	Phase 4
Phase 1	0			
Phase 2	1	0		
Phase 3	1	1	0	
Phase 4	1	1	1	0
p values	Phase 1	Phase 2	Phase 3	Phase 4
Phase 1	1.0000			
Phase 2	0.0411	1.0000		
Phase 3	0.0000	0.0000	1.0000	
Phase 4	0.0000	0.0125	0.0015	1.0000

Table 2.42: TLI1 Statistical T-test results for ME-1 for P08. *only ME-1 was performed for this participant.

P09 - ME-1 - TLI1				
H	Phase 1	Phase 2	Phase 3	Phase 4
Phase 1	0			
Phase 2	1	0		
Phase 3	1	1	0	
Phase 4	1	1	0	0
p values	Phase 1	Phase 2	Phase 3	Phase 4
Phase 1	1.0000			
Phase 2	0.0143	1.0000		
Phase 3	0.0000	0.0189	1.0000	
Phase 4	0.0000	0.0005	0.3120	1.0000

P09 - ME-2 - TLI1				
H	Phase 2	Phase 3	Phase 1	Phase 4
Phase 2	0			
Phase 3	1	0		
Phase 1	1	1	0	
Phase 4	0	1	1	0
p values	Phase 2	Phase 3	Phase 1	Phase 4
Phase 2	1.0000			
Phase 3	0.0000	1.0000		
Phase 1	0.0000	0.0000	1.0000	
Phase 4	0.4468	0.0000	0.0000	1.0000

Table 2.43: TLI1 Statistical T-test results for ME-1 and ME-2 for P09

P10 - ME-1 - TLI1				
H	Phase 1	Phase 2	Phase 3	Phase 4
Phase 1	0			
Phase 2	1	0		
Phase 3	1	1	0	
Phase 4	0	1	1	0
p values	Phase 1	Phase 2	Phase 3	Phase 4
Phase 1	1.0000			
Phase 2	0.0000	1.0000		
Phase 3	0.0000	0.0000	1.0000	
Phase 4	0.1611	0.0000	0.0002	1.0000

P10 - ME-2 - TLI1				
H	Phase 2	Phase 3	Phase 1	Phase 4
Phase 2	0			
Phase 3	1	0		
Phase 1	1	1	0	
Phase 4	1	1	1	0
p values	Phase 2	Phase 3	Phase 1	Phase 4
Phase 2	1.0000			
Phase 3	0.0000	1.0000		
Phase 1	0.0000	0.0000	1.0000	
Phase 4	0.0000	0.0000	0.0000	1.0000

Table 2.44: TLI1 Statistical T-test results for ME-1 and ME-2 for P10

P11 - ME-1 - TLI1				
H	Phase 1	Phase 2	Phase 3	Phase 4
Phase 1	0			
Phase 2	1	0		
Phase 3	0	1	0	
Phase 4	1	1	1	0
p values	Phase 1	Phase 2	Phase 3	Phase 4
Phase 1	1.0000			
Phase 2	0.0002	1.0000		
Phase 3	0.8161	0.0010	1.0000	
Phase 4	0.0000	0.0000	0.0000	1.0000

P11 - ME-2 - TLI1				
H	Phase 2	Phase 3	Phase 1	Phase 4
Phase 2	0			
Phase 3	0	0		
Phase 1	0	0	0	
Phase 4	1	1	1	0
p values	Phase 2	Phase 3	Phase 1	Phase 4
Phase 2	1.0000			
Phase 3	0.0569	1.0000		
Phase 1	0.8765	0.1308	1.0000	
Phase 4	0.0000	0.0076	0.0002	1.0000

Table 2.45: TLI1 Statistical T-test results for ME-1 and ME-2 for P11

P12 - ME-1 - TLI1				
H	Phase 1	Phase 2	Phase 3	Phase 4
Phase 1	0			
Phase 2	1	0		
Phase 3	1	1	0	
Phase 4	1	1	1	0
p values	Phase 1	Phase 2	Phase 3	Phase 4
Phase 1	1.0000			
Phase 2	0.0000	1.0000		
Phase 3	0.0000	0.0002	1.0000	
Phase 4	0.0000	0.0000	0.0000	1.0000

P12 - ME-2 - TLI1				
H	Phase 2	Phase 3	Phase 1	Phase 4
Phase 2	0			
Phase 3	1	0		
Phase 1	1	1	0	
Phase 4	1	1	1	0
p values	Phase 2	Phase 3	Phase 1	Phase 4
Phase 2	1.0000			
Phase 3	0.0072	1.0000		
Phase 1	0.0000	0.0088	1.0000	
Phase 4	0.0010	0.0000	0.0000	1.0000

Table 2.46: TLI1 Statistical T-test results for ME-1 and ME-2 for P12

P01 - ME-1 - TLI2				
H	Phase 1	Phase 2	Phase 3	Phase 4
Phase 1	0			
Phase 2	0	0		
Phase 3	1	1	0	
Phase 4	1	1	1	0
p values	Phase 1	Phase 2	Phase 3	Phase 4
Phase 1	1.0000			
Phase 2	0.1283	1.0000		
Phase 3	0.0000	0.0037	1.0000	
Phase 4	0.0000	0.0000	0.0000	1.0000

P01 - ME-2 - TLI2				
H	Phase 2	Phase 3	Phase 1	Phase 4
Phase 2	0			
Phase 3	1	0		
Phase 1	1	1	0	
Phase 4	1	0	1	0
p values	Phase 2	Phase 3	Phase 1	Phase 4
Phase 2	1.0000			
Phase 3	0.0000	1.0000		
Phase 1	0.0000	0.0000	1.0000	
Phase 4	0.0000	0.6463	0.0000	1.0000

Table 2.47: TLI2 Statistical T-test results for ME-1 and ME-2 for P01

P02 - ME-1 - TLI2				
H	Phase 1	Phase 2	Phase 3	Phase 4
Phase 1	0			
Phase 2	0	0		
Phase 3	0	1	0	
Phase 4	1	1	1	0
p values	Phase 1	Phase 2	Phase 3	Phase 4
Phase 1	1.0000			
Phase 2	0.2001	1.0000		
Phase 3	0.4523	0.0301	1.0000	
Phase 4	0.0001	0.0000	0.0001	1.0000

P02 - ME-2 - TLI2				
H	Phase 2	Phase 3	Phase 1	Phase 4
Phase 2	0			
Phase 3	0	0		
Phase 1	1	1	0	
Phase 4	0	0	1	0
p values	Phase 2	Phase 3	Phase 1	Phase 4
Phase 2	1.0000			
Phase 3	0.5057	1.0000		
Phase 1	0.0000	0.0000	1.0000	
Phase 4	0.5114	0.1443	0.0000	1.0000

Table 2.48: TLI2 Statistical T-test results for ME-1 and ME-2 for P02

P03 - ME-1 - TLI2				
H	Phase 1	Phase 2	Phase 3	Phase 4
Phase 1	0			
Phase 2	1	0		
Phase 3	1	1	0	
Phase 4	1	0	1	0
p values	Phase 1	Phase 2	Phase 3	Phase 4
Phase 1	1.0000			
Phase 2	0.0000	1.0000		
Phase 3	0.0000	0.0006	1.0000	
Phase 4	0.0000	0.4667	0.0000	1.0000

P03 - ME-2 - TLI2				
H	Phase 2	Phase 3	Phase 1	Phase 4
Phase 2	0			
Phase 3	0	0		
Phase 1	1	1	0	
Phase 4	1	1	1	0
p values	Phase 2	Phase 3	Phase 1	Phase 4
Phase 2	1.0000			
Phase 3	0.3373	1.0000		
Phase 1	0.0000	0.0000	1.0000	
Phase 4	0.0000	0.0000	0.0000	1.0000

Table 2.49: TLI2 Statistical T-test results for ME-1 and ME-2 for P03

P06 - ME-1 - TLI2				
H	Phase 1	Phase 2	Phase 3	Phase 4
Phase 1	0			
Phase 2	1	0		
Phase 3	1	1	0	
Phase 4	1	1	1	0
p values	Phase 1	Phase 2	Phase 3	Phase 4
Phase 1	1.0000			
Phase 2	0.0099	1.0000		
Phase 3	0.0000	0.0000	1.0000	
Phase 4	0.0000	0.0000	0.0000	1.0000

P06 - ME-2 - TLI2				
H	Phase 2	Phase 3	Phase 1	Phase 4
Phase 2	0			
Phase 3	1	0		
Phase 1	1	1	0	
Phase 4	1	1	1	0
p values	Phase 2	Phase 3	Phase 1	Phase 4
Phase 2	1.0000			
Phase 3	0.0000	1.0000		
Phase 1	0.0000	0.0000	1.0000	
Phase 4	0.0361	0.0000	0.0000	1.0000

Table 2.50: TLI2 Statistical T-test results for ME-1 and ME-2 for P06

P07 - ME-1 - TLI2				
H	Phase 1	Phase 2	Phase 3	Phase 4
Phase 1	0			
Phase 2	1	0		
Phase 3	0	1	0	
Phase 4	1	1	1	0
p values	Phase 1	Phase 2	Phase 3	Phase 4
Phase 1	1.0000			
Phase 2	0.0000	1.0000		
Phase 3	0.6334	0.0000	1.0000	
Phase 4	0.0033	0.0000	0.0000	1.0000

P07 - ME-2 - TLI2				
H	Phase 2	Phase 3	Phase 1	Phase 4
Phase 2	0			
Phase 3	1	0		
Phase 1	1	1	0	
Phase 4	1	1	1	0
p values	Phase 2	Phase 3	Phase 1	Phase 4
Phase 2	1.0000			
Phase 3	0.0000	1.0000		
Phase 1	0.0000	0.0000	1.0000	
Phase 4	0.0219	0.0000	0.0000	1.0000

Table 2.51: TLI2 Statistical T-test results for ME-1 and ME-2 for P07

P08 - ME-1 - TLI2				
H	Phase 1	Phase 2	Phase 3	Phase 4
Phase 1	0			
Phase 2	1	0		
Phase 3	0	1	0	
Phase 4	1	1	1	0
p values	Phase 1	Phase 2	Phase 3	Phase 4
Phase 1	1.0000			
Phase 2	0.0000	1.0000		
Phase 3	0.1928	0.0000	1.0000	
Phase 4	0.0000	0.0000	0.0000	1.0000

P08 - ME-1(2) - TLI2				
H	Phase 1	Phase 2	Phase 3	Phase 4
Phase 1	0			
Phase 2	0	0		
Phase 3	1	1	0	
Phase 4	1	1	1	0
p values	Phase 1	Phase 2	Phase 3	Phase 4
Phase 1	1.0000			
Phase 2	0.4388	1.0000		
Phase 3	0.0000	0.0000	1.0000	
Phase 4	0.0000	0.0000	0.0000	1.0000

Table 2.52: TLI2 Statistical T-test results for ME-1 for P08. *only ME-1 was performed for this participant.

P09 - ME-1 - TLI2				
H	Phase 1	Phase 2	Phase 3	Phase 4
Phase 1	0			
Phase 2	1	0		
Phase 3	1	0	0	
Phase 4	1	0	0	0
p values	Phase 1	Phase 2	Phase 3	Phase 4
Phase 1	1.0000			
Phase 2	0.0321	1.0000		
Phase 3	0.0072	0.4705	1.0000	
Phase 4	0.0001	0.1019	0.4438	1.0000

P09 - ME-2 - TLI2				
H	Phase 2	Phase 3	Phase 1	Phase 4
Phase 2	0			
Phase 3	1	0		
Phase 1	1	1	0	
Phase 4	1	1	1	0
p values	Phase 2	Phase 3	Phase 1	Phase 4
Phase 2	1.0000			
Phase 3	0.0000	1.0000		
Phase 1	0.0000	0.0000	1.0000	
Phase 4	0.0000	0.0000	0.0006	1.0000

Table 2.53: TLI2 Statistical T-test results for ME-1 and ME-2 for P09

P10 - ME-1 - TLI2				
H	Phase 1	Phase 2	Phase 3	Phase 4
Phase 1	0			
Phase 2	1	0		
Phase 3	1	1	0	
Phase 4	1	1	1	0
p values	Phase 1	Phase 2	Phase 3	Phase 4
Phase 1	1.0000			
Phase 2	0.0000	1.0000		
Phase 3	0.0000	0.0000	1.0000	
Phase 4	0.0000	0.0000	0.0487	1.0000

P10 - ME-2 - TLI2				
H	Phase 2	Phase 3	Phase 1	Phase 4
Phase 2	0			
Phase 3	1	0		
Phase 1	1	1	0	
Phase 4	1	1	1	0
p values	Phase 2	Phase 3	Phase 1	Phase 4
Phase 2	1.0000			
Phase 3	0.0000	1.0000		
Phase 1	0.0000	0.0000	1.0000	
Phase 4	0.0000	0.0000	0.0000	1.0000

Table 2.54: TLI2 Statistical T-test results for ME-1 and ME-2 for P10

P11 - ME-1 - TLI2				
H	Phase 1	Phase 2	Phase 3	Phase 4
Phase 1	0			
Phase 2	0	0		
Phase 3	1	1	0	
Phase 4	1	0	1	0
p values	Phase 1	Phase 2	Phase 3	Phase 4
Phase 1	1.0000			
Phase 2	0.2295	1.0000		
Phase 3	0.0000	0.0000	1.0000	
Phase 4	0.0006	0.3404	0.0000	1.0000

P11 - ME-2 - TLI2				
H	Phase 2	Phase 3	Phase 1	Phase 4
Phase 2	0			
Phase 3	0	0		
Phase 1	1	1	0	
Phase 4	0	0	1	0
p values	Phase 2	Phase 3	Phase 1	Phase 4
Phase 2	1.0000			
Phase 3	0.0835	1.0000		
Phase 1	0.0000	0.0000	1.0000	
Phase 4	0.5522	0.7692	0.0014	1.0000

Table 2.55: TLI2 Statistical T-test results for ME-1 and ME-2 for P11

P12 - ME-1 - TLI2				
H	Phase 1	Phase 2	Phase 3	Phase 4
Phase 1	0			
Phase 2	1	0		
Phase 3	1	0	0	
Phase 4	1	1	1	0
p values	Phase 1	Phase 2	Phase 3	Phase 4
Phase 1	1.0000			
Phase 2	0.0000	1.0000		
Phase 3	0.0000	0.5428	1.0000	
Phase 4	0.0000	0.0000	0.0000	1.0000

P12 - ME-2 - TLI2				
H	Phase 2	Phase 3	Phase 1	Phase 4
Phase 2	0			
Phase 3	1	0		
Phase 1	1	0	0	
Phase 4	0	1	1	0
p values	Phase 2	Phase 3	Phase 1	Phase 4
Phase 2	1.0000			
Phase 3	0.0000	1.0000		
Phase 1	0.0000	0.0939	1.0000	
Phase 4	0.4378	0.0001	0.0027	1.0000

Table 2.56: TLI2 Statistical T-test results for ME-1 and ME-2 for P12

From these results it can be concluded that a best marker cannot be identified since most respond in an average fashion across all participants. However, for some specific cases, one of the markers may lead to more information about the cognitive state of the participant it is acquired from. It is worth noting that these characteristics address the importance of using a pool of markers for the detection of mental stress, since these respond differently depending on the participant under study.

In Tables 2.57 through 2.66 the results for the AP are found. It can be concluded from these results that the MA experiment is able to cognitively impair the participants in the study. This can be observed from the fact that for the majority of the cases, the AP data vectors present significant differences demonstrating that the participants are affected by the change in DL. There are some issues related

to statistically indistinguishable adjacent DL phases, specially between phase 1 and 2. This may be attributed to the fact that for some participants phase 1 and 2 are equally difficult since their only difference resides in the amount of time given to produce a response.

P01 - ME-1 - AP				
H	Phase 1	Phase 2	Phase 3	Phase 4
Phase 1	0			
Phase 2	1	0		
Phase 3	1	1	0	
Phase 4	1	1	1	0
p values	Phase 1	Phase 2	Phase 3	Phase 4
Phase 1	1.0000			
Phase 2	0.0000	1.0000		
Phase 3	0.0000	0.0000	1.0000	
Phase 4	0.0000	0.0000	0.0000	1.0000

P01 - ME-2 - AP				
H	Phase 2	Phase 3	Phase 1	Phase 4
Phase 2	0			
Phase 3	1	0		
Phase 1	1	1	0	
Phase 4	1	1	1	0
p values	Phase 2	Phase 3	Phase 1	Phase 4
Phase 2	1.0000			
Phase 3	0.0000	1.0000		
Phase 1	0.0000	0.0000	1.0000	
Phase 4	0.0000	0.0000	0.0000	1.0000

Table 2.57: AP Statistical T-test results for ME-1 and ME-2 for P01

P02 - ME-1 - AP				
H	Phase 1	Phase 2	Phase 3	Phase 4
Phase 1	0			
Phase 2	0	0		
Phase 3	1	1	0	
Phase 4	1	1	1	0
p values	Phase 1	Phase 2	Phase 3	Phase 4
Phase 1	1.0000			
Phase 2	0.4913	1.0000		
Phase 3	0.0000	0.0000	1.0000	
Phase 4	0.0000	0.0000	0.0000	1.0000

P02 - ME-2 - AP				
H	Phase 2	Phase 3	Phase 1	Phase 4
Phase 2	0			
Phase 3	1	0		
Phase 1	1	1	0	
Phase 4	1	1	1	0
p values	Phase 2	Phase 3	Phase 1	Phase 4
Phase 2	1.0000			
Phase 3	0.0000	1.0000		
Phase 1	0.0000	0.0000	1.0000	
Phase 4	0.0000	0.0000	0.0000	1.0000

Table 2.58: AP Statistical T-test results for ME-1 and ME-2 for P02

P03 - ME-1 - AP				
H	Phase 1	Phase 2	Phase 3	Phase 4
Phase 1	0			
Phase 2	0	0		
Phase 3	1	0	0	
Phase 4	1	1	1	0
p values	Phase 1	Phase 2	Phase 3	Phase 4
Phase 1	1.0000			
Phase 2	0.0947	1.0000		
Phase 3	0.0027	0.2026	1.0000	
Phase 4	0.0000	0.0000	0.0000	1.0000

P03 - ME-2 - AP				
H	Phase 2	Phase 3	Phase 1	Phase 4
Phase 2	0			
Phase 3	1	0		
Phase 1	1	1	0	
Phase 4	1	1	1	0
p values	Phase 2	Phase 3	Phase 1	Phase 4
Phase 2	1.0000			
Phase 3	0.0000	1.0000		
Phase 1	0.0000	0.0000	1.0000	
Phase 4	0.0000	0.0000	0.0000	1.0000

Table 2.59: AP Statistical T-test results for ME-1 and ME-2 for P03

P06 - ME-1 - AP				
H	Phase 1	Phase 2	Phase 3	Phase 4
Phase 1	0			
Phase 2	1	0		
Phase 3	1	1	0	
Phase 4	1	1	1	0
p values	Phase 1	Phase 2	Phase 3	Phase 4
Phase 1	1.0000			
Phase 2	0.0003	1.0000		
Phase 3	0.0000	0.0000	1.0000	
Phase 4	0.0000	0.0000	0.0000	1.0000

P06 - ME-2 - AP				
H	Phase 2	Phase 3	Phase 1	Phase 4
Phase 2	0			
Phase 3	1	0		
Phase 1	0	1	0	
Phase 4	1	1	1	0
p values	Phase 2	Phase 3	Phase 1	Phase 4
Phase 2	1.0000			
Phase 3	0.0000	1.0000		
Phase 1	0.3630	0.0000	1.0000	
Phase 4	0.0000	0.0000	0.0000	1.0000

Table 2.60: AP Statistical T-test results for ME-1 and ME-2 for P06

P07 - ME-1 - AP				
H	Phase 1	Phase 2	Phase 3	Phase 4
Phase 1	0			
Phase 2	0	0		
Phase 3	1	1	0	
Phase 4	1	1	1	0
p values	Phase 1	Phase 2	Phase 3	Phase 4
Phase 1	1.0000			
Phase 2	0.4906	1.0000		
Phase 3	0.0000	0.0000	1.0000	
Phase 4	0.0000	0.0000	0.0000	1.0000

P07 - ME-2 - AP				
H	Phase 2	Phase 3	Phase 1	Phase 4
Phase 2	0			
Phase 3	1	0		
Phase 1	1	1	0	
Phase 4	1	1	1	0
p values	Phase 2	Phase 3	Phase 1	Phase 4
Phase 2	1.0000			
Phase 3	0.0000	1.0000		
Phase 1	0.0000	0.0000	1.0000	
Phase 4	0.0000	0.0000	0.0000	1.0000

Table 2.61: AP Statistical T-test results for ME-1 and ME-2 for P07

P08 - ME-1 - AP				
H	Phase 1	Phase 2	Phase 3	Phase 4
Phase 1	0			
Phase 2	1	0		
Phase 3	1	1	0	
Phase 4	1	1	1	0
p values	Phase 1	Phase 2	Phase 3	Phase 4
Phase 1	1.0000			
Phase 2	0.0278	1.0000		
Phase 3	0.0000	0.0000	1.0000	
Phase 4	0.0000	0.0000	0.0000	1.0000

P08 - ME-2 - AP				
H	Phase 1	Phase 2	Phase 3	Phase 4
Phase 1	0			
Phase 2	1	0		
Phase 3	1	1	0	
Phase 4	1	1	1	0
p values	Phase 1	Phase 2	Phase 3	Phase 4
Phase 1	1.0000			
Phase 2	0.0000	1.0000		
Phase 3	0.0000	0.0000	1.0000	
Phase 4	0.0000	0.0000	0.0000	1.0000

Table 2.62: AP Statistical T-test results for ME-1 for P08. *only ME-1 was performed for this participant.

P09 - ME-1 - AP				
H	Phase 1	Phase 2	Phase 3	Phase 4
Phase 1	0			
Phase 2	1	0		
Phase 3	1	1	0	
Phase 4	1	1	1	0
p values	Phase 1	Phase 2	Phase 3	Phase 4
Phase 1	1.0000			
Phase 2	0.0000	1.0000		
Phase 3	0.0000	0.0000	1.0000	
Phase 4	0.0000	0.0000	0.0000	1.0000

P09 - ME-2 - AP				
H	Phase 2	Phase 3	Phase 1	Phase 4
Phase 2	0			
Phase 3	1	0		
Phase 1	1	1	0	
Phase 4	1	1	1	0
p values	Phase 2	Phase 3	Phase 1	Phase 4
Phase 2	1.0000			
Phase 3	0.0000	1.0000		
Phase 1	0.0000	0.0000	1.0000	
Phase 4	0.0000	0.0000	0.0000	1.0000

Table 2.63: AP Statistical T-test results for ME-1 and ME-2 for P09

P10 - ME-1 - AP				
H	Phase 1	Phase 2	Phase 3	Phase 4
Phase 1	0			
Phase 2	1	0		
Phase 3	1	1	0	
Phase 4	1	1	1	0
p values	Phase 1	Phase 2	Phase 3	Phase 4
Phase 1	1.0000			
Phase 2	0.0000	1.0000		
Phase 3	0.0000	0.0000	1.0000	
Phase 4	0.0000	0.0000	0.0000	1.0000

P10 - ME-2 - AP				
H	Phase 2	Phase 3	Phase 1	Phase 4
Phase 2	0			
Phase 3	1	0		
Phase 1	1	0	0	
Phase 4	1	1	1	0
p values	Phase 2	Phase 3	Phase 1	Phase 4
Phase 2	1.0000			
Phase 3	0.0000	1.0000		
Phase 1	0.0000	0.5870	1.0000	
Phase 4	0.0000	0.0000	0.0000	1.0000

Table 2.64: AP Statistical T-test results for ME-1 and ME-2 for P10

P11 - ME-1 - AP				
H	Phase 1	Phase 2	Phase 3	Phase 4
Phase 1	0			
Phase 2	1	0		
Phase 3	1	1	0	
Phase 4	1	1	1	0
p values	Phase 1	Phase 2	Phase 3	Phase 4
Phase 1	1.0000			
Phase 2	0.0000	1.0000		
Phase 3	0.0000	0.0000	1.0000	
Phase 4	0.0000	0.0000	0.0000	1.0000

P11 - ME-2 - AP				
H	Phase 2	Phase 3	Phase 1	Phase 4
Phase 2	0			
Phase 3	1	0		
Phase 1	1	1	0	
Phase 4	1	1	1	0
p values	Phase 2	Phase 3	Phase 1	Phase 4
Phase 2	1.0000			
Phase 3	0.0000	1.0000		
Phase 1	0.0000	0.0000	1.0000	
Phase 4	0.0000	0.0000	0.0000	1.0000

Table 2.65: AP Statistical T-test results for ME-1 and ME-2 for P11

P12 - ME-1 - AP				
H	Phase 1	Phase 2	Phase 3	Phase 4
Phase 1	0			
Phase 2	1	0		
Phase 3	1	1	0	
Phase 4	1	1	1	0
p values	Phase 1	Phase 2	Phase 3	Phase 4
Phase 1	1.0000			
Phase 2	0.0021	1.0000		
Phase 3	0.0000	0.0000	1.0000	
Phase 4	0.0000	0.0000	0.0000	1.0000

P12 - ME-2 - AP				
H	Phase 2	Phase 3	Phase 1	Phase 4
Phase 2	0			
Phase 3	1	0		
Phase 1	1	1	0	
Phase 4	1	1	1	0
p values	Phase 2	Phase 3	Phase 1	Phase 4
Phase 2	1.0000			
Phase 3	0.0000	1.0000		
Phase 1	0.0000	0.0000	1.0000	
Phase 4	0.0000	0.0000	0.0000	1.0000

Table 2.66: AP Statistical T-test results for ME-1 and ME-2 for P12

In order to easily compare the prediction power of all studied markers, additional average Tables are presented in Tables 2.67 through 2.72. In these Tables the average test decision H is presented for ME-1 and ME-2, for all markers (i.e., PDM, HRV1, HRV2, TLI1 and TLI2) as well as for the task performance AP. For a fair comparison,

the Tables corresponding to PDM show the results without the baseline and for the ten participants that continued with the additional experiments (i.e., P01, P02, P03, P06, P07, P08, P09, P10, P11, P12).

PDM - All Participants Average - ME-1				
H	Phase 1	Phase 2	Phase 3	Phase 4
Phase 1	0.0000			
Phase 2	0.7000	0.0000		
Phase 3	0.8000	0.9000	0.0000	
Phase 4	1.0000	0.8000	1.0000	0.0000
Average	0.8667			

PDM - All Participants Average - ME-2				
H	Phase 2	Phase 3	Phase 1	Phase 4
Phase 2	0.0000			
Phase 3	0.8889	0.0000		
Phase 1	0.8889	0.7778	0.0000	
Phase 4	1.0000	1.0000	0.8889	0.0000
Average	0.9074			

Table 2.67: Average PDM Statistical T-test results for ME-1 and ME-2 for all participants (10 participants for ME-1 and 9 participants for ME-2).

HRV1 - All Participants Average - ME-1				
H	Phase 1	Phase 2	Phase 3	Phase 4
Phase 1	0.0000			
Phase 2	1.0000	0.0000		
Phase 3	0.8000	1.0000	0.0000	
Phase 4	1.0000	0.7000	0.7000	0.0000
Average	0.8667			

HRV1 - All Participants Average - ME-2				
H	Phase 2	Phase 3	Phase 1	Phase 4
Phase 2	0.0000			
Phase 3	0.8889	0.0000		
Phase 1	0.8889	0.6667	0.0000	
Phase 4	0.8889	0.7778	0.7778	0.0000
Average	0.8148			

Table 2.68: Average HRV1 Statistical T-test results for ME-1 and ME-2 for all participants (10 participants for ME-1 and 9 participants for ME-2).

HRV2 - All Participants Average - ME-1				
H	Phase 1	Phase 2	Phase 3	Phase 4
Phase 1	0.0000			
Phase 2	0.9000	0.0000		
Phase 3	0.9000	0.8000	0.0000	
Phase 4	0.9000	1.0000	0.8000	0.0000
Average	0.8833			

HRV2 - All Participants Average - ME-2				
H	Phase 2	Phase 3	Phase 1	Phase 4
Phase 2	0.0000			
Phase 3	0.7778	0.0000		
Phase 1	0.8889	0.7778	0.0000	
Phase 4	0.7778	0.7778	0.5556	0.0000
Average	0.7593			

Table 2.69: Average HRV2 Statistical T-test results for ME-1 and ME-2 for all participants (10 participants for ME-1 and 9 participants for ME-2).

TLI1 - All Participants Average - ME-1				
H	Phase 1	Phase 2	Phase 3	Phase 4
Phase 1	0.0000			
Phase 2	0.9000	0.0000		
Phase 3	0.7000	0.9000	0.0000	
Phase 4	0.8000	0.9000	0.8000	0.0000
Average	0.8333			

TLI1 - All Participants Average - ME-2				
H	Phase 2	Phase 3	Phase 1	Phase 4
Phase 2	0.0000			
Phase 3	0.7778	0.0000		
Phase 1	0.7778	0.6667	0.0000	
Phase 4	0.8889	1.0000	1.0000	0.0000
Average	0.8519			

Table 2.70: Average TLI1 Statistical T-test results for ME-1 and ME-2 for all participants (10 participants for ME-1 and 9 participants for ME-2).

TLI2 - All Participants Average - ME-1				
H	Phase 1	Phase 2	Phase 3	Phase 4
Phase 1	0.0000			
Phase 2	0.7000	0.0000		
Phase 3	0.7000	0.8000	0.0000	
Phase 4	1.0000	0.7000	0.9000	0.0000
Average	0.8000			

TLI2 - All Participants Average - ME-2				
H	Phase 2	Phase 3	Phase 1	Phase 4
Phase 2	0.0000			
Phase 3	0.6667	0.0000		
Phase 1	1.0000	0.8889	0.0000	
Phase 4	0.6667	0.6667	1.0000	0.0000
Average	0.8148			

Table 2.71: Average TLI2 Statistical T-test results for ME-1 and ME-2 for all participants (10 participants for ME-1 and 9 participants for ME-2).

AP - All Participants Average - ME-1				
H	Phase 1	Phase 2	Phase 3	Phase 4
Phase 1	0.0000			
Phase 2	0.7000	0.0000		
Phase 3	1.0000	0.9000	0.0000	
Phase 4	1.0000	1.0000	1.0000	0.0000
Average	0.9333			

AP - All Participants Average - ME-2				
H	Phase 2	Phase 3	Phase 1	Phase 4
Phase 2	0.0000			
Phase 3	1.0000	0.0000		
Phase 1	0.8889	0.8889	0.0000	
Phase 4	1.0000	1.0000	1.0000	0.0000
Average	0.9630			

Table 2.72: Average AP Statistical T-test results for ME-1 and ME-2 for all participants (10 participants for ME-1 and 9 participants for ME-2).

From the average Tables presented in Table 2.67 to Table 2.72, similar results are observed. In fact, a close inspection of the average score in each experimental session shows a similar value. It is important to stress the fact that from these results one can conclude that the PDM is as good a marker as the previously validated markers. Additionally, from the average results for AP one can also conclude that the MA operations experiment is very successful in cognitively impairing the participants with statistically different characteristics for every phase. In fact, Table 2.72 presents the highest average scores for both experiment configurations (i.e., ME-1 and ME-2).

2.4 Summary

This Chapter dealt with the experiment design for the exploration of a Human-Machine Interaction (HMI) system. It started by addressing the importance of adequate psychophysiological markers and their utilisation as a means of detecting the affective state of the human inside the HMI system. It highlighted from a thorough

literature review the fact that the most successfully used markers correspond to Heart Rate Variability (HRV) from cardiovascular measurements and to Task Load Index (TLI) from ElectroEncephalografic (EEG) recordings. Additionally, it introduced and validated, through a series of statistical tests, the use of the Pupil Diameter Marker (PDM), based on both eyes. This new marker was validated for its use as an incremental detector of mental stress levels and was also compared with the HRV and TLI markers obtaining similar results, with none of the former being identified as having an improved detection. Their prediction power was identified to be participant-specific, thus confirming the importance of their joint use on every experimental session. With regards to the task to induce mental stress in the participants, MA was selected given the supportive evidence previously found in the literature. Furthermore, its validity was tested through a statistical test to address its effect in producing mental stress identified with participants' reduced performance as the difficulty in the MA experiment increased.

Chapter 3

TYPE 2 FUZZY LOGIC MODELLING OF OPERATOR PERFORMANCE UNDER STRESS

3.1 Introduction

Fuzzy Logic was introduced by Zadeh in 1965 in the shape of Fuzzy Sets (FS) now referred to as Type 1 Fuzzy Sets (T1FS) in order to distinguish them from Type 2 Fuzzy Sets (T2FS). He later introduced T2FS in 1975 making the distinction necessary. T1FS have been used in many applications successfully despite their limited capability of handling uncertainty (understood as their restricted modelling capability for this type of data) [73].

T2FS address the well know phrase: "different words mean different things to different people" by being able of fully model heuristic uncertainty. This is what

is known as linguistic uncertainty. Additionally, one can also think of random uncertainty associated with unpredictability as is studied in probability theory. With the appropriate process, T2FS are able to model this kind of uncertainty as well. A T1FS cannot fully handle uncertainty since it associates one membership value for each input value (i.e., crisp membership grades) ; T2FS however, have grades of membership that are fuzzy, hence a collection of possible memberships can be associated with each input value; this makes T2FS tridimensional in shape.

A T2FS can be constructed with a collection of embedded T1FS (e.g., this would be the case when describing linguistic uncertainty). A T2FS would be reduced to a T1FS when all uncertainty disappears [73].

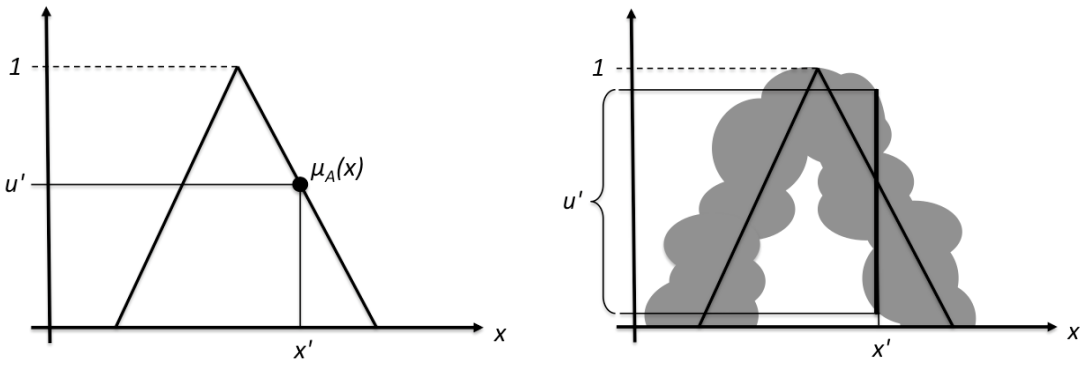

Figure 3.1: Triangular fuzzy membership functions. (a) Triangular Type 1 Membership Function (T1MF) illustrating the membership value $\mu(x)$ of the membership function u' at a specific input x'. (b) Triangular Type 2 Membership Function (T2MF) obtained after blurring a T1MF. This Figure illustrates the membership values $\mu(x, u)$ of the membership function u' at the intersection of x' with the blurred line, exemplifying the tridimensional shape of T2MF. [74]

To better understand what a T2FS is, one needs to refer to the triangular T1FS of Figure 3.1(a) and imagine blurring the line to either side in different amounts as is depicted in Figure 3.1(b). At a specific input value of x, say x', the T1FS of Figure 3.1(a) has a corresponding membership value $\mu(x)$ on its corresponding membership

function u'. Similarly, for the T2FS case of Figure 3.1(b), at x' the membership function u' has no longer a single membership value, but a collection of values where the projection of x' intersects the blur. Additionally, all these intersected values can have different weights, creating a tridimensional membership function [74, 78].

3.2 Definition of a Type 2 Fuzzy Set

A Type 2 Fuzzy Set (T2FS) denoted as $\tilde{A}$, with an associated Membership Function (MF) $\mu_{\tilde{A}}(x,u)$, where $x \in X$, and $u \in J_x$, is defined as follows [74, 78]:

$$\tilde{A} = \{ (x,u),\ \mu_{\tilde{A}}(x,u) \,|\, \forall x \in X,\ \forall u \in J_x \subseteq [0,1] \} \tag{3.1}$$

where $\tilde{A}$ represents a T2FS, $\mu_{\tilde{A}}(x,u)$ is its associated membership function, x is an input value, u is a coordinate space associated to x inside the secondary fuzzy-membership (i.e., a bi-dimensional membership space for each input x). For each combination of (x,u) the type 2 fuzzy membership can take values from 0 to 1. To better understand this membership please refer to Figure 3.2.

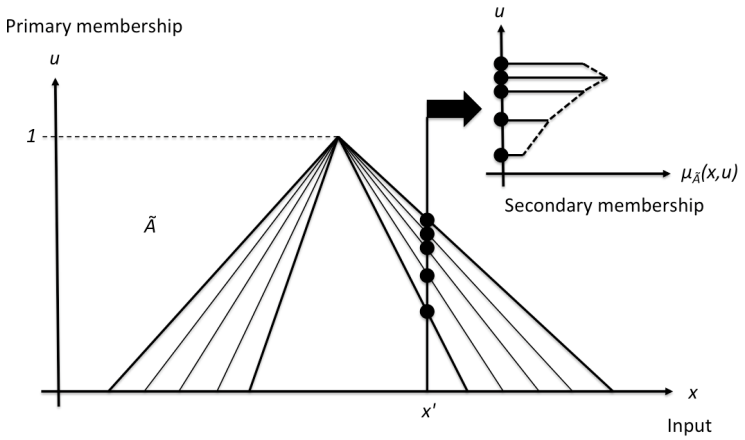

Figure 3.2: Triangular Type 2 Membership Function illustrating the secondary membership $\mu_{\tilde{A}}(x,u)$ at a specific input x'. The figure shows the tridimensional representation at discrete embedded type 1 fuzzy triangular membership functions. [73]

From Figure 3.2 a triangular type 2 fuzzy Membership Function (MF) can be observed. A collection of five embedded Type 1 (T1) MF are shown with solid lines. For an input value of x', discrete values of the primary membership space u are identified with black dots for each of the five T1 MF. On an additional coordinate plane on the upper-right corner, the secondary memberships $\mu_{\tilde{A}}(x, u)$ on the third dimension are shown. This Figure illustrates a discrete example of a type 2 MF, however, as defined by Equation 3.1, a number of infinite embedded T1 MF exist inside the triangular tridimensional MF illustrated.

3.3 Advantages and disadvantages of Type 2 Fuzzy Logic

Type 2 Fuzzy Logic inherits most of the benefits of working with T1FS as follows:

- A formal structure capable of describing complex linear and non-linear systems in the shape IF-THEN rules;
- The ability of interpret its rule-base;
- Its better handling of uncertainty.

However, its basic structure becomes more complex since it now requires an additional step known as the type-reduction process [73]. Additionally, the simple mathematical and numerical inference process of Type 1 Fuzzy Logic suffers from the addition of the extra dimension of T2FS, making it:

- Unsolvable mathematically at the present moment (i.e., there is no closed-form solution);
- Solvable numerically, but very computationally intensive;

- Not as simple to manipulate, understand and depict as T1FS given its extra dimension.

Despite the disadvantages of T2FS mainly introduced in the shape of computationally intensive calculations difficult to implement in real-time, T2FS are advantageous in the sense that they are more interpretable (transparent). This characteristic differentiates them from other techniques that have been used in practice for their application in data-driven modelling approaches such as neural-networks. Neural-network approaches are able to learn from data in a similar way as Fuzzy Systems do (i.e., when equipped with an appropriate learning algorithm). However, the end-model is 'opaque' and as a result may be more difficult to interpret. In contrast, the IF-THEN rule-base of Fuzzy approaches is fully interpretable, since it is designed to imitate the inference process us humans follow.

With regards to the intensive computations problematic, several approaches seek to solve this issue while retaining the advantages of T2FS like in [73, 74, 77, 80, 81]. One of such approaches is know as Interval Type 2 Fuzzy Sets (IT2FS) [73], where a simplification in the secondary membership of T2FS makes these systems able to be applied to real-time applications. In the next Section 3.4, IT2FS were applied to the modelling of participants undergoing mental stress in a simulation-based experiment. Since the introduction of IT2FS and its widespread application, a distinction from a complete T2FS was necessary. With this idea, most authors refer to the original and complete conception of T2FS as General Type 2 Fuzzy Logic Systems (GT2FLS) or General Type 2 Fuzzy Sets (GT2FS).

'Type 2 Fuzzy Systems' is a current and ongoing research area in control systems, with many approaches into the solution of the intensive computations of T2FS being addressed every day. In order to fully engage into this area, it is useful to refer to [73, 74, 75, 78, 79, 80, 81, 82].

3.4 Interval Type 2 Fuzzy Logic modelling and control

3.4.1 Introduction

The application of Fuzzy-based modelling techniques for the detection of operators undergoing cognitive load is not new. In fact, a series of experiments were previously performed in the Human Performance Laboratory at the University of Sheffield back in 2008 and published in [7, 8, 9, 11, 12]. The experiments performed in 2008 [8] consisted in a series mental stress induction experiments in a simulation configuration similar to the one presented in Chapter 2, the main difference relating to the mental stress induction experiment that for this case was based on the automation-enhanced Cabin Air Management System (aCAMS) of Figure 2.3. A series of training and validation (checking) data-sets were gathered for ten participants in that study. Participant-dependent Type 1 Fuzzy Logic models were trained with the aid of Genetic Algorithms (GA). These models contained an expert-designed "hand-crafted" rule-base common to all of them, providing a general logic. This fuzzy rule-base included information relating to the input-output mappings in their known operation ranges, and utilised HRV1 and TLI2 as its inputs. The system output was Time In Range (TIR), a variable related to the participant task performance in aCAMS [8].

The simulation-based results presented in this Section are a continuation of the experiments performed in [8] but with the application of Interval Type 2 Fuzzy Sets (IT2FS) as the modelling technique. This technique was used for modelling with the aid of GA in a similar configuration to the models of [8]. IT2FS were applied with the objective of improving the generalising properties of the participant-dependent models, given its more effective handling of uncertainty over the T1FS case. The

results of this Section were published in [13].

Besides presenting the results of utilising IT2FS for modelling, this Section is also concerned with addressing the shortcomings of this technique when dealing with systems with important parameter variations, in this case derived from the inter- and intra- differences across human participants. This Section will stress the necessity of an adaptive modelling technique, capable of handling uncertainty systematically.

3.4.2 Interval Type 2 Fuzzy Logic

3.4.2.1 Interval vs General Type 2 Fuzzy Logic

Interval Type 2 Fuzzy Sets (IT2FS) are a simplification of General Type 2 Fuzzy Sets (GT2FS). To better understand what this simplification means, it is convenient to first mathematically define IT2FS. An IT2FS denoted as $\tilde{A}_I$, has an associated Membership Function (MF) $\mu_{\tilde{A}}(x,u) = 1$, where $x \in X$, and $u \in J_x$, and is defined as [76]:

$$\tilde{A}_I = \left\{ (x,u),\ \mu_{\tilde{A}_I}(x,u) = 1 \,|\, \forall x \in X,\ \forall u \in J_x \subseteq [0,1] \right\} \tag{3.2}$$

where $\tilde{A}_I$ represents an IT2FS, $\mu_{\tilde{A}_I}(x,u)$ is its associated membership function that is always equal to 1, x is an input value, u is a coordinate space associated to x. The simplification of IT2FS consists in making all secondary memberships equiprobable by assigning to them a value of 1 [76]. This also simplifies their representations, since a tridimensional drawing is no longer necessary [74]. Figure 3.3 shows a discrete representation of a triangular IT2FS in a similar fashion to Figure 3.2 but with the added simplification of IT2FS.

As was previously mentioned, T2FS require an additional step in their inference: the type-reduction. For GT2FS this cannot be done in a mathematical closed form

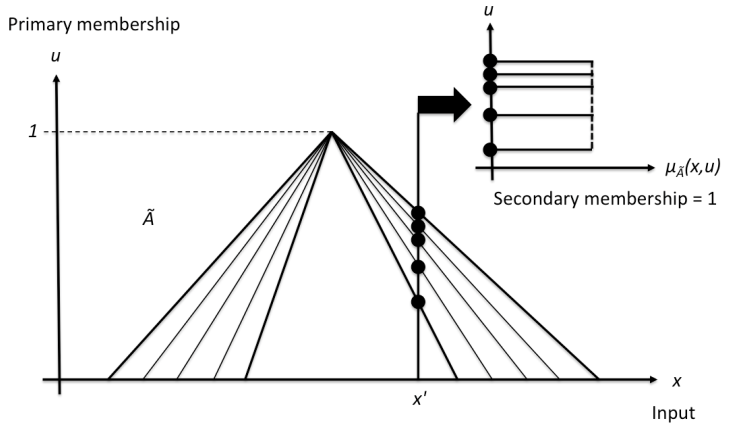

Figure 3.3: Triangular Interval Type 2 Membership Function illustrating the secondary membership simplification $\mu_{\tilde{A}}(x,u) = 1$ at a specific input x'. The figure shows the tridimensional representation at discrete embedded type 1 fuzzy triangular membership functions. [73]

since no solution exists to date, instead, discretisation allows for a computational solution with an associated computational cost. For most real-time applications, the use of GT2FS is problematic because of intensive computations. The simplification introduced with IT2FS retains a reduced handling of uncertainty with the benefit of reducing computational cost to an extent that makes them usable in real-time applications. The type-reduction process in IT2FS is handled with two parallel algorithms known as the Karnik-Mendel (KM) algorithms, that allow fast and simple computations [73]. Furthermore, other approaches into improving the speed of the KM algorithms exist. For the models constructed for this Section one of such approaches is used, the Enhanced Iterative Algorithm with Stop Condition (EIASC) type-reduction algorithm [82].

3.4.3 Interval Type 2 Fuzzy Sets for operator functional modelling

3.4.3.1 Experimental setup

In this Section a brief description of the experimental setup is dealt with. As was previously outlined, the automation-enhanced Cabin Air Management System (aCAMS) simulator of Figure 2.3 was used as a means of providing major mental demands on the operator's mental resources. The description of the experiment sessions performed can be found in more detail in [7, 8, 9, 11, 12, 13].

The experiments consisted of manual control of an increasing and decreasing number of key system parameters of breathable air quality. Each experiment session consisted of nine consecutive task periods of 15 minutes where difficulty was applied in a cyclic-loading manner by increasing and decreasing manual control in a stepwise form. Two sessions were performed for each participant. The experiment system allowed for the acquisition of psychophysiological markers and for the detection of near breakdown and recovery periods [8, 13].

The psychophysiological signals used were based in ECG and EEG recordings. Markers were processed to obtain HRV1 (Section 2.1.2.2) and TLI2 (Equation 2.2) with the procedure described in Section 2.1. For the output, a variable known as Time In Range (TIR) was used. TIR represents the performance state in the aCAMS and is related to the time during which key air-quality variables remain in their normal range. More information regarding the processing of the markers can be found in [12].

3.4.3.2 Participant-dependent model elicitation

Based on the results presented in [8], which explored the use of diverse configurations of rule-base, the most successful "hand-crafted" general (i.e., the term general acknowledges a uniformity in the way the inputs relate to the output for all participants) rule-base was used. This general rule-base can be found in Table 3.1.

		HRV1			
		S	M	B	VB
TLI2	S		H	VH	VH
	M	N		H	VH
	B	L	N		
	VB	L	L		

Table 3.1: General "hand-crafted" rule-base used for the construction of the participant-dependent models with Interval Type 2 Fuzzy Sets modelling [8, 12, 13]. In the Table, S, M, B, VB stand for input linguistic levels small, medium, big and very big respectively. Output TIR linguistic levels L, N, H and VH stand for low, neutral, high and very high respectively.

Model shells with equal MF shapes for each input label (i.e., S, M, B and VB) were defined and optimised with Genetic Algorithm (GA) using the Optimization Toolbox in MATLAB®. This shell was optimised for the training-dataset of each participant, obtaining participant-dependent models based on the acquired inputs-output mapping. Label initial ranges were used during the optimisation to retain logical categories for each IT2 MF (e.g., making sure S was in fact smaller that M). Seven optimisation procedures were performed for each participant training-dataset with slightly different characteristics related to the shape of the uncertainty optimised (i.e., by varying the mean, variance and maximum membership). Table 3.2 addresses these diverse optimisation characteristics [13].

The optimisation characteristics of Table 3.2 represent the optimisation of the uncertainty in the mean, variance or maximum membership value of the member-

IT2 Fuzzy Model	Uncertainty		
	Mean	Variance	MM
No. 1	Fixed	Variable	1
No. 2	Fixed	Variable	Variable
No. 3	Fixed	Variable	Variable
No. 4	Variable	Fixed	-
No. 5	Variable	Fixed	-
No. 6	Variable	Fixed	-
No. 7	Variable	Fixed	-

Table 3.2: Participant-dependent optimisation characteristics for the Interval Type 2 Fuzzy Sets modelling. MM stands for maximum membership value. [13]

ship functions defined for the general rule-base of Table 3.1. The GA optimisation procedure tuned the parameters correspondent to these variables to evaluate the model's prediction performance.

3.4.3.3 Modelling results

To illustrate the improvement of utilising IT2FS for modelling, a comparison of the performance of the seven models of Table 3.2 against T1FS model of [8] was obtained. This comparison included the overall Minimum Square Error (MSE) and the correlation values for the training and validation datasets. Such comparison was performed in simulation for the dataset corresponding to Participant 2 (P-02), as numbered in the experiments performed in [8]. Table 3.3 shows the evaluation of the different IT2FS models constructed for P-02 as well as their comparison with the T1FS model for the same participant.

From Table 3.3 it can be observed that the training and validation MSE values for the models GA-optimised with IT2FS are able to cope with validation data with a smaller error. Additionally, there are no important differences between all IT2FS models. What can also be concluded from these results is that there is a tradeoff in performance given the additional handling of uncertainty IT2 systems achieve in

P-02 Model	Minimum Square Error		Correlation	
	Training	Validation	Training	Validation
T1FS	**14.2252**	**163.2577**	**0.9626**	**0.5372**
IT2FS 1	17.8987	100.1359	0.9480	0.8247
IT2FS 2	**32.2605**	79.5631	**0.9119**	0.8636
IT2FS 3	24.8446	70.8343	0.9518	0.8191
IT2FS 4	17.7692	72.7647	0.9515	0.8399
IT2FS 5	20.4289	102.2802	0.9375	0.7915
IT2FS 6	28.4322	56.6657	0.9130	0.8659
IT2FS 7	26.2394	**51.1363**	0.9198	**0.8872**

Table 3.3: Interval Type 2 Fuzzy Sets GA-optimised models for Participant 2 (i.e., P-02 in [8]) and their comparison with a Mamdani Type 1 Fuzzy model trained with the same dataset. [13]

terms of a higher value for MSE in the training data with a lower value for MSE for the checking data.

To better illustrate these results, Figures 3.5 to 3.8 show performance plots for the T1FS model and three selected IT2FS models (i.e., IT2FS Models 1, 2 and 4) together with their corresponding MF plots. Figure 3.4 shows the used psychophysiological inputs HRV1 and TLI2 with the task performance output TIR for the training and validation P-02 datasets.

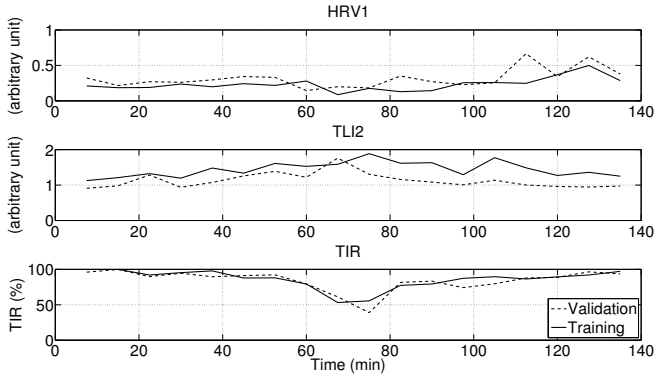

Figure 3.4: Training and validation inputs (HRV1 and TLI2) and output (TIR) for P-02 in [8]. Experimental sessions 1 (training) and 2 (validation) [13].

Similar input-output behaviour can be observed in Figure 3.4 when analysing the shape of the curves for the training and validation datasets. However, important variations exist as should be noted upon closer examination of such a figure. To evidence these differences, one should observe the minimum and maximum values for the recorded markers. For example, in the case of the TIR, the minimum percentage value in the validation dataset is smaller that the one for training.

For the IT2FS models of Figures 3.6 to 3.8, similar performances can be observed. However, upon examining their corresponding MF, it should be noted that important differences in their shapes exist given the stochastic nature of the optimisation with GA. Performances of similar characteristics were obtained for the other participants in the study, obtaining better predictions for the validation experiment than with the T1FS models, demonstrating the ability of IT2FS of handling uncertainty in data by obtaining more generalising results.

3.4.4 Summary

This Chapter addressed T2FS and their real-time application challenges, these being derived from a high computational cost given that T2FS have no closed-form mathematical solution to date. Practical solutions to these issues that can be found in the literature are usually dealt with by introducing the simplification of T2FS into IT2FS, ideal for real-time applications. Following this idea the Chapter introduced the modelling results obtained with IT2FS optimised with GA for operator performance under stress. The type-reduction method for these results was achieved with the EIASC algorithm in order to improve the computational performances. Several models were produced and compared with similar ones modelled with T1FS and sharing a common "hand-crafted" rule-base. From such results, the additional dimension of the IT2FS demonstrated its ability to handle uncertainty in data and

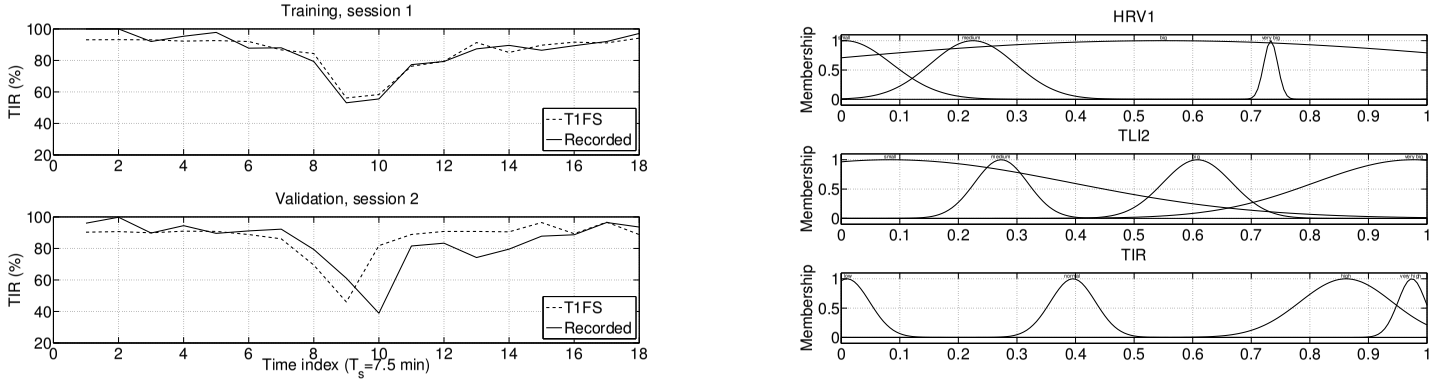

(a) (b)

Figure 3.5: Mamdani type 1 fuzzy model for P-02 (Numbering as in [8]). (a) Modelling results for the training and validation datasets. (b) Membership Functions for HRV1 and TLI2 as inputs and TIR as output[13].

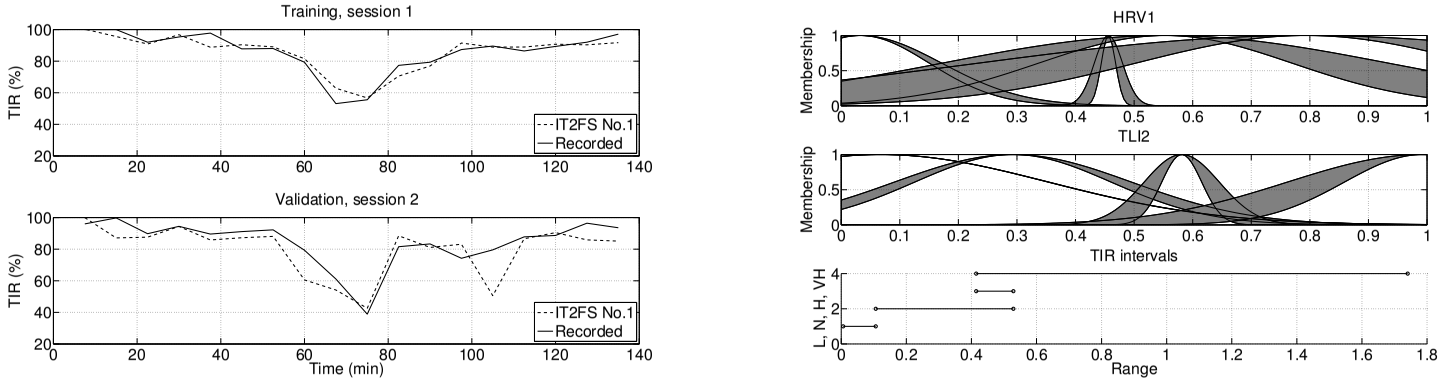

(a) (b)

Figure 3.6: Interval type 2 fuzzy model no. 1 for P-02 (Numbering as in [8]). (a) Modelling results for the training and validation datasets. (b) Membership Functions for HRV1 and TLI2 as inputs and TIR as output [13].

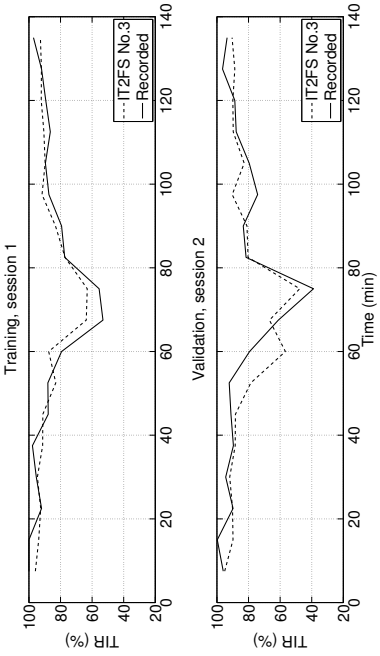

(a)

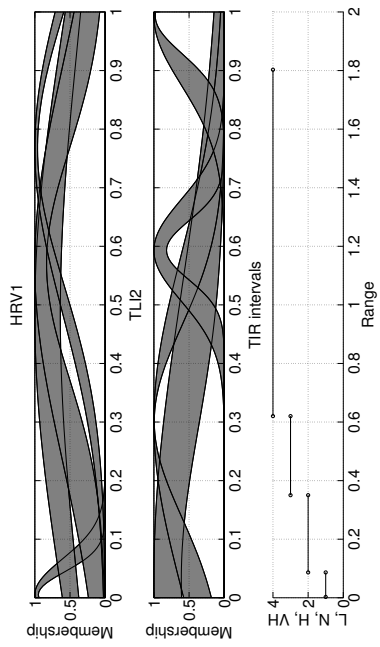

(b)

Figure 3.7: Interval type 2 fuzzy model no. 3 for P-02 (Numbering as in [8]). (a) Modelling results for the training and validation datasets. (b) Membership Functions for HRV1 and TLI2 as inputs and TIR as output [13].

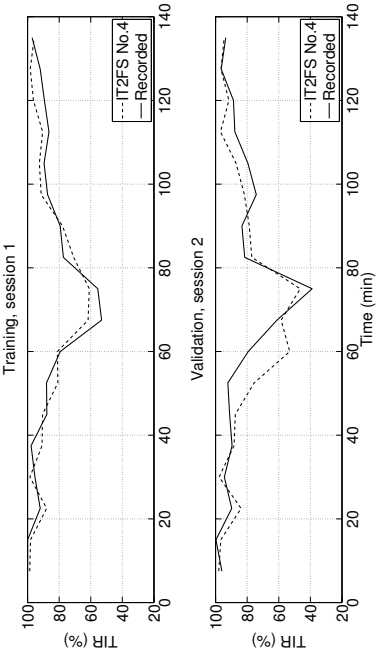

(a)

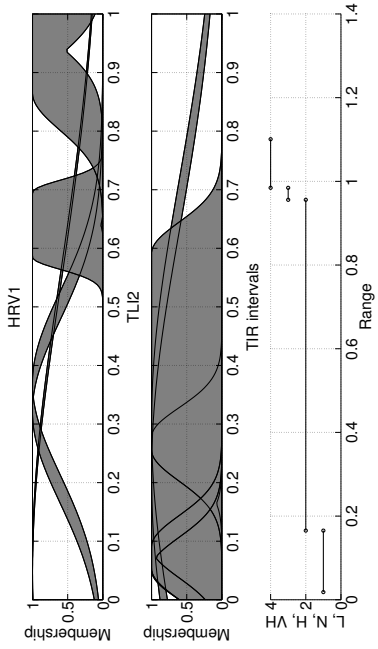

(b)

Figure 3.8: Interval type 2 fuzzy model no. 4 for P-02 (Numbering as in [8]). (a) Modelling results for the training and validation datasets. (b) Membership Functions for HRV1 and TLI2 as inputs and TIR as output [13].

as a result led to better predictions for unseen data in the validation experiments. However, a trade-off in performance was observed in the training fitting results.

Despite the obtained results, it was quickly apparent that an adaptive approach was required in order to adequately model Human Machine-Interactions of configurations similar to the ones studied. The results showed significant intra- and inter-variation across participants, making a fixed model unsuitable for this problematic. The next Chapter addresses a fuzzy-based modelling framework specifically designed to handle such differences. Fuzzy logic of type 2 was selected given its ability to handle uncertainty and its interpretability (transparency) as will be addressed.

Chapter 4

ADAPTIVE GENERAL TYPE 2 FUZZY C-MEANS MODELLING

4.1 Introduction

This Chapter introduces a new modelling algorithmic-design baptised as: Adaptive General Type 2 Fuzzy C-Means (A-GT2-FCM) modelling framework. This is a fuzzy-based approach that was validated with real-time experiments on human participants under the experimental framework of Chapter 2. Ten (10) participants experienced mental stress via mental arithmetic tasks that introduced a cognitive load. The mental stress state of these participants was evaluated through the acquisition of key psychophysiological markers based on ElectroEncephalographic (EEG), ElectroCardiographic (ECG) and pupil size signals as discussed in Section 2.1.

The A-GT2-FCM generates evolving models through a new adaptive, self-organising and interpretable modelling framework based on general Type 2 Fuzzy Sets (T2FS). Learning in real-time is achieved through a re-interpreted performance-learning algorithm that identifies features in data without the requirement of a prior training

phase. The interpretability feature of the A-GT2-FCM rule-base is later exploited for control as will be introduced in Chapter 5.

The next Section 4.2 introduces the background relating the original algorithms that inspired this new modelling framework. Section 4.2 also discusses the Fuzzy C-Means (FCM) clustering algorithm, and the way this algorithm was restructured in order to achieve a fast and efficient type-reduction and inference process for the A-GT2-FCM algorithm, a T2FS problematic that was introduced in Chapter 3. The adaptation capability of the A-GT2-FCM modelling framework is powered with the FCM restructured algorithm coupled with a modified Negative Reinforcement Learning algorithm (N-RL) that introduces the idea of evaluating the representativeness of the current rule-base to present conditions (i.e., in terms of current parameters) of the system to model (e.g., in this case, the Human Machine-Interaction system).

4.2 Background

4.2.1 Fuzzy C-Means (FCM) clustering algorithm

The Fuzzy C-Means (FCM) clustering algorithm was developed by Dunn in 1973 [91] and improved by Bezdek in 1981 [92] and has since been widely used. As any clustering algorithm, FCM refers to a clustering method that aims at dividing any dataset into subsets that contain members of similar characteristics. Since it is a fuzzy-based system, the FCM algorithm provides fuzzy bounds instead of well-defined and excluding ones. This clustering algorithm works on the premise that elements inside a cluster may still be somewhat similar to other cluster members. In this way, the algorithm provides a method for quantifying this similarity by utilising fuzzy memberships.

The FCM method is based in the minimisation of the following objective function:

$$J_m = \sum_{i=1}^{N} \sum_{j=1}^{C} u_{ij}^m \left\| x_i - c_j \right\|^2 \tag{4.1}$$

where m is the FCM constant that can be any real number greater than 1 ($1 \leq m \leq \infty$), N and C are the number of dataset elements and cluster centres respectively, u_{ij} is the fuzzy degree of membership of x_i in the j -cluster, x_i is the ith data element, c_j is the cluster centre (cluster representative), and $|| * ||$ is any norm expressing the similarity between any measured data and the centre.

The actual clustering is done through an iterative optimisation of the objective function of Equation 4.1. The membership u_{ij} and the centre c_j are updated at every step with:

$$u_{ij} = \sum_{k=1}^{C} \left(\frac{\|x_i - c_j\|}{\|x_i - c_k\|} \right)^{\frac{-2}{m-1}} \tag{4.2}$$

$$c_j = \frac{\sum_{i=1}^{N} u_{ij}^m \cdot x_i}{\sum_{i=1}^{N} u_{ij}^m} \tag{4.3}$$

The FCM iterative process stops when $\max_{\text{ij}} \left\{ \left| u_{ij}^{(k+1)} - u_{ij}^{(k)} \right| \right\} < \epsilon$. ϵ is a termination criterion and can take values between 0 and 1; k are the iteration steps. The method converges to a local minimum.

For the A-GT2-FCM modelling algorithm, the FCM degree of membership computation (Equation 4.2) was restructured since it provides a measurement of the fuzziness of the dataset elements as compared to cluster representatives. This way, a means of providing a fast inference procedure was achieved.

4.2.2 Adaptive clustering algorithms

The A-GT2-FCM modelling algorithm uses, as will be introduced in Section 4.3, a very simple inference process to avoid the computationally-costly type-reduction process that represents the bottleneck of T2FS implementations. However, despite having a simplified inference, it is still considered to be a very powerful algorithm given its ability to adapt and optimise its rule-base.

The requirement of an adaptive system was quickly apparent after the experiments in [7, 8, 9, 11, 12, 13] performed in the Human Performance Laboratory in The University of Sheffield. The intra- and inter- differences across the human participants studied, were observed to be of such a great measure that a fixed model was not enough to account for the quickly evolving parameter changes. Additionally, a generalising model (across subjects) was the prime objective of this project. After a thorough analysis it was concluded that a system aimed at modelling a HMI system would require an on-line adaptation procedure. Additionally, for control purposes, the system would need to exploit the information modelled in real-time (interpretability properties) for a truly intelligent control approach.

Several on-line adaptation methodologies were studied in the works presented in [85, 86, 87, 88, 95]. In [85, 86], Juang (2012) proposed a fuzzy-neural-based Takagi-Sugeno type adaptive modelling system where k-means clustering is used for rule generation by considering each cluster as a fuzzy rule. However, despite the excellent modelling results presented, the methodology was not directly chosen given that it uses a Neural Network (NN) approach, lacking direct interpretability properties required for intelligent control approaches. In [95] the idea of using adaptive clustering coupled with Reinforcement Learning (RL) (i.e., Q-learning) is introduced. The use of RL allows for the parallel exploration of different cluster representatives in real-time. Additionally, this work introduces the idea of learning from past experiences

in an adaptive system by rewarding clusters that performed well in the past. As will be seen in Section 4.2.3, negative rewards are used for on-line optimisation in the A-GT2-FCM modelling algorithm. The papers in [87, 88] present clustering-based self-organising fuzzy-based modelling methodologies. The rule generation procedure presented in these works was restructured in the A-GT2-FCM algorithm in order to allow for its implementation with T2FS. The A-GT2-FCM modelling framework re-interprets a similarity index (i.e., distance from the cluster representative) introduced in [87, 88] for its application with RL procedures.

In summary, the adaptive properties of the A-GT2-FCM modelling framework, are driven from the combination of adaptive clustering coupled with RL. It is also important to mention that the use of the FCM membership equation allows for fast inference via T2FS.

4.2.3 Negative Reinforcement Q-Learning algorithm (Q-L)

The Q-Learning (Q-L) algorithm was introduced by Watkins in 1989 [84]. The algorithm works by evaluating actions given at particular states. This algorithm has been proven to converge to optimum action-values with probability 1 when all actions are repeatedly sampled in all states and all actions are represented discretely. Q-L works under Markovian-domains, and learns from discounted- or negative- rewards on a long-term iterative experimentation of all actions in a finite action space [84].

The A-GT2-FCM modelling framework learns on the premise that after a sufficiently-long iterative learning process, the algorithm will have experienced the most important states of the phenomenon being modelled and will be equipped with a sufficiently-defined rule-base for every input-output combination probable. As with Q-L, negative-rewards are used as a means of introducing an optimisation system that works by negatively-rewarding bad predictions. With this procedure, the A-GT2-

FCM modelling algorithm learns the best-prediction cluster representatives in an on-line real-time manner.

The core differences between Q-L and the A-GT2-FCM Negative Reinforcement Learning (N-RL) process arise from the fact that Q-L supposes the existence of a fixed 'optimal-policy' (i.e., a best optimal fixed-model). In contrast, the A-GT2-FCM N-RL process works with the idea of infinite predictions into the future (that can never be optimal, since the future is not known *a priori*) and with a changing 'optimal-policy'. This means that the possible states are not well-defined and grow at each iteration in the future. However, we are sure that there is no fixed 'optimal-policy' (or fixed optimal-model) and that the best-prediction model is continuously changing as the phenomenon itself changes. In Q-L, discounted-rewards are worth less on every iteration. In contrast, the N-RL algorithm in the A-GT2-FCM modelling framework assumes that the parameter changes are always occurring, and rewards are weighted equally at every iteration step. In summary, the A-GT2-FCM N-RL algorithm borrows the idea of negative-rewards for continuously optimising the rule-base without the 'fixed' and 'optimal' implications of Q-L.

4.3 Adaptive General Type-2 Fuzzy C-Means Modelling Framework

This Section introduces the design of a new modelling framework named Adaptive General Type 2 Fuzzy C-Means (A-GT2-FCM). This algorithm was devised so as to take advantage of the mapping capability of T2FS with their ability to fully handle uncertainty systematically as discussed in Chapter 3, because of the simplicity of Fuzzy C-Means (FCM) clustering algorithm (Section 4.2.1) for a fast inference process (Equation 4.2); and the adaptive learning approach of Negative Reinforcement-

Learning (N-RL) (Section 4.2.3) to weight the uncertainty in data.

4.3.1 A-GT2-FCM rule-base

The idea behind A-GT2-FCM is one of a data-driven modelling framework capable of learning and storing information in real-time without the need for off-line training. The algorithm is based on a tridimensional rule-base R (Equation 4.4) whose first dimension (row) corresponds to the learned rules, its second dimension (column) corresponds to input and output variable mappings and the third dimension represents the uncertainty in the data. Part of the rule-base is the SM bi-dimensional matrix (see Equation 4.5) that holds the information regarding the weighting of the modelled uncertainty:

$$R = \left\{ \begin{array}{l} \left[\begin{array}{ccccc} x_{111} & x_{121} & \cdots & x_{1(d-1)1} & : \; y_{11} \\ x_{211} & x_{221} & \cdots & x_{2(d-1)1} & : \; y_{21} \\ & & \vdots & & \\ x_{r11} & x_{r21} & \cdots & x_{r(d-1)1} & : \; y_{r1} \end{array} \right] \\ \left[\begin{array}{ccccc} x_{112} & x_{122} & \cdots & x_{1(d-1)2} & : \; y_{12} \\ x_{212} & x_{222} & \cdots & x_{2(d-1)2} & : \; y_{22} \\ & & \vdots & & \\ x_{r12} & x_{r22} & \cdots & x_{r(d-1)2} & : \; y_{r2} \end{array} \right] \\ \left[\begin{array}{ccccc} x_{11g} & x_{12g} & \cdots & x_{1(d-1)g} & : \; y_{1g} \\ x_{21g} & x_{22g} & \cdots & x_{2(d-1)g} & : \; y_{2g} \\ & & \vdots & & \\ x_{r1g} & x_{r2g} & \cdots & x_{r(d-1)g} & : \; y_{rg} \end{array} \right] \end{array} \right. \tag{4.4}$$

$$SM = \begin{bmatrix} sm_{11} & sm_{12} & \cdots & sm_{1g} \\ sm_{21} & sm_{22} & \cdots & sm_{2g} \\ & & \vdots & \\ sm_{r1} & sm_{r2} & \cdots & sm_{rg} \end{bmatrix} \tag{4.5}$$

where x and y represent the input and output respectively in a MISO system, r is a variable number of fuzzy rules, d is a constant number of input and output variables, and g is the variable number that represents the size of the discrete uncertainty dimension. Finally, sm represent the weights for each rule and each uncertainty dimension.

4.3.2 FCM-based inference procedure

The FCM-based inference procedure for the A-GT2-FCM modelling framework follows the following next steps:

1. Calculate the uncertainty rule-base UNR of dimension r-by-d. This is where the use of the secondary membership lies; this calculation accounts for the type-reduction process:

$$UNR = \begin{bmatrix} unx_{11} & unx_{12} & \cdots & unx_{1(d-1)} & uny_1 \\ unx_{21} & unx_{22} & \cdots & unx_{2(d-1)} & uny_2 \\ & & \vdots & & \\ unx_{r1} & unx_{r2} & \cdots & unx_{r(d-1)} & uny_r \end{bmatrix} \tag{4.6}$$

$$UNR_{ij} = \frac{\sum_{m=1}^{g} SM_{im} \cdot R_{ijm}}{\sum_{n=1}^{g} SM_{in}} \tag{4.7}$$

where unx represents uncertainty-weighted inputs and uny the uncertainty weighted output in a MISO system. For Equation 4.7, $i = 1, 2, \ldots, r$; and $j = 1, 2, \ldots, d$.

2. Calculate the primary membership with the FCM algorithm and the UNR input-reduced matrix:

$$UNR_{in} = \begin{bmatrix} unx_{11} & unx_{12} & \cdots & unx_{1(d-1)} \\ unx_{21} & unx_{22} & \cdots & unx_{2(d-1)} \\ & & \vdots & \\ unx_{r1} & unx_{r2} & \cdots & unx_{r(d-1)} \end{bmatrix} \tag{4.8}$$

$$Dst_i = \sum_{n=1}^{(d-1)} (I_n - UNRin_{in})^2 \tag{4.9}$$

$$\mu_i = \sum_{l=1}^{r} \left(\frac{Dst_i}{Dst_l} \right)^{\frac{-1}{m-1}} \tag{4.10}$$

$$C_i = \frac{\mu_i - \min(\mu_i)}{\max(\mu_i) - \min(\mu_i)} \tag{4.11}$$

where $UNRin$ is the UNR input-reduced matrix, $I(t) = [in_1, in_2, \ldots, in_{(dim-1)}]$ is the input vector with the information needed to perform a prediction and is of size 1-by-$(d-1)$, Dst_i is the 1-by-r distance vector, m is an FCM algorithm constant (i.e., usually equal to 2), μ_i is the 1-by-r membership vector (with the FCM restructured membership algorithm) and C is the normalised 1-by-r μ. $i = 1, 2, \ldots, r$; and $n = 1, 2, \ldots, (d-1)$.

The FCM restructured membership algorithm (see Equation 4.10) weights for each rule, the sums of the squared distances between all $UNRin$ elements and the current input vector (see Equation 4.9). This way, a normalised membership (see Equation 4.11) is computed for each rule.

3. Obtain the Predicted Output, PO, with the UNR output-reduced vector. This corresponds to the defuzzification process;

$$UNRout = \begin{bmatrix} uny_1 \\ uny_2 \\ \vdots \\ uny_r \end{bmatrix} \tag{4.12}$$

$$PO = \frac{\sum_{m=1}^{r} C_m \cdot UNRout_m}{\sum_{n=1}^{r} C_n} \tag{4.13}$$

where $UNRout$ is the UNR output reduced matrix and C is the normalised 1-by-r membership vector.

The A-GT2-FCM modelling algorithm is a T2FS approach since it utilises tridimensional membership sets in the computation of a predicted output. The secondary membership weights inside SM are used to calculate an uncertainty type-reduced rule-base UNR (step 1) that is later used to calculate the primary membership (step 2). This membership is computed with the FCM restructured algorithm and compares each new input vector $I(t)$ to all the rules in UNR. Predictions (step 3, Equation 4.13) are based on the comparison of the current state with the information stored in the tridimensional rule-base (R and SM).

The A-GT2-FCM algorithm utilises a very simplified inference by avoiding the costly Mamdani-type rule interpretation process. This way, it is able to take advantage of the uncertainty present in the data without the need of a computationally expensive type-reduction process that represents the bottleneck of many approaches to T2FS [80]. It is nevertheless a very powerful algorithm because of its learning and adaptive capability reinterpreted from the ideas in [85, 86, 87, 88, 95] (as discussed in Section 4.2.2). Figure 4.1 shows a diagram of the A-GT2-FCM modelling framework.

From the diagram of Figure 4.1 it can be seen how the input vector is used in the A-GT2-FCM modelling framework to generate a predicted output. The past-

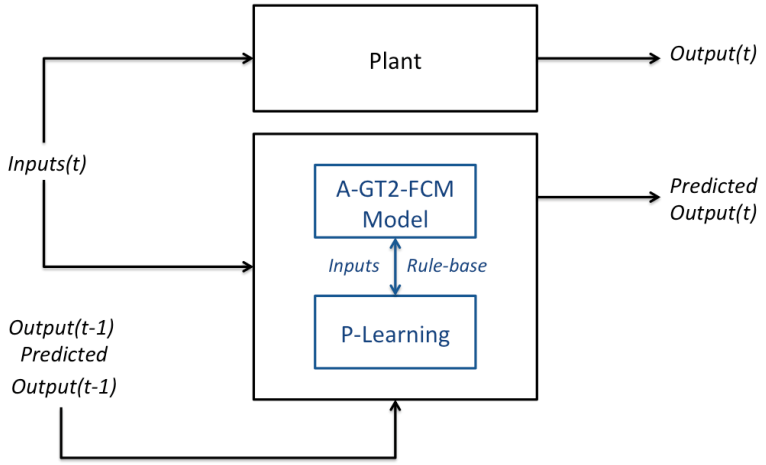

Figure 4.1: Diagram of the Adaptive General Type-2 Fuzzy C-Means, A-GT2-FCM, modelling framework with its p-learning algorithm routine.

predicted output is compared with the actual plant's output, and the difference is used in the p-learning algorithm to restructure the model's rule-base. The functioning of the p-learning algorithm will be introduced in Section 4.3.4. The next Section presents a numerical practical example showing the simplified FCM-based inference of the A-GT2-FCM algorithm.

4.3.3 Numerical example of the A-GT2-FCM inference process

An example of a simple rule-base with $r = d = g = 3$ is as follows:

$$R_{ex} = \left\{ \begin{bmatrix} 0.91 & 0.22 & 0.52 \\ 0.76 & 0.39 & 0.77 \\ 0.80 & 0.36 & 0.90 \end{bmatrix}_1 \begin{bmatrix} 0.95 & 0.18 & 0.59 \\ 1.00 & 0.79 & 1.00 \\ - & - & - \end{bmatrix}_2 \begin{bmatrix} 0.86 & 0.21 & 0.37 \\ - & - & - \\ - & - & - \end{bmatrix}_3 \right.$$

$$SM_{ex} = \begin{bmatrix} 0.75 & 0.32 & 1.00 \\ 0.35 & 0.00 & 0.00 \\ 1.00 & - & - \end{bmatrix}$$

As can be observed, R_{ex} is a tridimensional matrix (the symbol - represents an empty matrix value; empty here is different than zero). Each row is a rule; for this example we can observe two inputs and one output. The $-$ symbolises empty matrix spaces.

To calculate UNR_{ex} with Equation 4.7 consider the following calculation of one of its output elements:

$$uny_1 = (sm_{11} \cdot y_{11} + sm_{12} \cdot y_{12} + sm_{13} \cdot y_{13}) / (sm_{11} + sm_{12} + sm_{13})$$

$$= (0.75 \cdot 0.52 + 0.32 \cdot 0.59 + 1 \cdot 0.37) / (0.75 + 0.32 + 1) = 0.46$$

Similarly, all UNR_{ex} elements were obtained:

$$UNR_{ex} = \begin{bmatrix} 0.89 & 0.21 & 0.46 \\ 0.76 & 0.39 & 0.77 \\ 0.80 & 0.36 & 0.90 \end{bmatrix}$$

Consider an input vector:

$$I_{ex} = \begin{bmatrix} 0.66 & 0.27 \end{bmatrix}$$

with:

$$UNRin_{ex} = \begin{bmatrix} 0.89 & 0.21 \\ 0.76 & 0.39 \\ 0.80 & 0.36 \end{bmatrix}$$

Then, the first element in the distance vector of Equation 4.9 is:

$$Dst_1 = (in_1 - unx_{11})^2 + (in_2 - unx_{12})^2$$

$$= (0.66 - 0.89)^2 + (0.27 - 0.21)^2 = 0.0576$$

with similar calculations, $Dst_2 = 0.0244$ and $Dst_3 = 0.0277$.

The FCM membership (Equation 4.10) for the first rule can be calculated with $m = 2$ as follows:

$$\mu_1 = {Dst_1}^{\frac{-1}{m-1}} \Big/ \left({Dst_1}^{\frac{-1}{m-1}} + {Dst_2}^{\frac{-1}{m-1}} + {Dst_3}^{\frac{-1}{m-1}} \right)$$

$$= {(0.0576)^{-1}} \Big/ {[(0.0576)^{-1} + (0.0244)^{-1} + (0.0277)^{-1}]} = 0.1838$$

similarly, $\mu_2 = 0.4339$ and $\mu_3 = 0.3822$; and $C_1 = 0$, $C_2 = 1$, $C_3 = 0.7932$ after the normalisation process in Equation 4.11.

With:

$$C_{ex} = [\ 0.00 \quad 1.00 \quad 0.7932\ ]$$

and:

$$UNRout_{ex} = [\ 0.46 \quad 0.77 \quad 0.90\ ]^T$$

the inference output of Equation 4.13 is as follows:

$$PO_{ex} = \frac{C_1 \cdot uny_1 + C_2 \cdot uny_2 + C_3 \cdot uny_3}{C_1 + C_2 + C_3}$$

$$= \frac{(0 \cdot 0.46) + (1 \cdot 0.77) + (0.7932 \cdot 0.90)}{0 + 1 + 0.7932} = 0.8275$$

This procedure is repeated after the arrival of every new input vector. UNR_{ex} should be recalculated at every iteration since the rule-base composed of R_{ex} and SM_{ex} is constantly changed with the p-learning algorithm.

4.3.4 The performance learning (p-learning) algorithm in the A-GT2-FCM

The learning algorithm in the A-GT2-FCM is named performance learning (p-learning) and was inspired from the learning process presented in [87, 88] with its use of similarity measurements in the form of the inverse exponential function (see Equations 4.14, 4.15, 4.17 and 4.18). The p-learning algorithm includes the incorporation of similarity measurements to account for uncertainty and uses N-RL to weight this uncertainty in a similar way as the Q-L algorithm (See Section 4.2.3). Additionally, rules are not replaced as in [87] but combined (or added) to the uncertainty dimension (3rd dimension) with the aid of two similarity thresholds.

The p-learning algorithm operates with the following learning procedure:

1. After prediction (see Equations 4.7 to 4.13) acquire the output $O(t-1)$ and check the maximum error tolerance ET (constant defined by the user) to decide if p-learning should be applied. In case the difference between the prediction and the acquired output surpasses the ET, then apply p-learning.

If $E(t) = |PO(t-1) - O(t-1)| > ET$, apply p-learning (Steps $2-13$, Equations 4.14 to 4.19)

2. In p-learning, calculate the similarity index vector RS of size 1-by-$(r-1)$ among rules in the uncertainty rule-base UNR. Use $i = 1, 2, \ldots, (r-1)$; $j = 1, 2, \ldots, d$. This step identifies similar rules in the type-reduced rule-base (see Equations 4.6 and 4.7) using the constant rad (defined by the designer) as follows:

$$RS_i = e^{-\left(\sum_{j=1}^{d} \frac{UNR_{ij} - UNR_{(i+1)j}}{d \cdot rad}\right)} \tag{4.14}$$

3. Check r dimension combination threshold CT (constant defined by the designer and constrained by $1 > CT > 0$). Obtain new R and SM using $i = 1, 2, \ldots, (r-1)$; $j = 1, 2, \ldots, d$; $k = 1, 2, \ldots, g$. If two or more rules are above the threshold, they are combined with λ_1 and λ_2 (constants defined by the designer). If two rules are too similar, then they are combined as follows:

If $RS_i > CT$, then

$$R_{ijk} = \lambda_1 \cdot R_{ijk} + \lambda_2 \cdot R_{(i+1)jk}$$

$$SM_{ik} = \lambda_1 \cdot SM_{ik} + \lambda_2 \cdot SM_{(i+1)k}$$

$$\lambda_1 + \lambda_2 = 1$$

Erase $R_{(i+1)}$ for all d and g

Erase $SM_{(i+1)}$ for all g

Reduce size of r by one

4. Calculate similarity index matrix GS of size r-by-$(g-1)$ among rules in uncertainty dimension g with $i = 1, 2, \ldots, r$; $j = 1, 2, \ldots, d$; $k = 1, 2, \ldots, (g-1)$; and with rad, defined similarly to step 2. This step identifies similar representatives (rule-mappings) in the uncertainty dimension as follows:

$$GS_i = e^{-\left(\sum_{j=1}^{d} \frac{\left|g_{ijk} - g_{ij(k+1)}\right|}{d \cdot rad}\right)} \tag{4.15}$$

$$g_{ijk} = SM_{ik} \cdot R_{ijk} \tag{4.16}$$

5. Check the g dimension generality threshold GT (constant defined by the designer with the constraint $1 > CT > GT > 0$) and obtain new R and SM with $i = 1, 2, \ldots, r$; $j = 1, 2, \ldots, d$; $k = 1, 2, \ldots, (g-1)$. If two or more uncertainty rule-mappings are similar, then they are combined as in step 3 as follows:

If $GS_{ik} > GT$,

$$R_{ijk} = \lambda_1 \cdot R_{ijk} + \lambda_2 \cdot R_{ij(k+1)}$$

$$SM_{i(k+1)} = 0$$

Erase $R_{i(k+1)}$ for all d

6. Resize the rule-base by eliminating unnecessary dimensions after similarity checks of steps 3 and 5.

7. Calculate the similarity index matrix DS of size r-by-d with the past input-output vector $D(t-1) = [\ I(t-1) \quad O(t-1)\ ]$ of size 1-by-d, and rules in the

rule-base. Use $i = 1, 2, \ldots, r$; $k = 1, 2, \ldots, g$ with constant rad defined similarly to steps 2 and 4. This identifies the match of the input-output past mapping with the rule-base used for the prediction to decide if to combine with and existing rule, if to add as an additional uncertainty representative, or if a new rule is required.

$$DS_i = e^{-\left(\sum_{j=1}^{d} \frac{\left|D_i - R_{ijk}\right|}{d \cdot rad}\right)} \tag{4.17}$$

8. Check the combination threshold CT to identify if new data is similar to an existing rule in the rule-base. If true, combine with existing rule and obtain new R and SM by combining D with the combination constant σ (chosen by de designer under the constraint$0 < \sigma < 1$). The combination constant σ expresses the degree of importance given to incoming new information. Use $i = 1, 2, \ldots, r$; $j = 1, 2, \ldots, d$; $k = 1, 2, \ldots, g$. This step can be summarised as follows:

$$\text{If } DS_{ik} > CT,$$

$$R_{ijk} = \sigma \cdot D_j + (1 - \sigma) \cdot R_{ijk}$$

$$SM_{ik} = \sigma + (1 - \sigma) \cdot SM_{ik}$$

9. Check the generality threshold GT. Add to the uncertainty dimension of one of the rules and obtain the new R and SM. If no similar rule is found in the rule-base, but D vector is similar enough as defined by the GT, then add D to the uncertainty dimension g. Use $i = 1, 2, \ldots, r$; $j = 1, 2, \ldots, d$; $k = 1, 2, \ldots, g$. This step ensures the uncertainty in the data is taken into account. This step can be summarised as follows:

$$\text{Else if } DS_{ik} > GT,$$

$$R_{ij(k+1)} = D_j$$

$$SM_{ij(k+1)} = 1$$

10. If the input-output mapping D is different to existing rules and their uncertainty dimension, add as a new rule for all g and obtain the new R and SM. This step generates new data rule-representatives for the rule-base. Use $i = 1, 2, \ldots, r$; $j = 1, 2, \ldots, d$; $k = 1$.

Else,

$$R_{(r+1)j1} = D$$

$$SM_{(r+1)1} = 1 \text{ Increment size of } r \text{ by one}$$

11. Re-order rule-base sorting by output (d) column for interpretability of model.

12. Calculate the N-RL algorithm-based distance with the scaling constant α. Use $i = 1, 2, \ldots, r$; $j = 1, 2, \ldots, d$; $k = 1, 2, \ldots, g$. This step weights the uncertainty dimension mappings for a true GT2FS.

$$d_{ijk} = |\alpha(D_j - R_{ijk})|$$

$$\text{If } \alpha = 1, d_{ijk} = |D_j - R_{ijk}|$$

13. Calculate the N-RL based similarity matrix RLS of size r-by-g. Use constant rad defined similarly to steps 2, 4 and 7. Obtain the new SM matrix. In this step, Equation 4.19 uses N-RL to reduce the weight of dissimilar representatives in dimension g. With this process and enough experienced data, the weights for less occurring cases stored in the uncertainty are reduced. This ensures that the predictions are more highly influenced by the most occurring cases when SM is used for the calculation of UNR (see Equation 4.7). Use $i = 1, 2, \ldots, r$; $k = 1, 2, \ldots, g$.

$$RLS_{ik} = e^{-\left(\sum_{j=1}^{d} \frac{d_{ijk}}{d \cdot rad}\right)} \tag{4.18}$$

$$SM_{ik} = \frac{SM_{ij} \cdot RLS_{ik}}{\max\left(RLS_i\right)} \tag{4.19}$$

As can be observed from the inference process and the p-learning process of the A-GT2-FCM modelling framework, the inter- and intra-parameter variabilities across humans in a HMI system are handled inside the model learning operation without the need for calibration process and in real-time.

4.4 Summary

This Chapter addressed the new A-GT2-FCM modelling framework together with its two main algorithms; the FCM-based inference, and the p-learning procedure based in N-RL. The Chapter started by presenting the background that inspired the A-GT2-FCM modelling framework, followed by an introduction to the FCM clustering algorithm, the idea behind adaptive clustering approaches found in the literature, the Q-L RL algorithm as well as the use of a similarity index to measure distances between data mappings, and the use of cluster representatives. Finally, in order to demonstrate the simple but powerful inference process of the A-GT2-FCM modelling framework, a numerical example is also presented, showing how this process solves the type-reduction issues that most T2FS approaches encounter.

In the next Chapter, the application of the A-GT2-FCM modelling and control algorithm for the proposed HMI system which was described in Chapter 2 will be addressed. In this Chapter besides the application of this new modelling technique, its use for control purposes in the form of the Energy Model-Based Controller (E-MBC) is also presented.

Chapter 5

THE A-GT2-FCM FRAMEWORK APPLIED TO OPERATOR FUNCTIONAL MODELLING AND CONTROL

5.1 Off-line modelling

In Section 2.3.2 it was explained how a series of preliminary experiments on four participants (i.e., P01, P02, P03 and P04) were performed to evaluate the use of PDM as a psychophysiological marker for mental stress detection under the MA experimental configuration of Chapter 2. The data collected for this preliminary study were further utilised with the objective of testing the A-GT2-FCM modelling framework of Chapter 4 in a simulated real-time experiment. The markers utilised (i.e., HRV_1, HRV_2, TLI_1, TLI_2 and PDM) were calculated off-line and fed to the A-GT2-FCM algorithm on an iterative configuration to simulate the real-time

experiment.

With this simulation-based experiment, the speed of the programmed A-GT2-FCM was evaluated, concluding that it was suitable to be implemented in real-time with the aid of the MATLAB® GUI environment (see Section 2.2.4). Additionally, the modelling performance of the A-GT2-FCM algorithm was tested and compared with the off-line constructed participant-dependent Adaptive Network-based Fuzzy Inference System (ANFIS) models (i.e., one model for each participant) designed with the aid of the GUI-ANFIS editor in the 'Fuzzy Logic Toolbox' of MATLAB®. The data corresponding to ME-1 were used for the ANFIS training and the ME-2 were used for validation (see Figure 2.13 in Chapter 2). ANFIS was selected given its extensive use in the control systems community. ANFIS provides a neural network architecture and a powerful learning algorithm capable of finding relationships in data with a training procedure in off-line. Additionally, it is easily implemented due to the availability of the GUI-ANFIS editor of MATLAB®. More information on ANFIS can be found in [96]. With regards to the designed ANFIS-models, its structure was automatically constructed with 'Subset clustering' and its default settings (i.e., Range of influence=0.5, Squash factor=1.25, Accept ratio=0.5 and Reject ratio=0.15). Training was done with the 'hybrid' algorithm [96].

Table 5.1 presents the modelling results of the A-GT2-FCM compared to the fixed participant-dependent ANFIS-models constructed. For this test, the Error was calculated as follows:

$$Error = 100 \cdot \sqrt{\frac{\sum_{i=1}^{N} (AP_i - PAP_i)^2}{N}} \tag{5.1}$$

where N is the total number of data-points, AP is the Accuracy Performance acquired during the MA operations experiment and PAP is the Predicted Accuracy

Performance obtained from the model. For every modelling experiment, $N = 690$ data-points as is detailed in Chapter 2.

The Correlation was calculated as follows:

$$Correlation = \frac{\text{cov}\,(AP, PAP)}{\sqrt{\text{cov}\,(AP, AP) \cdot \text{cov}\,(PAP, PAP)}} \tag{5.2}$$

	A-GT2-FCM				participant-dependent ANFIS			
	Error		Correlation		Error		Correlation	
	ME-1	ME-2	ME-1	ME-2	ME-1	ME-2	ME-1	ME-2
P01	8.4150	12.5287	0.9623	0.8906	16.8354	41.5638	0.8256	0.2876
P02	13.4517	12.2430	0.9199	0.9322	13.7193	51.7388	0.9034	-0.0134
P03	10.0642	8.6569	0.9371	0.9534	7.5707	31.6411	0.9607	0.5270
P04	5.3565	7.2997	0.8863	0.9400	5.6937	34.0883	0.8548	-0.1343
Avg.	**9.3219**	**10.1821**	**0.9264**	**0.9291**	10.9548	39.7580	0.8861	0.1667

Table 5.1: Modelling performance results for the off-line preliminary study (see Equations 5.1 and 5.2). Comparison between the A-GT2-FCM modelling framework and participant-dependent ANFIS fixed models. ME-1 corresponds to training phase and ME-2 to validation phase.

From Table 5.1 it can be observed how the A-GT2-FCM modelling framework performs better in average when compared with the participant-dependent ANFIS models trained the ME-1 data. The benefit of the adaptive technique is more evident in the ME-2, were the inter-differences across participants result in deficient ANFIS predictions as can be observed in the Table. In all cases, the A-GT2-FCM ME-2 results, greatly surpass the ANFIS models with a small Error and high Correlation for the adaptive modelling case. For the ME-1, results for both modelling approaches are comparable. In fact, for P03, the ANFIS model obtains marginally better results.

The results presented in this section are important since they highlight the modelling capabilities of the A-GT2-FCM algorithm and its applicability in real-time. Additionally, the comparison with the commonly used ANFIS technique functions

as a benchmark to put into perspective the obtained results. However, since the A-GT2-FCM modelling framework is an adaptive approach, its validation has to be performed in real-time to truly test its adaptive properties. The next Section presents a series of real-time modelling experiments performed for all ten participants in the study.

5.2 On-line real-time modelling

This Section presents the on-line real-time modelling results of the A-GT2-FCM modelling framework for the ten (10) participants in the MA operations experiment of Chapter 2. As a means of validating the modelling results, a comparison with participant-dependent off-line trained ANFIS fixed-models is also presented. This experiment was performed with the designed MATLAB® GUI environment. The designed GUI calculated markers as well as the A-GT2-FCM algorithm (including the p-learning algorithm) predicted performance in real-time. The computed input-output dataset obtained for ME-1 was used in off-line to train the participant-dependent ANFIS models; the ME-2 dataset was used as validation for the trained ANFIS models. The results of the A-GT2-FCM real-time predictions were compared with the ANFIS models and can be found in Table 5.2.

Table 5.2 presents the modelling results calculated via equations 5.1 and 5.2 for the predictions in real-time which were obtained via the A-GT2-FCM algorithm and compared with the off-line predictions with the same experimental data of the participant-specific ANFIS models. From this Table it can be observed that the A-GT2-FCM performs better and in a consistent way for all participants in the study. Errors and Correlations show an excellent performance throughout, demonstrating the fast learning capabilities of the algorithm that needs no training phase. In the

case of ANFIS, a very small training error and a high correlation index are observed for every participant in ME-1. However, the performance for ME-2 is not consistent and shows inferior prediction results for most participants. Overall, the A-GT2-FCM algorithm is able to obtain superior predictions; which can mainly be attributed to its adaptive properties.

A-GT2-FCM real-time / ANFIS off-line. Modelling

	Error					
	ME-1			ME-2		
P01	5.4197	/	2.0520	6.1525	/	71.8948
P02	5.2753	/	2.2577	6.7112	/	52.0001
P03	5.7502	/	1.8520	6.2016	/	34.0385
P06	8.1281	/	3.1923	6.7512	/	58.8248
P07	6.4311	/	2.5943	6.9501	/	43.7482
P08*	4.7957	/	1.7297	5.1479	/	6.9308
P09	5.1887	/	1.4180	5.2014	/	8.2639
P10	5.1957	/	1.9126	6.4262	/	9.4716
P11	5.0032	/	2.3427	5.8235	/	6.4813
P12	6.4129	/	2.2724	6.7505	/	14.3965
Avg.	5.7601	/	**2.1624**	**6.2116**	/	30.6051
	Correlation					
	ME-1			ME-2		
P01	0.9828	/	0.9971	0.9587	/	0.1716
P02	0.9820	/	0.9966	0.9732	/	0.4876
P03	0.9638	/	0.9833	0.9574	/	0.6257
P06	0.9751	/	0.9955	0.9818	/	0.3718
P07	0.9866	/	0.9976	0.9826	/	0.3332
P08*	0.9852	/	0.9977	0.9682	/	0.9601
P09	0.9662	/	0.9972	0.9553	/	0.9073
P10	0.9818	/	0.9970	0.9860	/	0.9662
P11	0.9859	/	0.9968	0.9856	/	0.9834
P12	0.9845	/	0.9975	0.9814	/	0.9216
Avg.	0.9794	/	**0.9956**	**0.9730**	/	0.6729

* Both experiments with incremental difficulty profile

Table 5.2: Modelling performance results for the real-time modelling study (see Equations 5.1 and 5.2). Comparison between the A-GT2-FCM modelling framework and participant-dependent ANFIS fixed models. ME-1 corresponds to training phase and ME-2 to validation phase.

To further demonstrate the ability of A-GT2-FCM, Figures 5.1 through 5.10 show the results for ME-1 and ME-2 for all participants in the study.

From Figure 5.1 it can be observed how the A-GT2-FCM algorithm was able to successfully predict the performance of P01 in the MA experiment for both 'difficulty' configurations (ME-1 and ME-2). Furthermore, correlation, as shown in Table 5.2, is very high and the error is very small. This Figure also shows the predictions for P01-specific ANFIS model, demonstrating the inability of ANFIS fixed model to handle the inter-parameter differences in P01 for the ME-2 case.

The information used by A-GT2-FCM to calculate its predictions (psychophysiological markers) is presented in Figure 5.11 and corresponds to the studied markers of Chapter 2.1. Similar performances were obtained for all participants in the study despite the intra-differences between them. For the P01-specific ANFIS model used as a benchmark comparison in Table 5.2, the inputs correspond to the same markers of Figure 5.11 but with the inclusion of $AP(t-1)$.

Despite the bad predictions observed in ME-2 for the P01-specific ANFIS model, it can be observed in Table 5.2, how some of the ANFIS models were also able to lead to good predictions (e.g., P08, P09, P10 and P11).

To further demonstrate the inability of a fixed model to handle the parameter variations (apparent in the previous Figures) in the collected data, Section 5.2.1 addresses the adaptive properties of the A-GT2-FCM modelling framework and how it compares with the designed participant-specific ANFIS models.

5.2.1 Adaptive properties of the A-GT2-FCM modelling framework

This Section discusses the adaptive properties of the A-GT2-FCM modelling framework. Throughout this work, it has been stated that the A-GT2-FCM algorithm

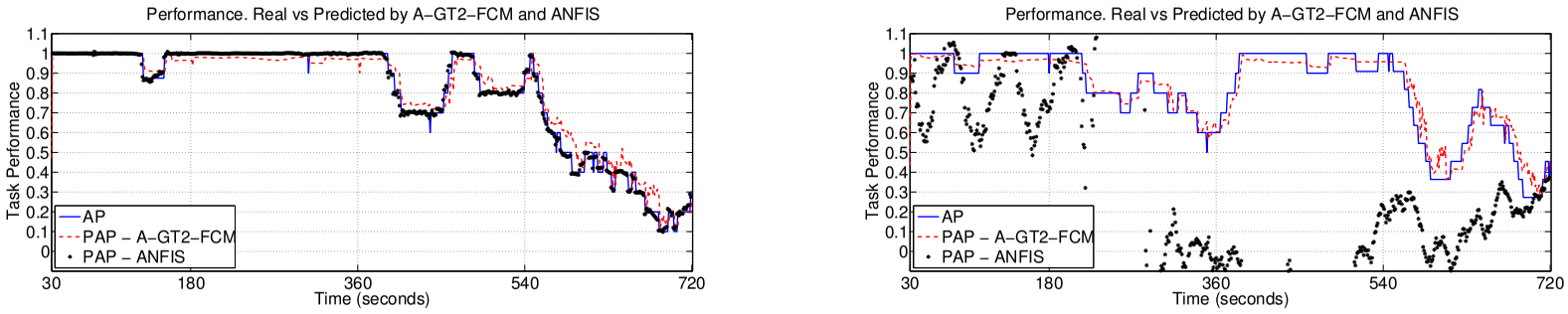

(a) (b)

Figure 5.1: P01 Accuracy performance, AP, and predicted accuracy performance, PAP obtained with A-GT2-FCM in real-time and off-line with the P01-specific ANFIS model. (a) Incremental difficulty (ME-1 with $DL = 1, 2, 3, 4$) MA experiment. (b) Scrambled difficulty (ME-2 with $DL = 2, 3, 1, 4$) MA experiment.

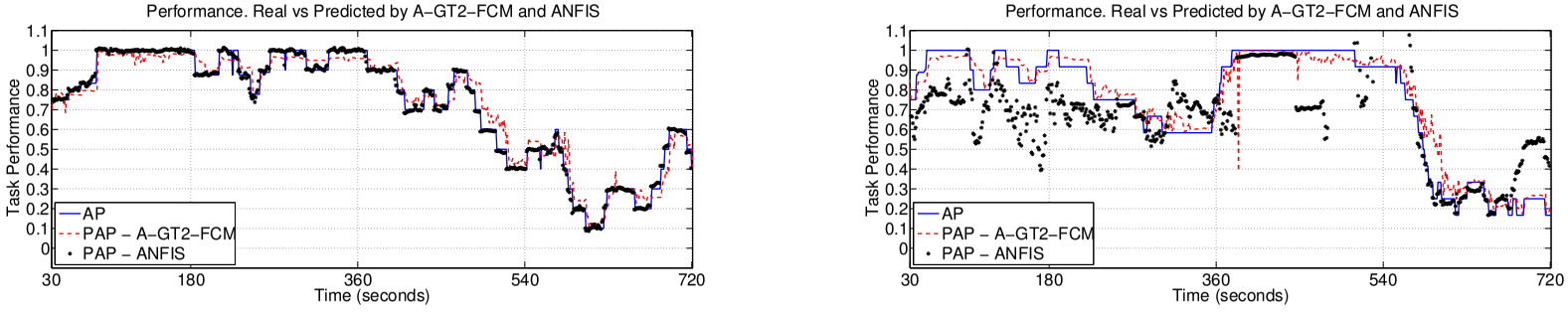

(a) (b)

Figure 5.2: P02 Accuracy performance, AP, and predicted accuracy performance, PAP obtained with A-GT2-FCM in real-time and off-line with the P02-specific ANFIS model. (a) Incremental difficulty (ME-1 with $DL = 1, 2, 3, 4$) MA experiment. (b) Scrambled difficulty (ME-2 with $DL = 2, 3, 1, 4$) MA experiment.

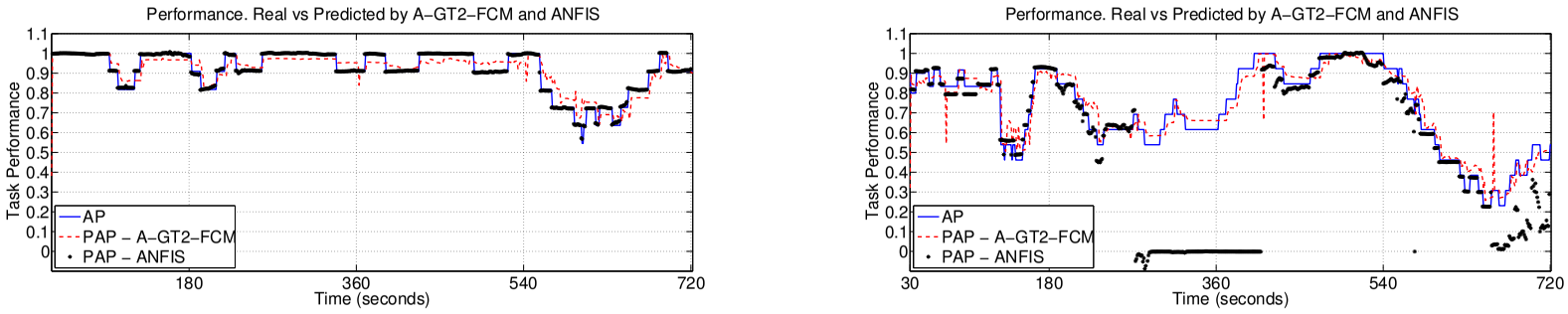

(a) (b)

Figure 5.3: P03 Accuracy performance, AP, and predicted accuracy performance, PAP obtained with A-GT2-FCM in real-time and off-line with the P03-specific ANFIS model. (a) Incremental difficulty (ME-1 with $DL = 1, 2, 3, 4$) MA experiment. (b) Scrambled difficulty (ME-2 with $DL = 2, 3, 1, 4$) MA experiment.

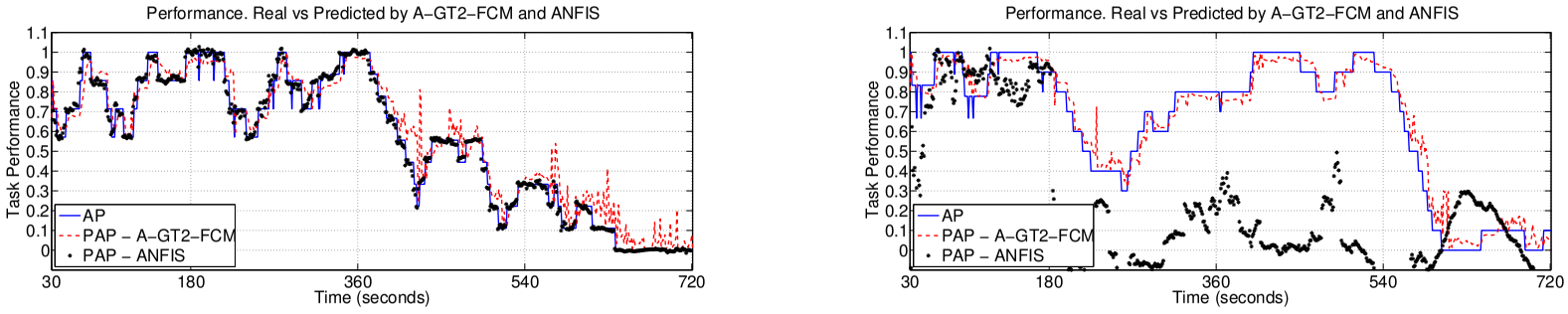

(a) (b)

Figure 5.4: P06 Accuracy performance, AP, and predicted accuracy performance, PAP obtained with A-GT2-FCM in real-time and off-line with the P06-specific ANFIS model. (a) Incremental difficulty (ME-1 with $DL = 1, 2, 3, 4$) MA experiment. (b) Scrambled difficulty (ME-2 with $DL = 2, 3, 1, 4$) MA experiment.

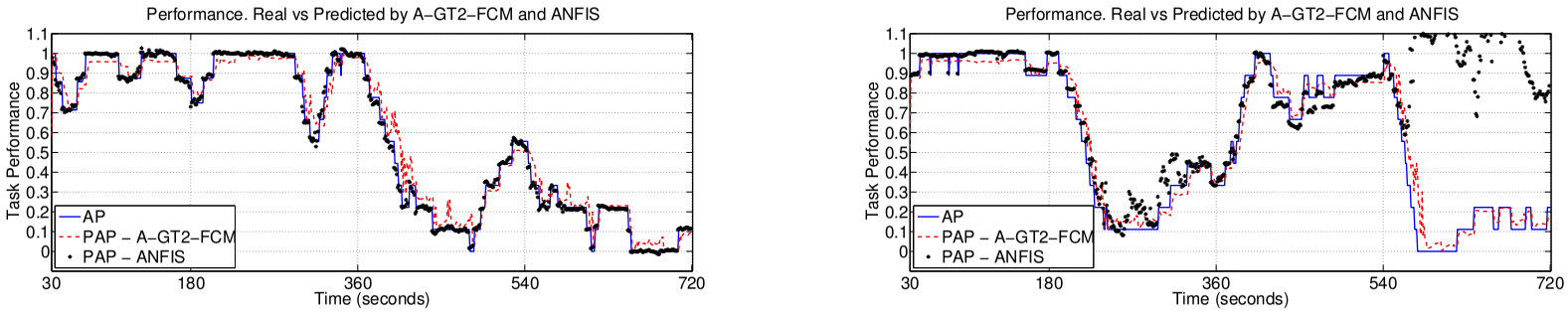

(a) (b)

Figure 5.5: P07 Accuracy performance, AP, and predicted accuracy performance, PAP obtained with A-GT2-FCM in real-time and off-line with the P07-specific ANFIS model. (a) Incremental difficulty (ME-1 with $DL = 1, 2, 3, 4$) MA experiment. (b) Scrambled difficulty (ME-2 with $DL = 2, 3, 1, 4$) MA experiment.

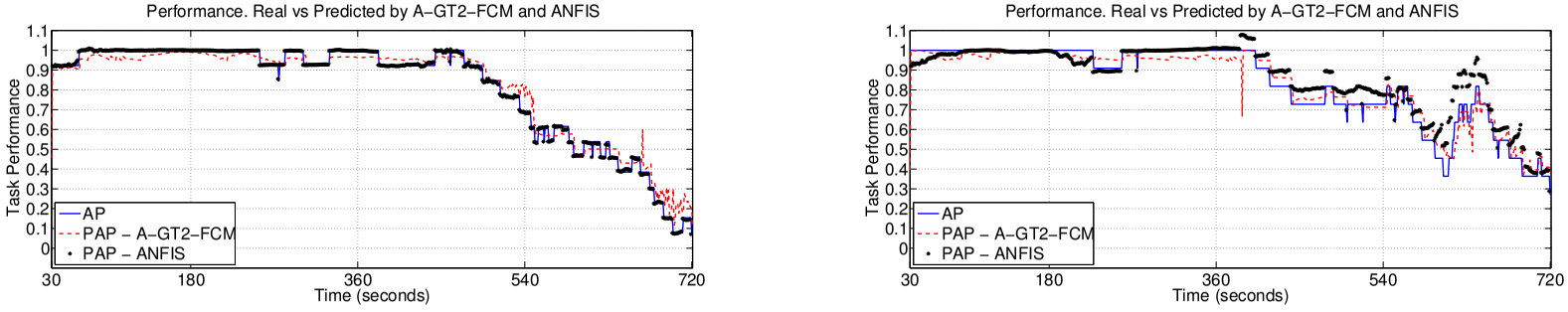

(a) (b)

Figure 5.6: P08 Accuracy performance, AP, and predicted accuracy performance, PAP obtained with A-GT2-FCM in real-time and off-line with the P08-specific ANFIS model. (a) Incremental difficulty (ME-1 with $DL = 1, 2, 3, 4$) MA experiment. (b) Additional Incremental difficulty (ME-1 with $DL = 1, 2, 3, 4$) MA experiment.

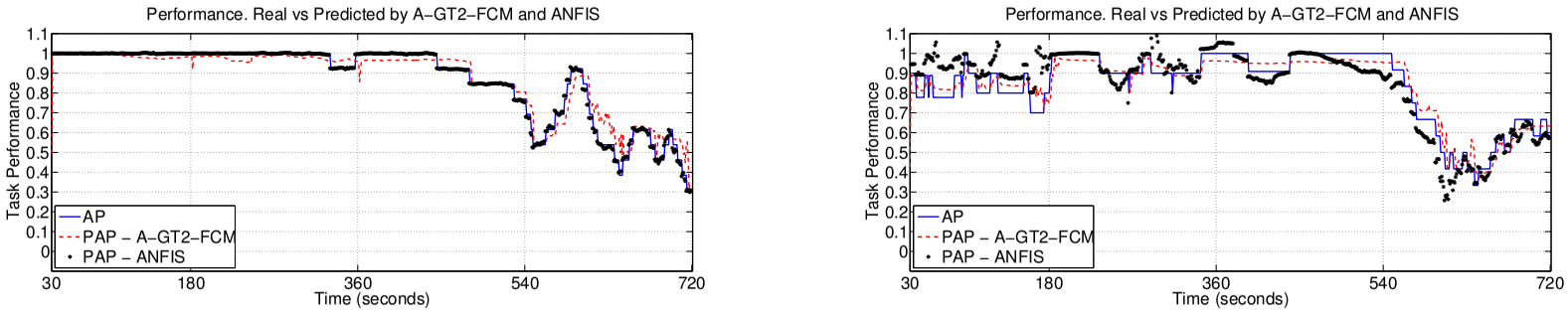

Figure 5.7: P09 Accuracy performance, AP, and predicted accuracy performance, PAP obtained with A-GT2-FCM in real-time and off-line with the P09-specific ANFIS model. (a) Incremental difficulty (ME-1 with $DL = 1, 2, 3, 4$) MA experiment. (b) Scrambled difficulty (ME-2 with $DL = 2, 3, 1, 4$) MA experiment.

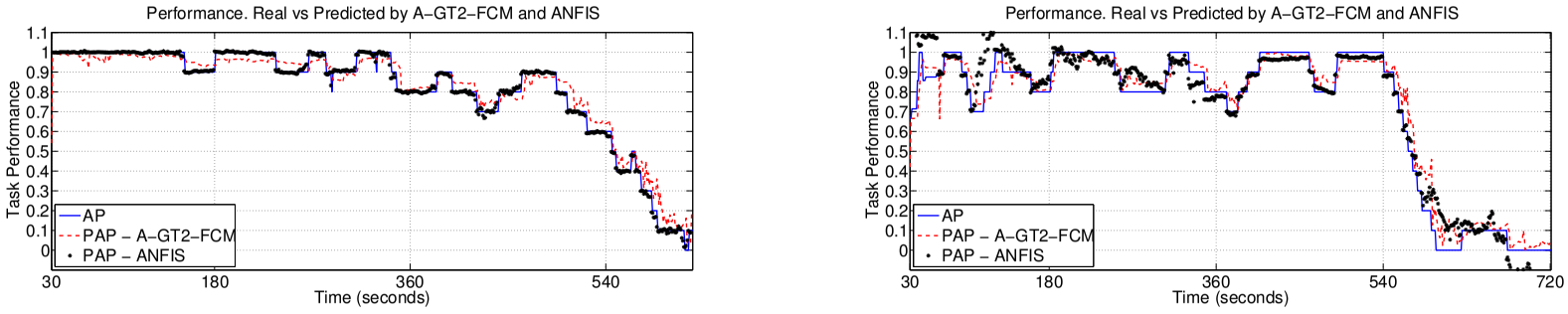

Figure 5.8: P10 Accuracy performance, AP, and predicted accuracy performance, PAP obtained with A-GT2-FCM in real-time and off-line with the P10-specific ANFIS model. (a) Incremental difficulty (ME-1 with $DL = 1, 2, 3, 4$) MA experiment. (b) Scrambled difficulty (ME-2 with $DL = 2, 3, 1, 4$) MA experiment.

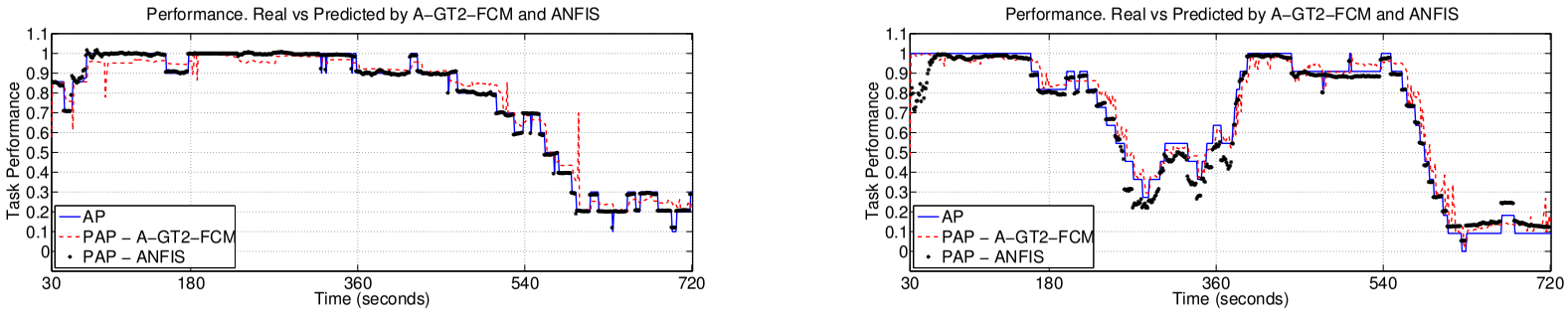

(a) (b)

Figure 5.9: P11 Accuracy performance, AP, and predicted accuracy performance, PAP obtained with A-GT2-FCM in real-time and off-line with the P11-specific ANFIS model. (a) Incremental difficulty (ME-1 with $DL = 1, 2, 3, 4$) MA experiment. (b) Scrambled difficulty (ME-2 with $DL = 2, 3, 1, 4$) MA experiment.

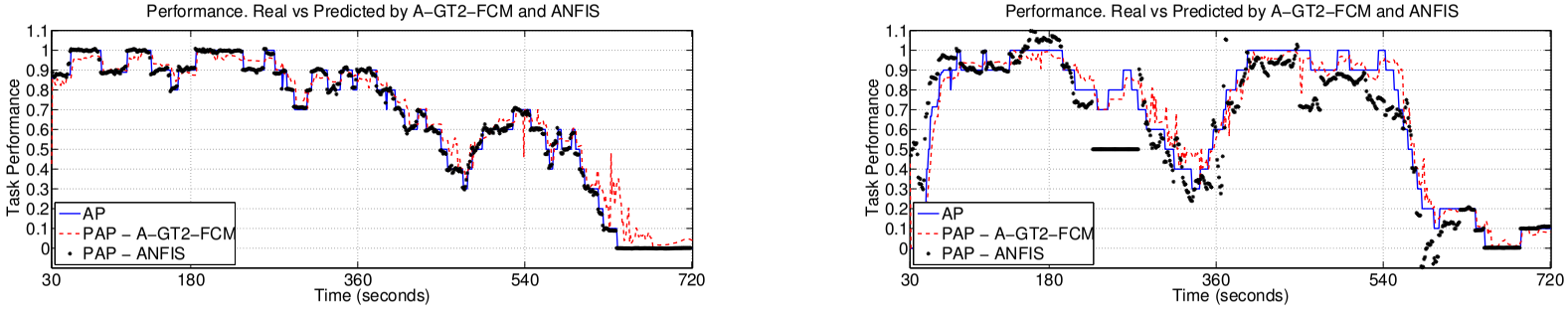

(a) (b)

Figure 5.10: P12 Accuracy performance, AP, and predicted accuracy performance, PAP obtained with A-GT2-FCM in real-time and off-line with the P12-specific ANFIS model. (a) Incremental difficulty (ME-1 with $DL = 1, 2, 3, 4$) MA experiment. (b) Scrambled difficulty (ME-2 with $DL = 2, 3, 1, 4$) MA experiment.

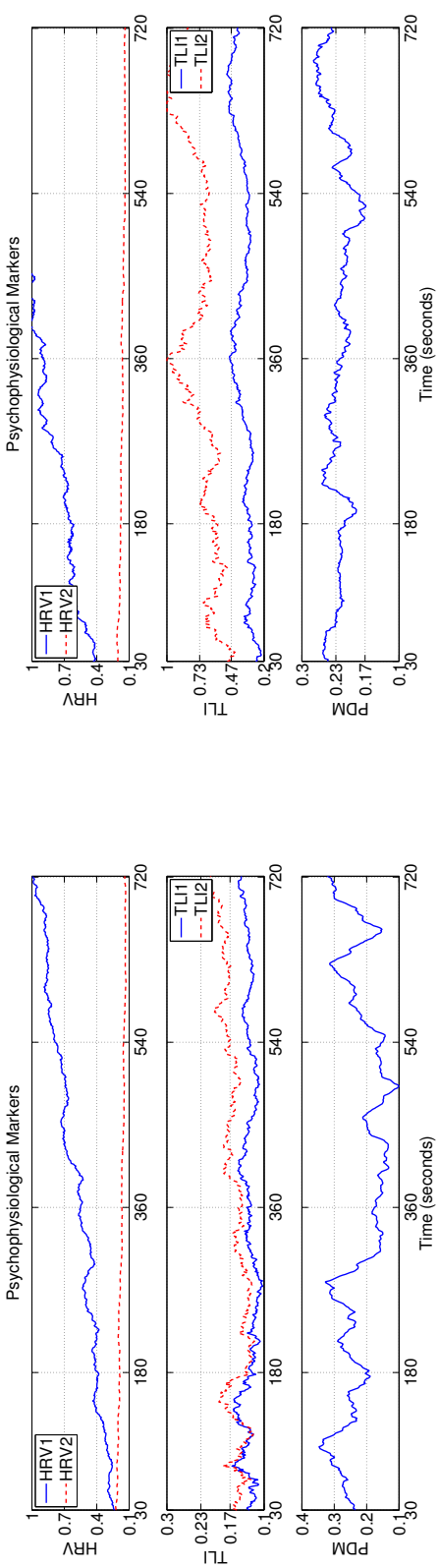

Figure 5.11: P01 Psycho-physiological markers inputs (HRV_1, HRV_2, TLI_1, TLI_2 and PDM) to A-GT2-FCM. (a) Incremental difficulty (ME-1 with $DL = 1, 2, 3, 4$) MA experiment. (b) Scrambled difficulty (ME-2 with $DL = 2, 3, 1, 4$) MA experiment.

presents characteristics that make it adaptable to inter- and intra-parameter variabilities between the participants in the study. The A-GT2-FCM modelling framework is able to handle uncertainty from its T2FS configuration and its real-time p-learning algorithm (see Chapter 4). The evidence that supports these adaptive characteristics is addressed via the following remarks:

1. The model is able to self-organise and operate in real-time. The real-time modelling results presented in Table 5.2 and Figures 5.1 through 5.10 demonstrate the ability of the A-GT2-FCM algorithm to learn from features in the data and in real-time by producing good predictions even without a training phase. With regards to the self-organisation properties of the modelling framework, Figure 5.12 illustrates how the p-learning algorithm operates by displaying the number of rules in r and g dimensions as the DL changes for P12 in the ME-1. For the designed P12-specific ANFIS model, the rule-base was of 12 rules, leading to good off-line predictions of the training ME-1 data.

2. The modelling framework is generalising for all participants; there was no need for a participant-based calibration and off-line model construction, an important contribution when compared with the ANFIS case and the works in [7, 8, 13]. For the first prediction, the same 'dummy' rule-base was used for all participants. Furthermore, despite having important variations in the psychophysiological inputs from participant to participant and among participants themselves, the model was able to capture these in a transparent way. In fact, the same constant values were used to re-scale the markers for all participants. In order to demonstrate the variability in the markers an example comparison between the input data from P11 and P01 in the ME-2 is presented in Figure 5.13. From this figure it can be observed that the scaling in the numerical values for both participants significantly varied (see y-axis). This is

especially evident for the TLI markers in the middle plot, since for P11 these are double in magnitude as compared to the ones from P01 for the same experimental configuration. Additionally, inter-differences exist as well, as can be seen in Figure 5.11 by examining the TLI markers for P01. For this particular case, the markers for the ME-2 (Figure 5.11(b)) are double in magnitude when compared with the ones for the ME-1 (Figure 5.11(a)). Derived from this important change in marker scaling is the degraded predictions observed for the P01-specific ANFIS model for ME-2 (see Figure 5.1(b)).

3. The A-GT2-FCM modelling algorithm can handle and adapt to temporal loss of information. Given the real-time conditions in the the MA operations experiment, where acquisition and calculation of markers was achieved, there were occasional losses of information resulting from reference disconnection on the head scalp during EEG acquisition and/or disconnection of ECG electrodes derived from natural movements during some of the experiments. Despite these data losses (disturbances), the A-GT2-FCM was able to adapt without significant loss in performance; Figures 5.14 through 5.16 show some of these cases. Figure 5.14 shows a scenario whereby the EEG-based TLI markers are lost during phase 3 of ME-2 for P02. The effect of this temporal loss of data can be observed for the modelling results (Figure 5.14(b)) with evident lower than average prediction for the location. Figures 5.15 and 5.16 show similar scenarios where the TLI1 and TLI2 markers are lost respectively. With respect to the effect of this loss in their modelling results, no evident or noticeable changes in the predictions can be observed. In these graphs, the ability of the adaptive model to recover quickly at the next iteration can be observed, ensuring successful adaptation and disturbance rejection. For the ANFIS model during validation (ME-2, Figure 5.14), the situation appears to be rather different, lead-

ing to a poor performance with no robustness properties for intra-parameter changes in P02 due to temporal loss of marker information. For the ANFIS models of Figures 5.15 and 5.16, no noticeable effect derived from this loss of information is observed in the predictions. However, it is worth noting that these two examples are for the ME-1, the training phase of the ANFIS models.

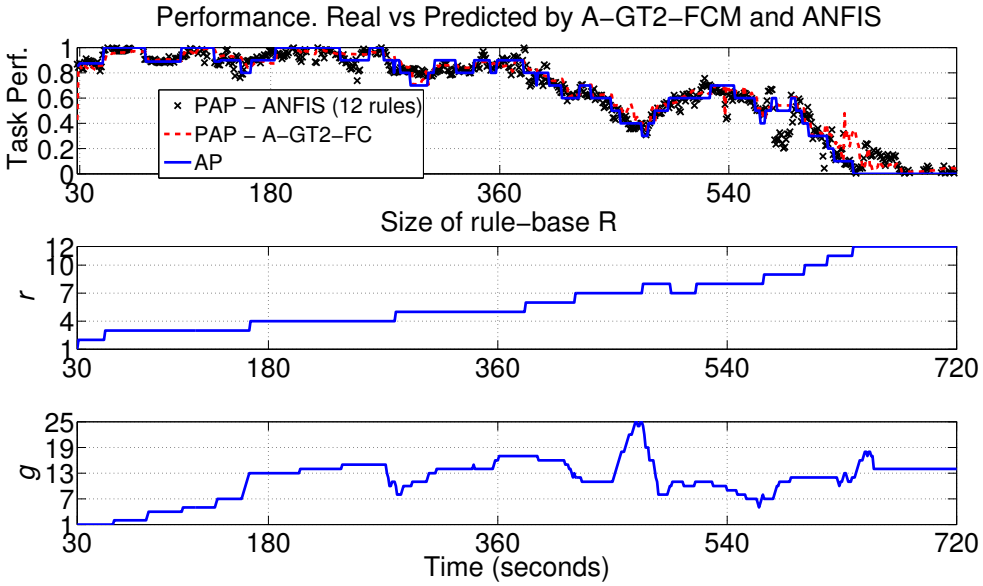

Figure 5.12: P12 Evolution in the size of the rule-base R during ME-1. Top plot, Task Performance (A-GT2-FCM and P12-specific ANFIS). Middle and bottom plots show the size of the rule-base R in its r and g dimensions.

5.3 Online real-time control

In Chapter 2 the experiment designed to induce mental stress on human participants in a HMI configuration was introduced. In addition to the modelling aspects of the participants in this study, this work includes a set of control experiments with such participants included in the loop. In fact, the ultimate aim of this work relates to the development of a synergetic approach for modelling and control of humans participants within the framework of a HMI system.

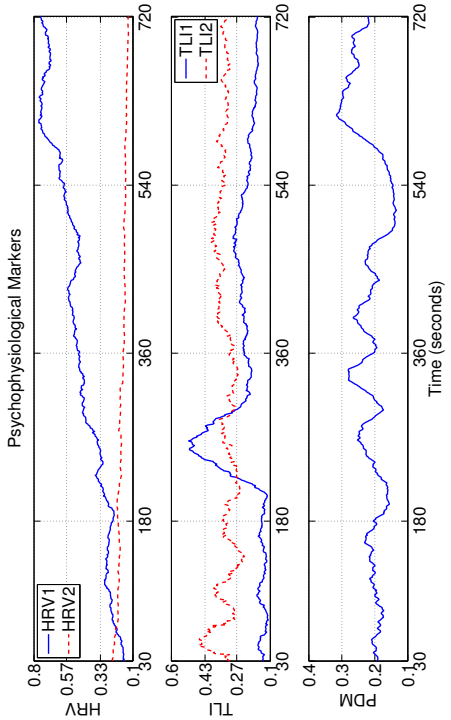

(a)

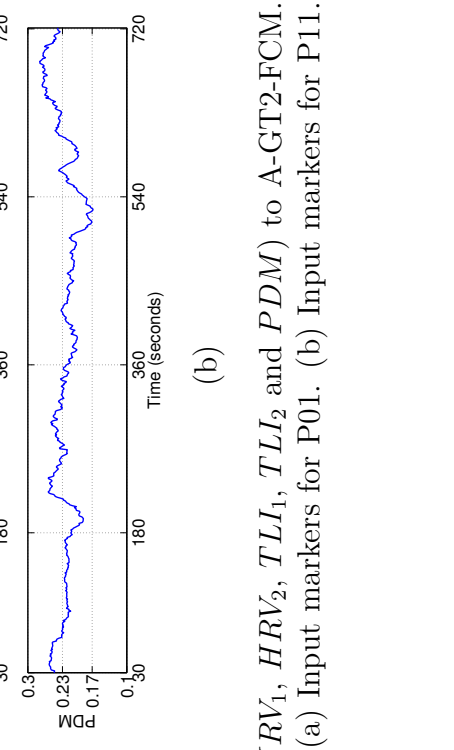

(b)

Figure 5.13: P01 and P11 Psycho-physiological markers inputs (HRV_1, HRV_2, TLI_1, TLI_2 and PDM) to A-GT2-FCM. Scrambled difficulty (ME-2 with $DL = 2, 3, 1, 4$) MA experiment. (a) Input markers for P01. (b) Input markers for P11. Observe intra-differences in marker scaling between P01 and P11.

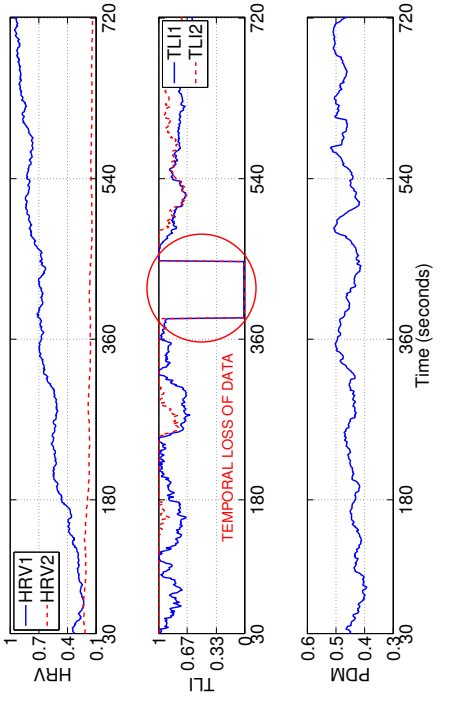

(a)

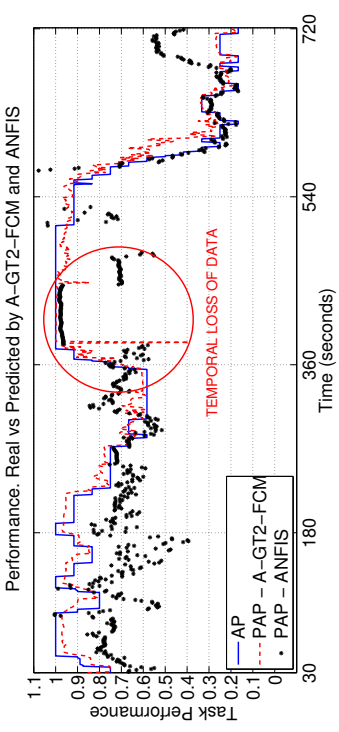

(b)

Figure 5.14: P02 A-GT2-FCM algorithm adaptiveness to temporal loss of data in input TLI markers for ME-2 MA experiment. (a) Input markers for P02. (b) A-GT2-FCM and P02-specific ANFIS modelling results. The effect of the temporal loss of data is signalled with a red circle.

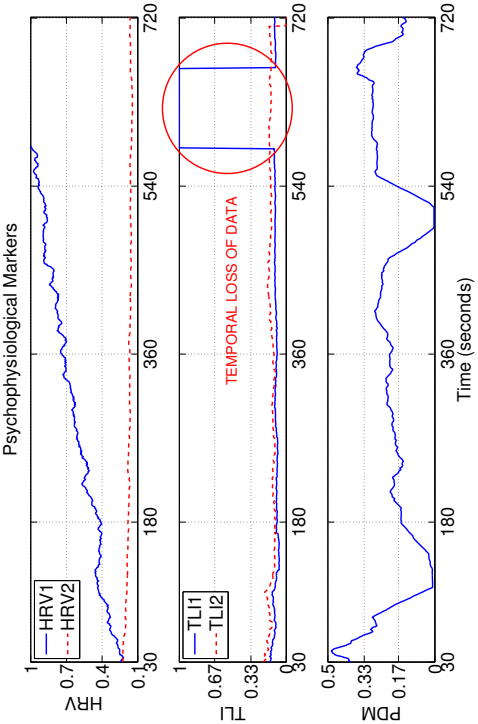

(a)

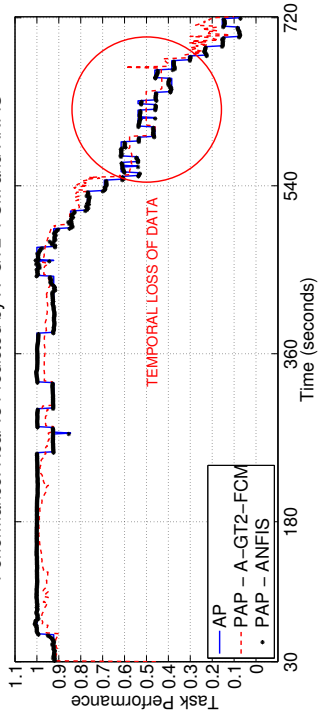

(b)

Figure 5.15: P08 A-GT2-FCM algorithm adaptiveness to temporal loss of data in input TLI1 marker for ME-1 MA experiment. (a) Input markers for P08. (b) A-GT2-FCM and P08-specific ANFIS modelling results. The effect of the temporal loss of data is signalled with a red circle.

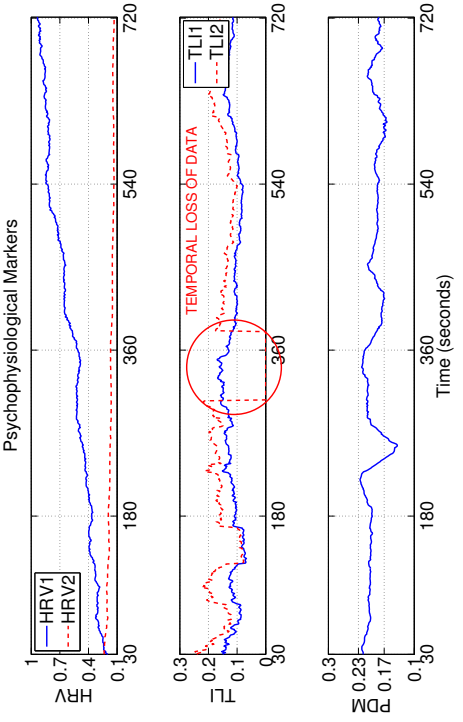

(a)

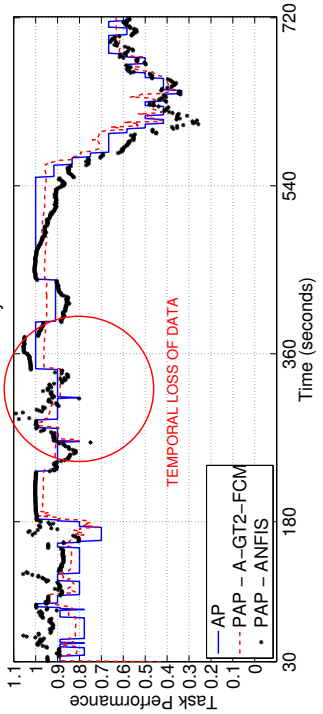

(b)

Figure 5.16: P09 A-GT2-FCM algorithm adaptiveness to temporal loss of data in input TLI1 marker for ME-1 MA experiment. (a) Input markers for P09. (b) A-GT2-FCM and P09-specific ANFIS modelling results. The effect of the temporal loss of data is signalled with a red circle.

In the following sections, two controller designs are presented, namely, the Energy Model-Based Controller (E-MBC) and an ANFIS Model-Based Controller (ANFIS-C). The E-MBC (see Section 5.3.1) is a new controller design that works by interpreting the information learned and stored in the tridimensional rule-base of the A-GT2-FCM modelling framework (see Chapter 4). This new controller design is also compared with an ANFIS model-based controller (ANFIS-C) which uses a simple reference-based control logic that was successfully implemented in [62].

The selection of T2FS as the base for the A-GT2-FCM modelling framework was based on the interpretability properties of fuzzy techniques. Interpretability for adaptive modelling techniques is very important since the model is constructed in an online manner and the information in it is not known before the start of the actual experiment. With fuzzy-based adaptive techniques (with exception to Fuzzy-Neural-Network approaches) the interpretation of the rule-base is possible for the design of intelligent control algorithms.

5.3.1 The Energy Model-Based Controller

The inference process (based on the FCM membership calculation of Equation 4.10) of the A-GT2-FCM algorithm was re-utilised with a series of simple modifications for its use as the Energy Model-Based Controller (E-MBC).

The elicited real-time model includes the learnt system's information. However, the model itself may not directly guide the system into a desired sate accurately; for this task, a controller design that exploits the information in the model is necessary. For the case of the E-MBC, an energy function f_E needs to be defined for an intelligent control approach. The idea behind this function is to maximise 'energy extraction' by directing the system to states with 'maximum energy extraction'. The energy extraction concept may mean different things to different systems. For the

case of the HMI under study, this maximum energy extraction refers to the direction of the human participant into the highest difficulty state without any significant loss in task performance, i.e., this function will guide the system into a desirable operation stage.

With the aid of this energy function f_E, an additional energy membership vector E will be used in combination with the FCM membership C (that directs the inference into the most probable state given present conditions, see Equation 4.11) for the derivation of a control output. Figure 5.17 is a diagram illustrating the E-MBC architecture.

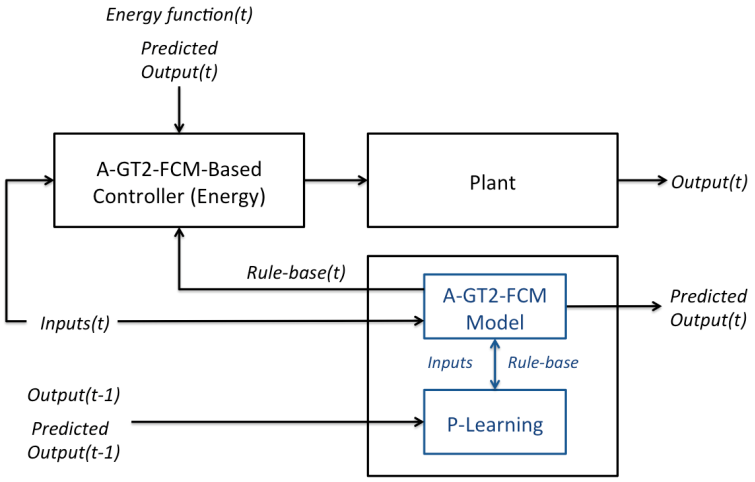

Figure 5.17: Diagram of the Energy Model Based Controller, E-MBC, showing how it uses the information included in the A-GT2-FCM model.

From Figure 5.17 it can be observed how $Output(t-1)$ and $PredictedOutput(t-1)$ are used for the p-learning algorithm (see Section 4.3.4). The current inputs are passed to the inference process of the A-GT2-FCM algorithm to provide the $PredictedOutput(t)$. As can also be observed in the diagram, the E-MBC is based on the rule-base of the A-GT2-FCM model, the $PredictedOutput(t)$ and the $f_E(t)$ to produce a control output that directs the Plant into a desired state.

The inference process in the E-MBC is the following:

1. Obtain the latest rule-base model for use with the controller (Rc and SM) from the A-GT2-FCM and calculate the controller uncertainty-weighted rule-base UNR similarly as in Equation 4.7 with $i = 1, 2, \ldots, r$; and $j = 1, 2, \ldots, d$. Use Rc with the included control variable xc. See the following:

$$Rc = \left[\begin{array}{ccccccc} x_{i1k} & x_{i2k} & \cdots & x_{i(d-2)k} & \boldsymbol{xc_{i(d-1)k}} & : & y_{ik} \end{array} \right]$$

$$UNR_{ij} = \frac{\sum_{m=1}^{g} SM_{im} \cdot Rc_{ijm}}{\sum_{n=1}^{g} SM_{in}}$$

$$UNRc = \left[\begin{array}{c} unxc_1 \\ unxc_2 \\ \vdots \\ unxc_r \end{array} \right] \tag{5.3}$$

where x represent inputs to the system, y represents the output, and $i = 1, 2, \ldots, r$; and $k = 1, 2, \ldots, g$. r is the variable number of rules in the rule-base and g is the variable number that represents the size of the discrete uncertainty dimension. $unxc$ represent the uncertainty-weighted control variable input to the system. As with the case for Equation 4.4, Rc is tridimensional in shape.

2. Obtain an energy membership from the energy function f_E evaluated at each rule in the A-GT2-FCM rule-base (i.e., matrix R and SM). The energy function f_E is defined by the designer to guide the controller towards the desired state and is an application specific function. This membership is calculated as follows:

$$E_i = f_E(unx_{i1}, unx_{i2}, \ldots, unx_{i(d-1)}, uny_i) \tag{5.4}$$

where E is the energy membership vector of size 1-by-r. unx and uny are uncertainty-weighted input and output elements from the uncertainty matrix UNR respectively; for a MISO system and $i = 1, 2, \ldots, r$. The energy membership may use any combination of inputs and output as specified by the designer.

3. Obtain the FCM normalised membership C with the process outlined in step 2 of the A-GT2-FCM inference in Section 4.3 (Equations 4.9 through 4.11).

4. Use the energy membership E in combination with the normalised FCM membership C of Equation 4.11 for the calculation of a control output CO:

$$CO = \frac{\sum_{m=1}^{r} \left(\epsilon E_m + (1-\epsilon)\, C_m\right) \cdot UNRc_m}{\sum_{n=1}^{r} \left(\epsilon E_n + (1-\epsilon)\, C_n\right)} \tag{5.5}$$

where $UNRc$ is the uncertainty-weighted control variable vector of size r-by-1 from the uncertainty matrix UNR. C and E are the FCM and Energy memberships respectively (of size 1-by-r). The constant ϵ is a user-selected weight.

As a requirement, the control variable should be used as an input in the rule-base during the modelling with the A-GT2-FCM modelling framework to ensure its relationship to other variables is stored and learned. The calculation of the CO action re-uses the inference process defined for the modelling framework as should be observed by comparing Equation 5.5 with the A-GT2-FCM inference process of Equation 4.13. The only difference in both Equations resides in the inclusion of the E membership.

5.3.1.1 Energy Model-Based Controller design for the MA operations experiment

This Section presents the specific E-MBC design for the MA operations experiment of the HMI system described in Chapter 2. The E-MBC was tested with the same 10 participants in the real-time modelling experiments of Section 5.2. As previously ex-

plained, the E-MBC reuses the rule-base structure inside the A-GT2-FCM algorithm to operate; for this reason and since the A-GT2-FCM learns from the data in real-time, the E-MBC needs to be provided with an 'experienced' rule-base in order for it to generate meaningful control actions from the start. This requirement translates into a modelling session where no controller is present (open loop mode). Once the most prominent operating regions of the system have been explored and learnt, the E-MBC is able to provide intelligent control actions (closed loop functioning) based on the 'experienced' rule-base structure (R and SM matrices, see Section 4.3).

For the control of the MA operations experiment (Section 2.2.3), the control variable is represented by the Difficulty Level (DL) of the experiment. The A-GT2-FCM works by learning in real-time the most important input-output relationships; for this reason, the DL had to be added as another input for the model (stored inside the A-GT2-FCM rule-base), with the mappings in R (Equation 4.4 with an augmented size of r-by-7-by-g) becoming ($i = 1, 2, \ldots, r; k = 1, 2, \ldots, g$):

$$R = [\ HRV_{1_{ik}} \quad HRV_{2_{ik}} \quad TLI_{1_{ik}} \quad TLI_{2_{ik}} \quad PDM_{ik} \quad DL_{ik} \quad : \quad PAP_{ik}\ ] \tag{5.6}$$

As previously stated, for the E-MBC to operate efficiently and optimally it is important that the fuzzy rule-base (e.g., R and SM) explores and learns from the main operation regions of the system. For the MA experiment specifically, this translates to having experienced all the four difficulty levels. Figure 5.18 shows the diagram of the E-MBC that was designed for the MA experiment.

The E-MBC for the MA experiment used the following inference steps:

1. Use DL (i.e., the control variable) as the control output.

2. Use the PAP (e.g., the output of the model) as an input for the E-MBC.

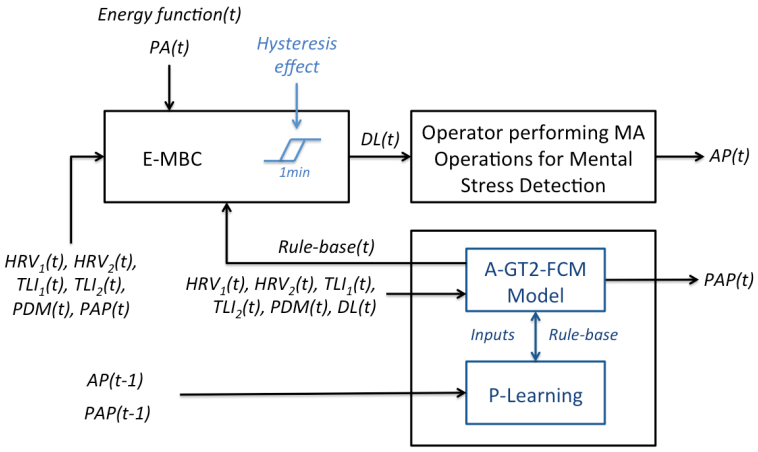

Figure 5.18: Diagram of the Energy Model Based Controller designed for the MA experiment. The diagram shows how E-MBC uses the A-GT2-FCM model information stored in its rule-base and the inclusion of a 1min hysteresis effect.

3. Calculate the UNR matrix with Equation 4.7 and with the augmented R of Equation 5.6 ($i = 1, 2, \ldots, r$):

$$UNR = [\ unHRV_{1_i} \quad unHRV_{2_i} \quad unTLI_{1_i} \quad unTLI_{2_i} \quad unPDM_i \quad unPAP_i \quad : \quad unDL_i\ ] \tag{5.7}$$

4. Define the energy function (f_E) (see Equation 5.4) as dependent on the PAP and the DL:

$$f_E(PAP, DL) = PAP \cdot DL/4 \tag{5.8}$$

5. Calculate the energy membership (E) and normalise it similarly to C in Equation 4.11 ($i = 1, 2, \ldots, r$):

$$\mu_{E_i} = \sum_{m=1}^{r} \frac{unPAP_i \cdot unDL_i}{unPAP_m \cdot unDL_m} \tag{5.9}$$

$$E_i = \frac{\mu_{E_i} - \min(\mu_{E_i})}{\max(\mu_{E_i}) - \min(\mu_{E_i})} \tag{5.10}$$

6. Calculate the FCM membership C following Equations 4.9 to 4.11.

7. Calculate the controller output (CO) using Equation 5.5 with $\epsilon = 0.5$.

The controller is guided with the use of PAP together with the DL (see the energy membership E, Equations 5.9 and 5.10). The use of these variables is driven by the fact that the control should maximise the DL without compromising on accuracy. The ideal state (e.g., maximum DL without great loss in AP) for each participant is variable, and is influenced by his/her personal ability and current state identified through the psychophysiological markers and the PAP from his derived A-GT2-FCM model. Another important feature of the E-MBC designed for the MA experiment is its use of a 1 min hysteresis that ensures that control actions have enough time to have a causal effect on the participant and to avoid 'bang-bang' control effect.

In order to visualise the ideal PAP-DL combination, Figure 5.19 shows the normalised outcomes for the defined energy function $f_E(PAP, DL)$. In this Figure it can be seen how the ideal state corresponds to $DL = 4$ with an $PAP = 1$. As will be seen in the results of the online real-time control experiments, this DL proved to be a challenge for all participants; making a lower DL their ideal level of performance. It is worth noting that performance is significantly affected by the varying psychophysiological state of the participant (e.g., influenced by fatigue, time of day, engagement, etc.); this is the part where the adaptive knowledge of the model output contributes most.

5.3.2 A-GT2-FCM real-time modelling and E-MBC for Mental Arithmetic operations experiment

This Section is concerned with the results for the real-time implementation of the E-MBC for the 10 participants in the MA operations experiment. As previously outlined, before the actual E-MBC experiments were performed, a sufficiently 'experi-

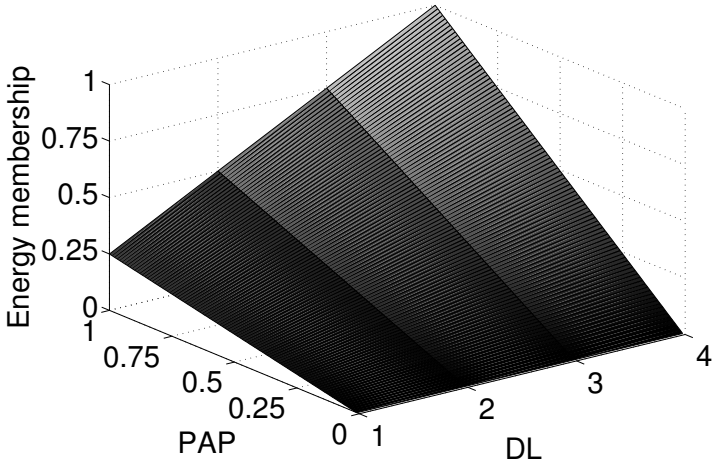

Figure 5.19: Membership for the energy function $f_E(PAP, DL)$.

enced' model had to be derived with the A-GT2-FCM modelling algorithm. For this purpose, the data obtained during ME-1 was used in an off-line real-time-simulated experiment to obtain one initial model for each of the 10 participants in the study. These models were later used for the E-MBC real-time experiments, obtaining the results presented from Figures 5.20 through 5.29. It should be noted that these initial derived models suffer changes during the actual E-MBC experiments; these changes resulting from the adaptive properties of the A-GT2-FCM modelling framework that evolves to provide the most current description of the current state of the participant in the experiment.

In order to illustrate the E-MBC capability, most experiments included disturbances (represented by a finite number of forced changes in DL) which were introduced at time stamps $t = \{180, 360, 540\}$ and identified with an asterisk on the next plots. In all Figures, the bottom plot corresponds to the energy membership E, included to illustrate the changes in the 'extracted energy' amount with the objective of evaluating the benefit of the control action. It should also be noted that the CO changes the DL with 1 min intervals due to the implementation of a hysteresis period, which

was introduced to ensure the participants had enough time to respond and adapt to the new state.

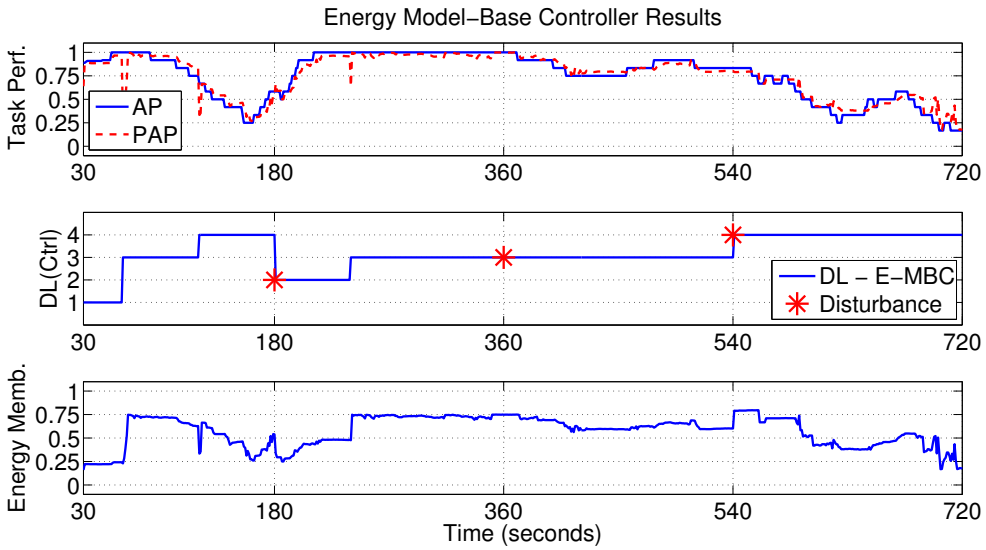

Figure 5.20: E-MBC real-time experiment for P01. Disturbances identified with an asterisk.

In Figure 5.20 it can be seen how the E-MBC quickly identified $DL = 3$ as the best state for P01. After a period of increased 'energy extraction' the E-MBC selects $DL = 4$, lowering the amount of 'extracted energy'. As should be observed, this is not the best decision, a fact that is learned by the E-MBC, which reduces the DL from $t = 180$ towards $t = 540$. Again, after the last disturbance at $t = 540$ the new performance information experienced by the E-MBC showed that $DL = 4$ increased the 'energy extraction'. This new state influenced the decision of the E-MBC to remain at $DL = 4$ throughout the remaining of the experiment.

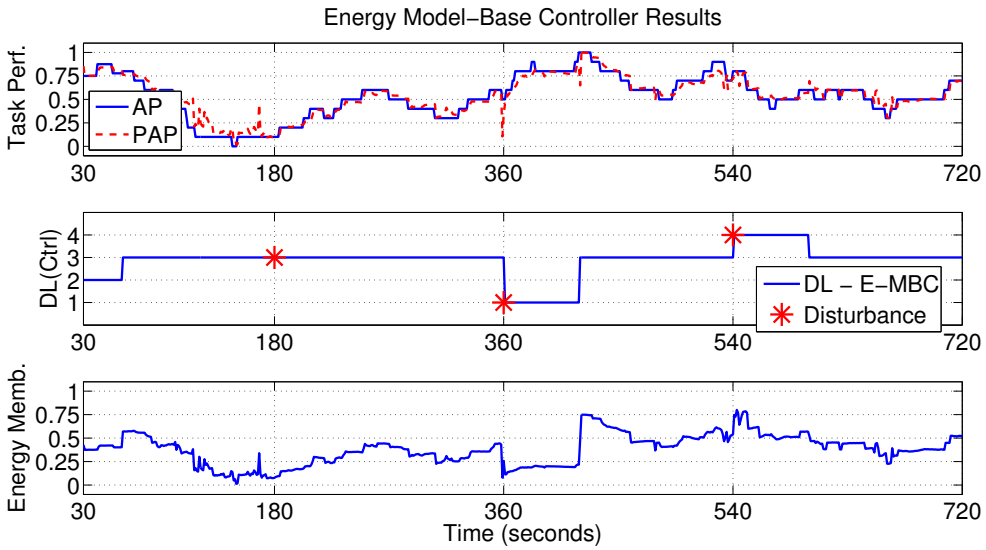

Figure 5.21: E-MBC real-time experiment for P02. Disturbances identified with an asterisk.

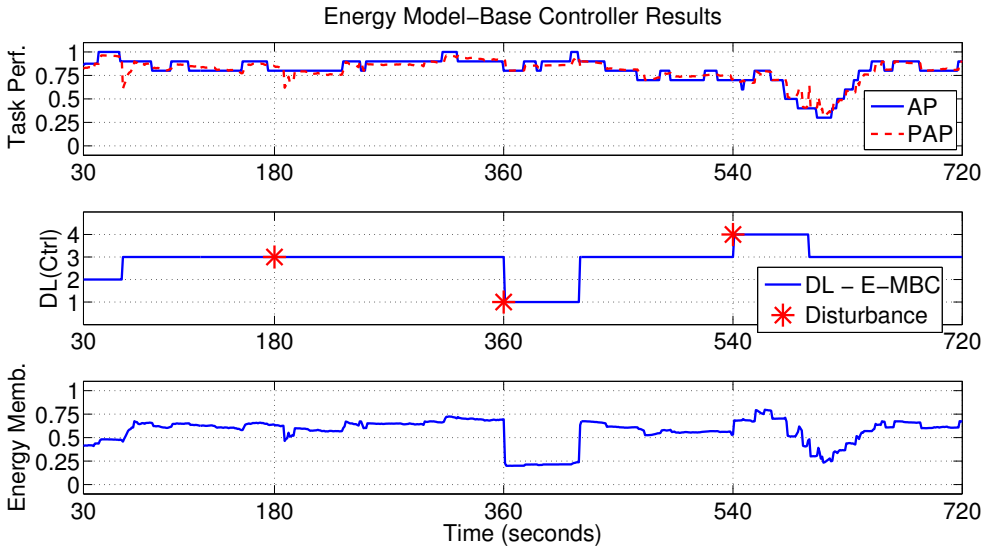

Figure 5.22: E-MBC real-time experiment for P03. Disturbances identified with an asterisk.

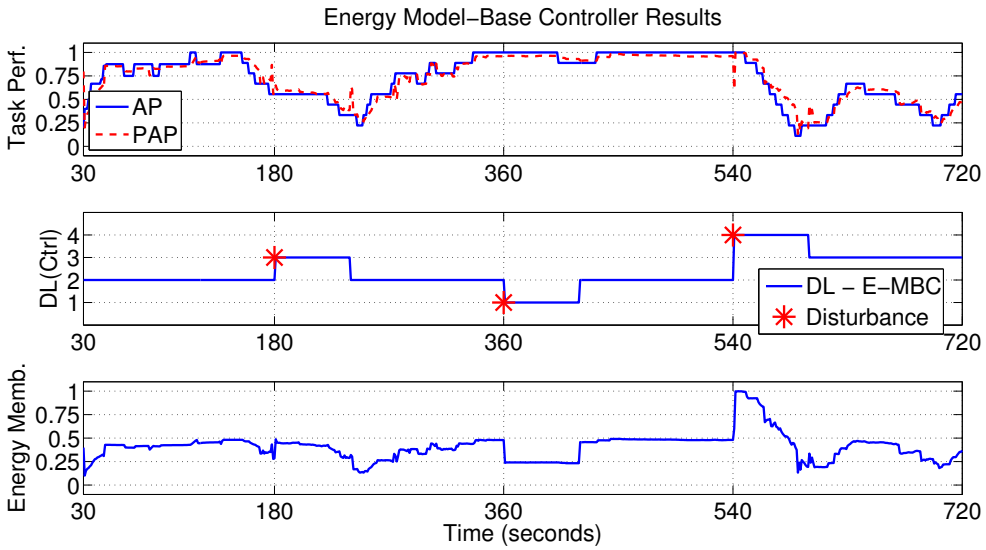

Figure 5.23: E-MBC real-time experiment for P06. Disturbances identified with an asterisk.

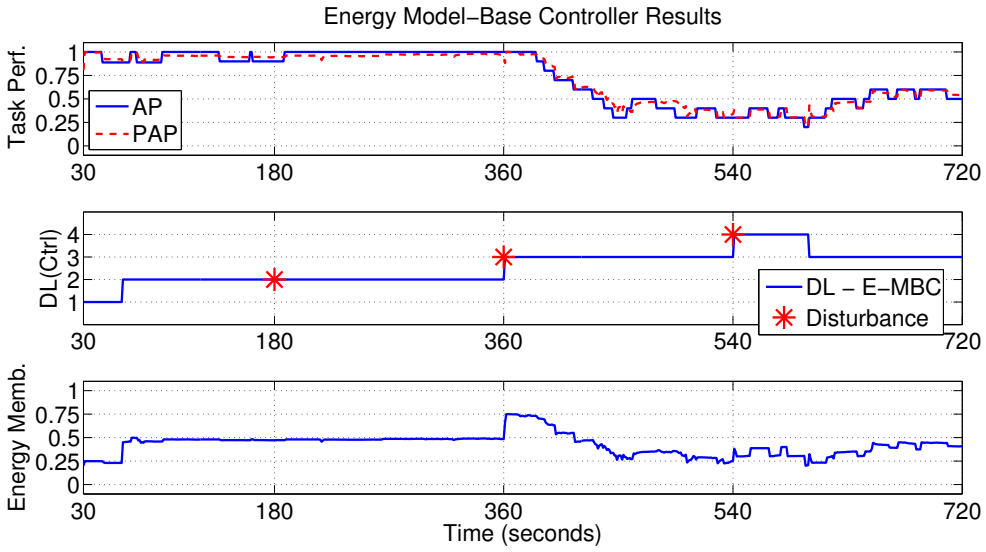

Figure 5.24: E-MBC real-time experiment for P07. Disturbances identified with an asterisk.

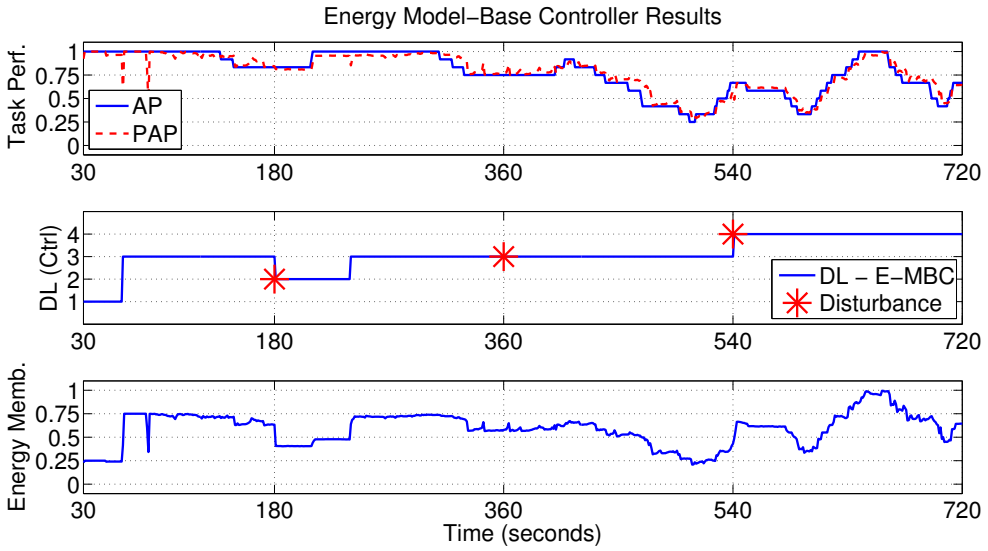

Figure 5.25: E-MBC real-time experiment for P08. Disturbances identified with an asterisk.

Figure 5.25 illustrates the implementation of the E-MBC in real-time for P08 in the study; with disturbances identified with an asterisk. In this Figure, the E-MBC identified that the best performance was achieved at $DL = 3$ (similarly to Figure 5.28 for P01 and P11) by interpreting P08 ability from the information stored in its rule-base (learned from the data contained in ME-1). From previous experience, the E-MBC avoids $DL = 4$ during most of the experiment. However, after the disturbance at $t = 540$ the E-MBC adapted by leaving the $DL = 4$ unchanged given new experience of increased ability from P08. This example highlights the advantage of an adaptive controller that responds to changes in the human behaviour of P08 (inter-parameter variability).

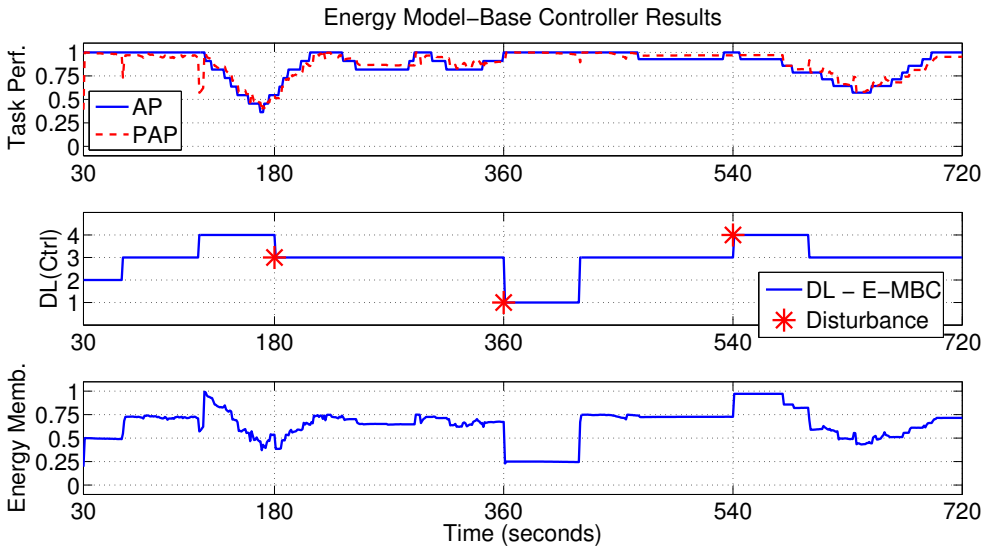

Figure 5.26: E-MBC real-time experiment for P09. Disturbances identified with an asterisk.

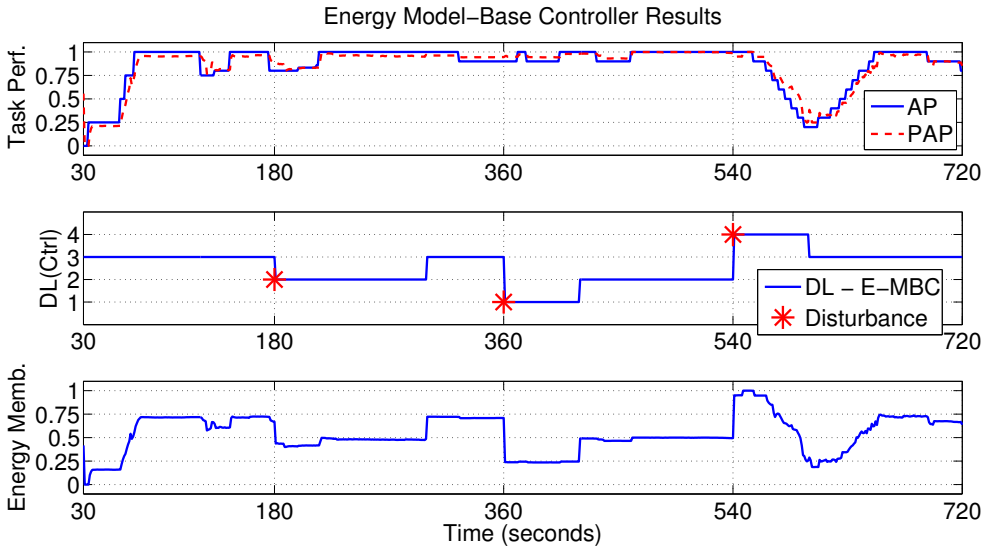

Figure 5.27: E-MBC real-time experiment for P10. Disturbances identified with an asterisk.

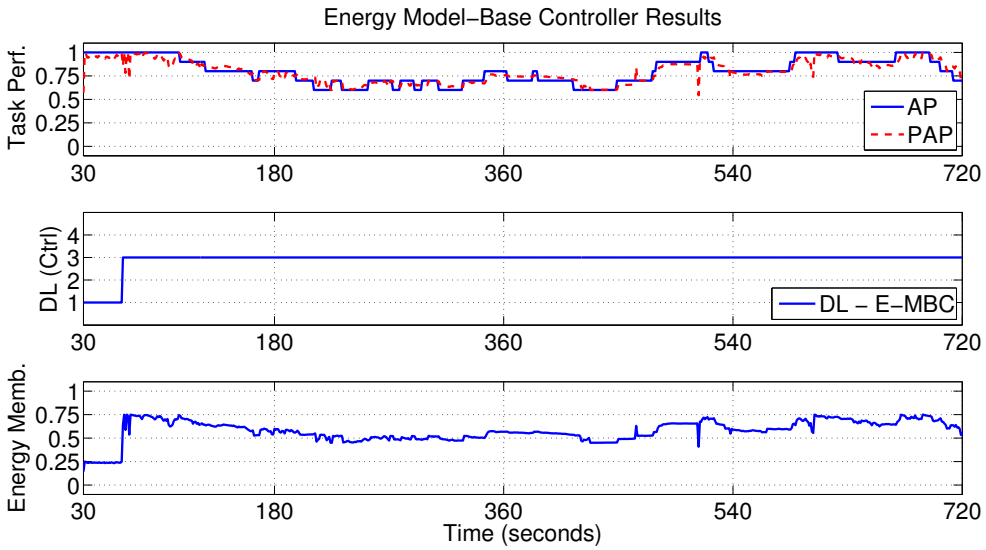

Figure 5.28: E-MBC real-time experiment for P11. Disturbances identified with an asterisk.

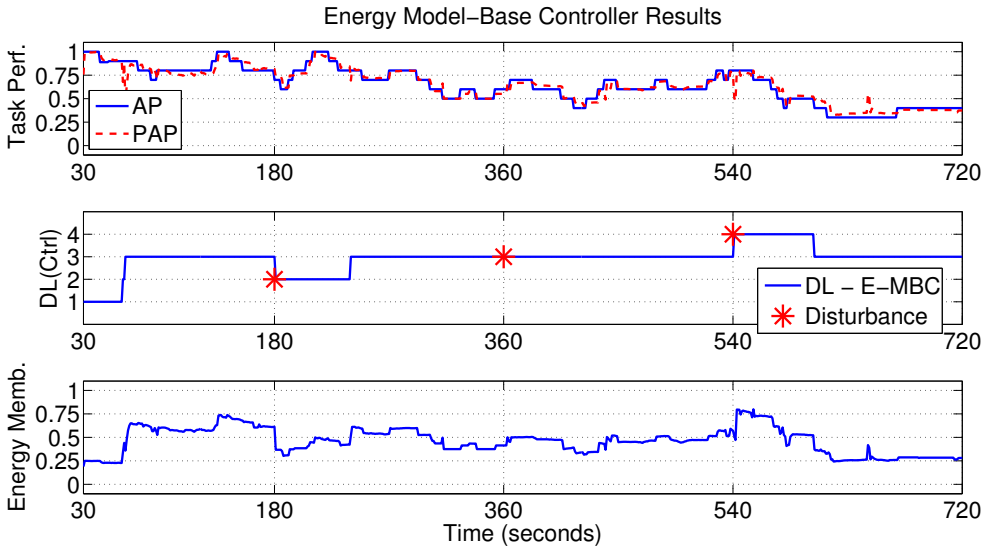

Figure 5.29: E-MBC real-time experiment for P12. Disturbances identified with an asterisk.

From Figure 5.28 it can be observed that after one minute of operation the E-

MBC selected $DL = 3$ from an initial $DL = 1$ as the best combination of PAP and the highest DL (following the logic in the energy function $f_E(PAP, DL)$). After the selection of this DL there was an increase in the energy extraction that was maintained throughout the experiment. This experiment was performed without any inclusion of disturbances.

From the various examples of the implementation of the E-MBC for all participants in the study, it can be observed how this adaptive and intelligent approach contributes positively and effectively towards the control law defined by f_E, maximising 'energy extraction' throughout. In order to validate the importance of the obtained results, the next Section compares the E-MBC with a similar implementation with the well-known ANFIS approach.

5.3.3 Comparison with an ANFIS Model-Based Controller

This Section addresses the controller validation results of the E-MBC when compared with an ANFIS model-based controller (ANFIS-C) to show how intelligent and adaptive properties contribute towards an increase in participant performance. The ANFIS-C design was based on the work of [62], where predictions from a fuzzy modelling framework were used together with a reference-based control approach. The ANFIS-C is based on the same reference configuration, but with last minute averaged predicted performance from fixed ANFIS models to select the DL as the control output. The ANFIS-C is governed by the following steps [62]:

1. Obtain mean of last minute of PAP by participant-specific ANFIS model.
2. If $PAP > 0.9$, then $DL = DL + 1$; with maximum $DL = 4$.
3. Else if $PAP < 0.6$, then $DL = DL - 1$; with minimum $DL = 1$.
4. Else, DL remains unchanged.

The ANFIS-C was tested in real-time for all ten (10) participants in the study, following the same disturbance profiles to the ones implemented for the E-MBC. It is important to note that a like-for-like experiment is not possible since participants perform differently on each experiment session (real-time mode), however, all experiments were carefully performed so as they would follow the same experiment criteria (i.e., same Disturbance locations, same length, same DL structure).

As already shown in Section 5.2, a fixed model was not able to completely capture the inter- and intra- parameter variabilities in humans on a HMI system. However, for some specific cases (e.g., P08, P09, P10 and P11) the prediction results obtained with the participant-specific ANFIS fixed-models show an acceptable performance both in training and validation. It is important to note that the ANFIS-C controller is fully dependent on the quality of its ANFIS predictions, and as will be observed, its performance suffers whenever there is a change in the participants' parameters.

Figures 5.30 through 5.39 show the comparisons between the E-MBC and the ANFIS-C. Every Figure presents the prediction performance of both modelling techniques (e.g., A-GT2-FCM and participant-specific ANFIS), the controllers output (e.g., CO for E-MBC and for ANFIS-C), including a comparative plot of the Energy Memberships for both controllers.

ANFIS-C results for P02 (Figure 5.31) show how good P02-specific predictions positively impact the controller's action. In this Figure one can observe how both controllers are very similar in their control output (DL). However, it is important to stress the advantage in the use of the Energy Membership (E-MBC) that can be appreciated during the last minute of Phase 1 ($t = 30$ to $t = 180$). During this period, the ANFIS-C selects $DL = 4$ given the last minute average performance for P02 (over 90%). As can also be observed, this happens to be the wrong selection given the reduction in performance that follows soon after. For the E-MBC, this

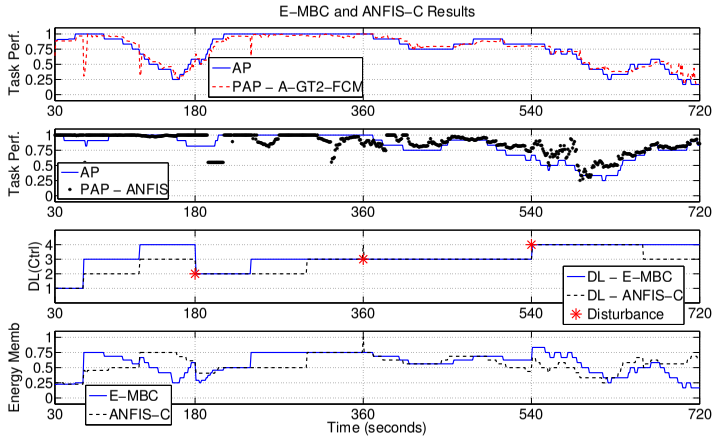

Figure 5.30: P01 Comparative E-MBC and ANFIS-C real-time control experiment results.

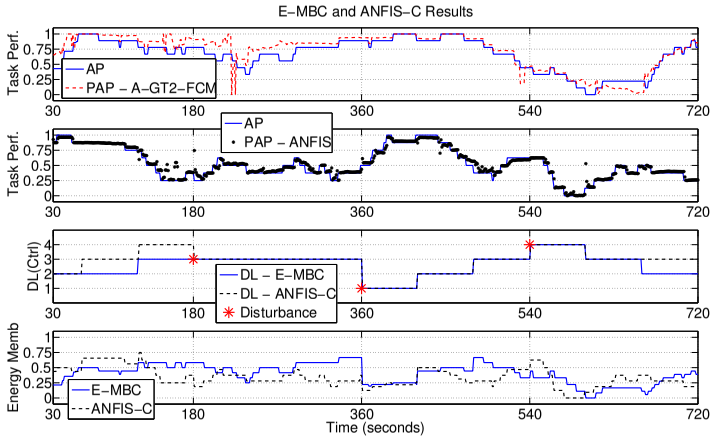

Figure 5.31: P02 Comparative E-MBC and ANFIS-C real-time control experiment results.

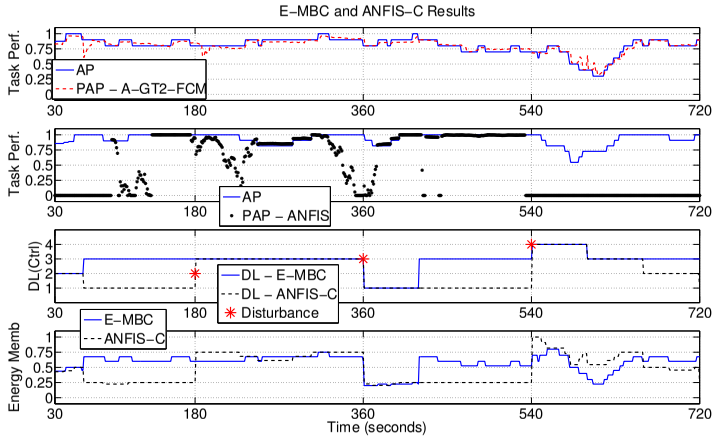

Figure 5.32: P03 Comparative E-MBC and ANFIS-C real-time control experiment results.

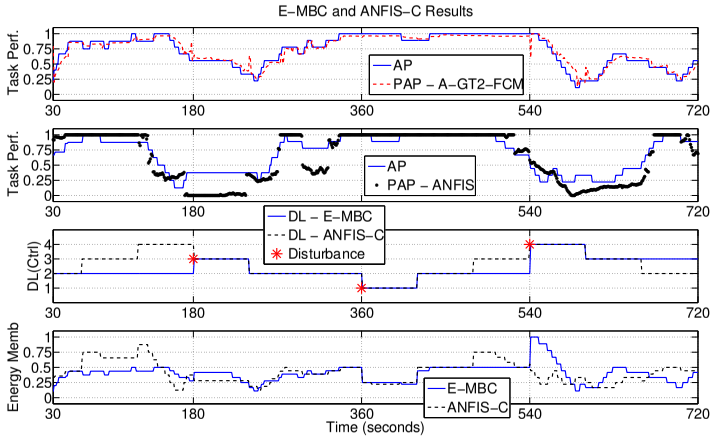

Figure 5.33: P06 Comparative E-MBC and ANFIS-C real-time control experiment results.

is not the case, since this controller knows from previous experience that $DL = 4$ would be too challenging for this participant, hence avoiding it throughout the whole experiment.

From Figure 5.34 a different scenario can be observed. Here, the P07-specific ANFIS model bad predictions negatively impacted on the operation of the ANFIS-C. During Phase 1 ($t = 30$ to $t = 180$) errors in the predictions made the ANFIS-C select the control output as $DL = 1$, hence generating a reduced energy extraction. Again, for Figure 5.35 we can observe prediction errors for the P08-specific ANFIS model during Phase 4 ($t = 540$ to $t = 720$). These bad predictions lead to ANFIS-C maintaining $DL = 4$ throughout the rest of this phase, leading to reduced energy extraction as can be identified in the bottom plot. For the E-MBC we can observe that during Phase 4 this controller also maintained DL equal to 4. However, in this case, this action was not derived from bad predictions, but from the adaptation to the new good performance experience observed after the last disturbance. Before this Phase we can observe that the controller selected $DL = 3$ for its operation throughout, following its previous experienced past performance (gathered in the rule-base of the A-GT2-FCM model).

Figure 5.38 shows the controller results comparison for P11. From this Figure it can be observed that despite having acceptable predictions, ANFIS-C increases the control DL in the second stage ($t = 180$s to $t = 360$s), which leads to a significant reduction in the task performance. This example also illustrates the importance of accurate performance predictions and model interpretability (e.g., the Energy Membership) at each operation stage in order to avoid reductions in accuracy and to maximise 'energy extraction'. In this respect the ANFIS-C is disadvantageous since it is only based on performance and does not consider the ideal $PAP-DL$ combination (i.e., the Energy Membership) for each participant. With respect to the E-MBC it

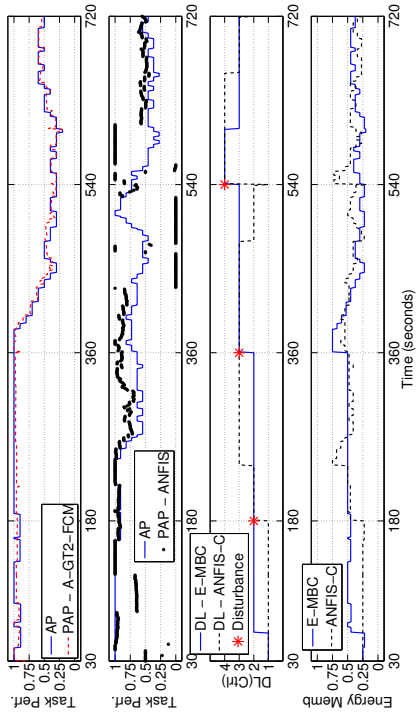

Figure 5.34: P07 Comparative E-MBC and ANFIS-C real-time control experiment results.

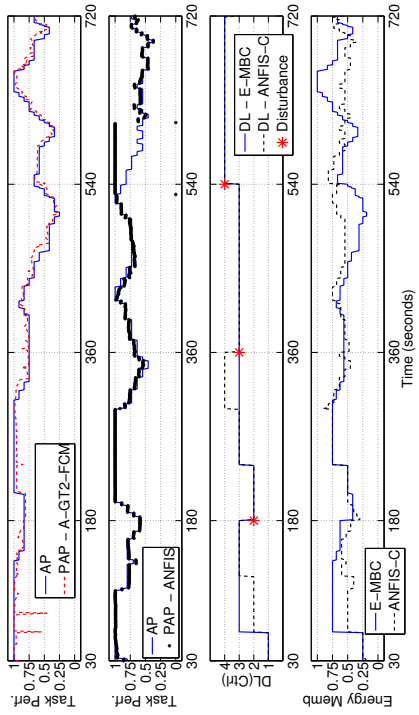

Figure 5.35: P08 Comparative E-MBC and ANFIS-C real-time control experiment results.

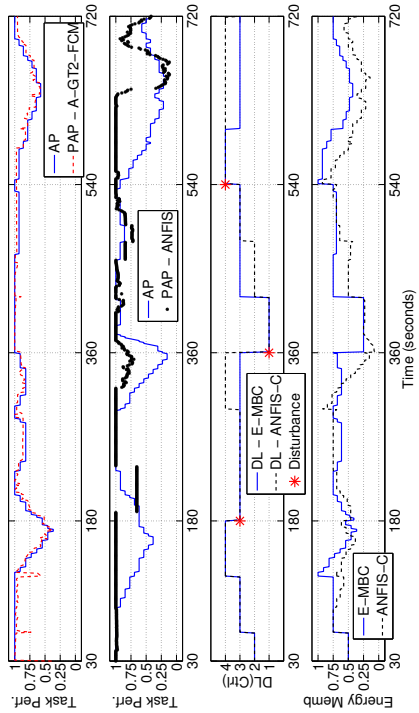

Figure 5.36: P09 Comparative E-MBC and ANFIS-C real-time control experiment results.

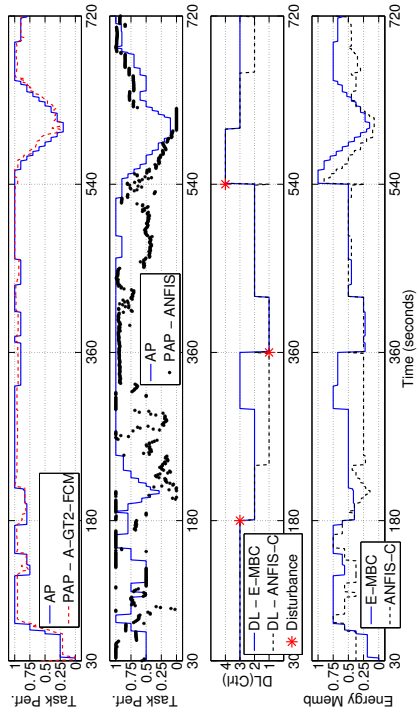

Figure 5.37: P10 Comparative E-MBC and ANFIS-C real-time control experiment results.

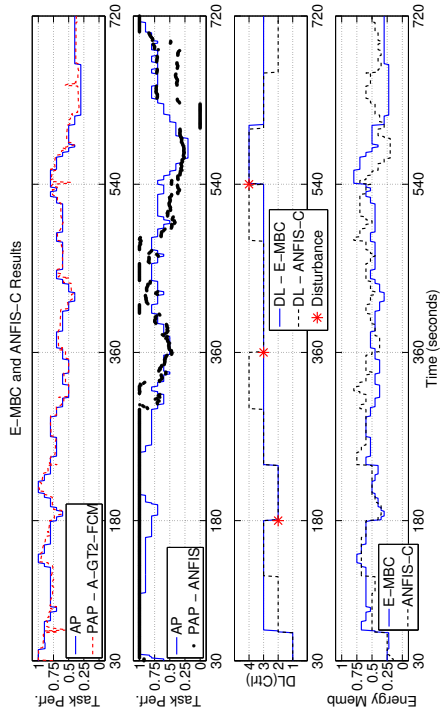

Figure 5.39: P12 Comparative E-MBC and ANFIS-C real-time control experiment results.

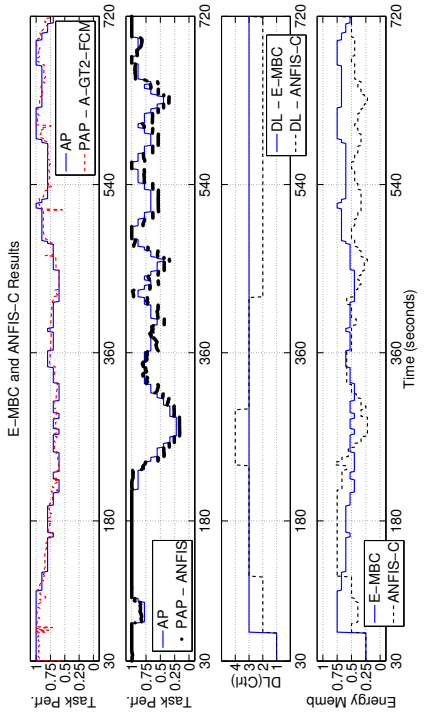

Figure 5.38: P11 Comparative E-MBC and ANFIS-C real-time control experiment results.

Control Energy Extraction Mean			
	ANFIS - C	E-MBC	No Control
	ME-1 (Disturbance profile)		
P01	0.5558	0.5699	0.4568
P07	0.4048	0.4247	0.2811
P08	0.5730	0.5848	0.4681
P12	0.5146	0.4614	0.3500
	ME-2 (Disturbance profile)		
P02	0.4049	0.3722	0.4046
P03	0.4760	0.5706	0.4104
P06	0.4163	0.4020	0.3340
P09	0.5286	0.6402	0.4969
	Disturbance profile: $DL = 3, 2, 1, 4$		
P10	0.3951	0.5389	-
	No disturbance profile		
P11	0.4722	0.5809	-
Avg.	0.4741	0.5146	0.4002

Table 5.3: Energy extraction means for all participants in the real-time control experiments with the E-MBC, the ANFIS-C and without controller.

is observed how the knowledge of the ideal Energy Membership contributes to an increased 'energy extraction'. In fact, for this example, the average energy extraction for the E-MBC is of 0.5809, while for the ANFIS-C it is of 0.4722.

Similar results to those described in the previous lines can be observed for the remaining participants' control results. In order to demonstrate numerically the increase in 'energy extraction', Table 5.3 presents the average energy extraction values for all real-time control experiments with the E-MBC, the ANFIS-C and with no controller (i.e., corresponding to the DL profiles of ME-1 or ME-2 of the real-time modelling experiments of Section 5.2).

From Table 5.3 it can be observed how for all participants with the exception

of P02, E-MBC leads to an improvement in the amount of energy extracted when compared with the energy extraction without control. When compared with ANFIS-C, E-MBC shows better energy extraction in most cases. Overall, and for these ten (10) cases, there is an increase in energy performance as can be observed in the average values at the bottom of the Table. Furthermore, Figure 5.40 shows the energy extraction results for P03 in the study with and without control. From this Figure it can be observed that during the experiment, the real energy membership was mostly higher in the case of E-MBC. This is also evident from Table 5.3 for the mean energy extraction values for P03. This demonstrates how control actions derived from accurate predictions and model interpretability result in an increase in energy extraction.

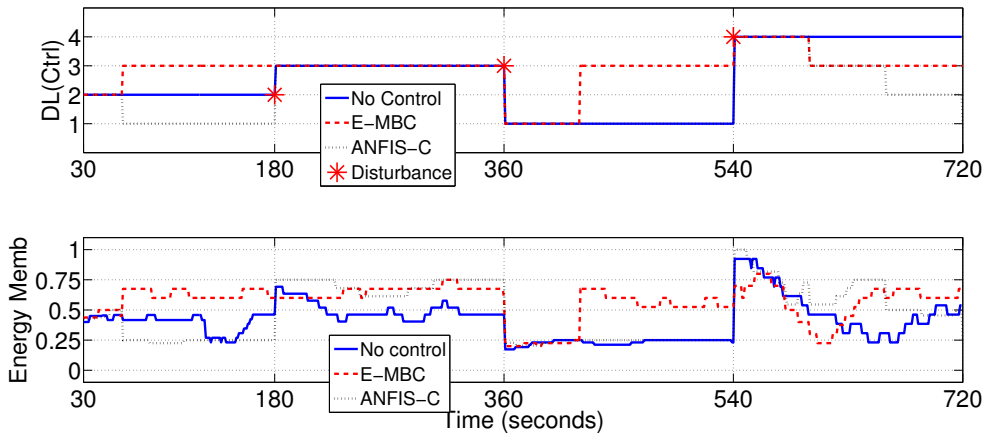

Figure 5.40: Energy extraction results in real-time for P03 with and without controllers. Difficulty level profiles (top plot) and real energy membership (bottom plot).

5.4 Summary

This Chapter presented the application of the A-GT2-FCM modelling algorithm (Chapter 5) for the HMI configuration of operators performing a MA operations

based experiment as described in Chapter 2. Additionally, this Chapter also presented a new architecture in which the interpretability property of the fuzzy rule-base in the A-GT2-FCM can be used for control purposes. This new control algorithm was referred to here as the Energy Model-Based Controller (E-MBC) since it makes use of an 'energy membership' to guide the system into 'maximum energy extraction' operating regions as defined by the designer with an energy function. Both algorithms, i.e., the A-GT2-FCM and the E-MBC, demonstrated much improved performances for the modelling and control of operators performing mental stress tasks as compared with ANFIS participant-dependent constructed models and with participant-specific ANFIS model-based controllers (ANFIS-C). The adaptive properties of the A-GT2-FCM modelling algorithm were also addressed in this Chapter by demonstrating the way the model learns in real-time and how an updated interpretable rule-base impacts in the E-MBC mechanism.

In the next and final Chapter, the conclusions and research recommendations relating to this study are presented.

Chapter 6

CONCLUSIONS AND RECOMMENDATIONS

6.1 Conclusions

This study started by introducing the role of the human operating inside a Human-Machine Interaction System (HMI), the Psychophysiology an Ergonomics fields of study, and the modelling difficulties of these systems. The most commonly used psychophysiological markers for the detection of mental stress (e.g., cognitive load) were also highlighted by describing the characteristics of Heart Rate Variability (HRV) and its two main calculation methods (e.g., HRV1 and HRV2), together with the Task Load Index (TLI) under two configurations as well (e.g., TLI1 and TLI2). The use of a new marker, the Pupil Diameter Marker (PDM), was investigated with the introduction of a statistical-based series of real-time experiments for the validation of its mental load predictive power. This new marker was also compared to HRV and TLI under the same experimental configuration to demonstrate its contribution as an additional valuable marker for the detection of incremental levels of mental

stress.

The experimental design selected to produce mental stress on the HMI configuration was also introduced, namely, the Mental Arithmetic (MA) operations experiment. This work stressed that the MA experiment was capable of producing 'stress entrainment' of participants as evidenced by the previously published literature and validated via statistical tests. Furthermore, it should also be stressed that this experiment design is simple enough to be replicated for validation with no training required for participants. A Graphical-User-Interface-based (GUI) software, the Mental Stress Evaluation (MSE) GUI was designed for the deployment of the experiment as well. This system was capable of handling all processes in the experiment that ranged from the acquisition of key psychophysiological markers, signal processing aspects, to intelligent modelling and real-time control calculations, achieving fast computations able to respond to the requirements of the deployment of the MA experiment in real-time.

The main contribution of this work is the introduction of a new modelling technique named Adaptive General Type-2 Fuzzy C-Means, proposed and applied to modelling humans undergoing psychological (mental) stress. This new modelling technique was compared with participant-specific trained ANFIS models, and was shown to lead to superior predictions for all participants. The design of the A-GT2-FCM technique incorporates features that make it adaptive to inter- and intra- parameter variability across subjects. This capability arises from its performance-learning algorithm based on negative Reinforcement Learning. Its implementation in real-time was possible given its restructured inference mechanism based on the Fuzzy C-Means algorithm that can fully handle uncertainty under this configuration. The performance-learning algorithm proved its ability in the extraction of features from data in real-time, taking advantage of the capability of Type-2 Fuzzy Sets (T2FS)

to truly handle uncertainty. For all ten (10) participants in the study, successful modelling was achieved with a small error and a high correlation with the actual performance.

A controller design that re-exploits the A-GT2-FCM inference mechanism and information in the form of its tridimensional fuzzy rule-base was also presented. This controller, named Energy Model Based Control (E-MBC) incorporates an Energy-based Membership that allows it to acquire maximum 'energy extraction'. Evidence to the controller's good performance was presented and compared with another set of real-time experiments of the same structure performed with a participant-specific ANFIS prediction-based reference control. E-MBC achieved superior performance with an increase in the extraction of 'energy' for experiments without control.

The validated in real-time and through comparison modelling and control techniques (e.g., A-GT2-FCM and E-MBC) presented in this work, highlighted the importance of the use of adaptive models with self-organising properties for such harsh environments as the HMI system under investigation. This work stressed the fact that fixed models are simply not able to handle applications characterised by uncertainty and significant inter/intra subject parameter variability, hence proving emphatically the robustness of the new design for fast adaptive modelling and control techniques such as the A-GT2-FCM and E-MBC.

The results of this study show true promise in the further evaluation of the A-GT2-FCM modelling framework for applications with similar characteristics in the field of HMI. Furthermore, the simplicity of the designed inference mechanism makes it truly open to new and exciting control configurations for the many other challenging real-world environments where man-machine synergies and the switching between manual control and automation in real-time to avoid operator breakdown are of paramount importance.

6.2 Further recommendations for research

The application of adaptive and intelligent modelling/control techniques to HMI configurations as the one studied in this work is particularly important because of the indirect nature of acquired signals for the detection of human stress (i.e., physical or mental). From this viewpoint, the study of new bio-markers that may lead to an improved understanding of the complex processes inside the human body is of paramount importance. In this work, the inclusion of the pupil size measurement marker (i.e., the PDM) as an incremental detector of mental stress represented a new research direction, however, there are yet many more markers to explore that have not received much attention even on the presence of supportive evidence of their predictive power; one of these being the heat-footprints acquired from images of the face of operators performing mentally stressful tasks. As a recommendation for future research focused in the improvement of the quality of the models constructed for HMI, other markers should be explored in addition to the ones investigated previously. Additionally, researchers should try to answer more specific questions regarding the nature of mental stress with carefully designed experiments for this purpose, since to this date, no clear understanding of its complex structure exists.

On the development of new modelling/control algorithms for a much broader field of applications, the Adaptive General Type-2 Fuzzy C-Means algorithm renders itself as a methodology yet to be fully explored. The presented algorithm answered one of the most important questions in the field of type 2 fuzzy logic, i.e., the type-reduction issue. However, since this work presented a validation through experimentation only, a mathematical proof of convergence for the learning properties of the A-GT2-FCM p-learning algorithm is still required. For a fully generalising algorithmic structure within a broader application range, this mathematical solution needs indeed to be explored in detail.

Bibliography

[1] C. E. Billings, Aviation Automation: The Search for a Human-Centered Approach. Lawrence Erlbaum Associates, Mahwah, 1996.

[2] T. B. Sheridan, Humans and Automation: System Design and Research Issues. Willey, Santa Monica, 2002.

[3] P. A. Hancock and Desmond, P. A., Stress, Workload, and Fatigue. Lawrence Erlbaum Associates, Mahwah, 2001.

[4] P. A. Hancock, "On the process of automation transition in multitask human–machine systems", IEEE Transactions on Systems, Man and Cybernetics, Part A: Systems and Humans, Vol. 37, No. 4, pp. 586–598, 2007.

[5] N. Meshkati, "Control rooms' design in industrial facilities", Human Factors and Ergonomics in Manufacturing Journal, Vol. 13, No. 4, pp. 269-277, 2003.

[6] O. Uncu and I. B. Turksen, "Discrete Interval Type 2 Fuzzy System Models Using Uncertainty in Learning Parameters", in IEEE Transactions on Fuzzy Systems, Vol. 15, No. 1, pp. 90-106, Feb. 2007.

[7] C. H. Ting, M. Mahfouf, D. A. Linkens, A. Nassef, P. Nickel, A. C. Roberts, M. H. Roberts and G. R. J. Hockey, "Real-time Adaptive Automation for Performance Enhancement of Operators in a Human Machine System", in IEEE 16th

Mediterranean Conference on Control and Automation, Ajaccio, pp. 552-557, 2008.

[8] C. H. Ting, M. Mahfouf, A. Nassef, D. A. Linkens, G. Panoutsos, P. Nickel, A. C. Roberts and G. R. J. Hockey, "Real-Time Adaptive Automation System Based on Identification of Operator Functional State in Simulated Process Control Operations", IEEE Transactions on Systems, Man and Cybernetics, Vol. 40, No. 2, pp. 251-262, 2010.

[9] A. Roberts, M. Roberts, B. Hockey, P. Nickel, A. Nassef, M. Mahfouf, D. Linkens and C. H. Ting, "Real-Time Adaptive Control of Automation in Response to Operator Strain", *Annual Meeting of Human Factors and Ergonomics Society Europe Chapter*, The Netherlands, 2008.

[10] M. Mahfouf, J. Zhang, D. A. Linkens, A. Nassef, P. Nickel, G. R. J. Hockey and A. C. Roberts, "Adaptive Fuzzy Approaches to Modelling Operator Functional States in a Human-Machine Process Control System", *IEEE International Conference on Fuzzy Systems London*, pp. 234 - 239, London, July 2007.

[11] A. Nassef, C. H. Ting, M. Mahfouf, D. A. Linkens, P. Nickel, G. R. J. Hockey and A. C. Roberts, "A New Framework for Real-Time Adaptive Fuzzy Monitoring and Control for Humans under Psychophysiological Stress", *BIOSIGNALS 2008, International Conference on Bio-inspired Systems and Signal Processing*, pp. 320 - 325, Portugal, January 2008.

[12] A. Nassef, "On-line Monitoring and Adaptive Control of Psychophysiological Markers Relating to Humans under Stress", unpublished doctoral dissertation, University of Sheffield, Sheffield, UK, 2009.

[13] L. A. Torres-Salomao, M. Mahfouf and O. Obajemu, "Interval Type-2 Fuzzy Logic Adaptive Modelling for Human Operators Undergoing Mental Stress", in Proceedings of 19th World Congress of the International Federation of Automatic Control, Cape Town, pp. 9880-9885, 2014.

[14] R. M. Stern, W. J. Ray and K. S. Quigley, Psychophysiological Recording, New York : Oxford University Press, 2001.

[15] J. T. Cacioppo, L. G. Tassinary and G. Berntson, Handbook of Psychophysiology, New York : Cambridge University Press, 2007.

[16] J. R. Stroop, "Studies of Interference in Serial Verbal Reactions", Journal of Experimental Psychology, Vol. 121, No. 1, pp. 15-23, 1992.

[17] W. J. Kop, D. S. Krantz, R. H. Howell, M. A. Ferguson, V. Papademetriou, D. Lu, J. J. Pompa, J. F. Quigley, M. Vernalis and J. S. Gottdiener., "Effects of Mental Stress on Coronary Epicardial Vasomotion and Flow Velocity in Coronary Artery Disease: Relationship With Hemodynamic Stress Responses", Journal of the American College of Cardiology, Vol. 37, No. 5, pp. 1359-1366, 2001.

[18] S. Akselrod, D. Gordon, F. A. Uvel, D. Shannon, C. A. Barger and R. J. Cohen, "Power Spectrum Analysis of Heart Rate Fluctuation: A Quantitative Probe of Beat - To - Beat Cardiovascular Control", Science, Vol. 213, No. 4504, pp. 220-222, 1981.

[19] Y. Kuriyagawa and I. Kageyama, "A Modelling of Heart Rate variability to Estimate Mental Work Load", IEEE International Conference on Systems, Man and Cybernetics, Vol. 2, pp. 294-299, 1999.

[20] R. P. Sloan, P. A. Shapiro, E. Bagiella, S. M. Boni, M. Paik, J. T. Bigger Jr., R. C. Steinman and J. M. Gorman, "Effect of mental stress throughout the day on cardiac autonomic control" Biological Psychology, Vol. 37, pp. 89-99, 1994.

[21] R. Colombo, G. Mazzuero, F. Soffiantino, M. Ardizzoia, G. Minuco, "A comprehensive PC solution to heart rate variability analysis in mental stress", Proceedings of Computers in Cardiology, pp. 475-478, 1989.

[22] S. W. Porges, "Cardiac Vagal Tone: A Physiological Index of Stress", Neuroscience and Biobehavioral Reviews, Vol. 19, No. 2, pp. 225-233, 1995.

[23] A. H. Garde, B. Laursen, A. H. Jorgensen and B. R. Jensen, "Effects of mental and physical demands on heart rate variability during computer work", European Journal of Applied Physiology, Vol. 87, pp. 456-461, 2002.

[24] N. Hjortskov, D. Rissén, A. K. Blangsted, N. Fallentin, U. Lundberg and K. Sogaard, "The effect of mental stress on heart rate variability an blood pressure during computer work", European Journal of Applied Physiology, Vol. 92, pp. 84-89, 2003.

[25] L. Bernardi, J. WdowczykSzulc, C. Valenti, S. Castoldi, C. Passino, G. Spadacini and P. Sleight, "Effects of Controlled Breathing, Mental Activity and Mental Stress With or Without Verbalization on Heart Rate Variability", Journal of the American College of Cardiology, Vol. 35, No. 6, pp. 1462-1469, 2000.

[26] A. Vincent, I. M. Craik, and J. J. Furedy, "Relations among memory performance, mental workload and cardiovascular responses", International Journal of Psychophysiology, Vol. 23, pp. 181-198, 1996.

[27] J. Taelman, S. Vandeput, I. Gilgorijevic, A. Spaepen and S. Van Huffel, "Time-frequency heart rate variability characteristics of young adults during physical,

mental and combined stress in laboratory environment", 33rd Annual International Conference of the IEEE EMBS, pp. 1973-1976, 2011.

[28] M. Horsten, M. Ericson, A. Perski, S. P. Wamala, K. Schenck-Gustafsson and K. Orth-Gomér, "Psychosocial Factors and Heart Rate Variability in Healthy Women", Psychosomatic Medicine, Vol. 61, pp. 49-57, 1999.

[29] Karhikeyan P., Murugappan M. and S. Yaacob, "ECG Signals Based Mental Stress Assessment Using Wavelet Transform" 2011 IEEE International Conference on Control System, Computing and Engineering, pp. 258-262, 2011.

[30] W. Wu, J. Lee and H. Chen, "Estimation of Heart Rate Variability Changes during Different Visual Stimulation using Non-invasive Real-Time ECG Monitoring System", 2009 IJBS'09 International Joint Conference on Bioinformatics, Systems Biology and Intelligent Computing, pp. 344-347, 2009.

[31] M. Myrtek, D. Weber, G. Brungner and W. Muller, "Ocupational stress and strain of female students: results of physiological, behavioural, and psychological monitoring", Biological Psychology, Vol. 42, pp. 379-391, 1996.

[32] R. McCraty, M. Atkinson, W. A. Tiller, G. Rein and A. P. Watkins, "The Effects of Emotions on Short-Term Power Spectrum Analysis of Heart Rate Variability", Brief Reports of The American Journal of Cardiology, Vol. 76, 1995.

[33] W. Zhang, J. Wang and H. He, "The effects of operational and emotional mental stress on the cardiovascular response", Biomedical Engineering and Biotechnology, 2012 IEEE International Conference on, pp. 921-924, 2012.

[34] R. Perini, S. Milesi, N. M. Fisher, D. R. Pendergast and A. Veicsteinas, "Heart rate variability during dynamic exercise in elderly males and females", European Journal of Applied Physiology, Vol. 82, pp. 8-15, 2000.

[35] P. Karthikeyan, M. Murugappan and S. Yaacob, "A Review on Stress Inducement Stimuli for Assessing Human Stress Using Physiological Signals", IEEE 7th International Colloquium on Signal Processing and its Applications, pp. 420-425, 2011.

[36] D. W. Watson, "Physiological Correlates of Heart Rate Variability (HRV) and the subjective assessment of workload and fatigue inflight crew: a practical study", in People in Control: An International Conference on Human Interfaces in Control Rooms, Cockpits and Command Centres, pp. 159-163, 2001.

[37] J. A. Healey and R. W. Picard, "Detecting Stress During Real-World Driving Tasks Using Physiological Sensors", IEEE Transactions on Intelligent Transportation Systems, Vol. 6, No. 2, pp. 156-166, 2005.

[38] E. S. Mezzacappa, R. M. Kelsey, E. S. Katkin and R. P. Sloan, "Vagal Rebound and Recovery From Psychological Stress", Psychosomatic Medicine, Vol. 63, pp. 650-657, 2001.

[39] A. Sul, J. Shin, C. Lee, Y. Yoon and J. Principe, "Evaluation of Stress Reactivity and Recovery using Biosignals and Fuzzy Theory", in Proceedings of the Second Joint EMBS/BMES Conference, pp. 32-33, 2002.

[40] B. Lorenz and R. Parasuraman, "Human operator functional state in automated systems: The role of compensatory control strategies", in Operator Functional State: The Assessment and Prediction of Human Performance Degradation in Complex Tasks, G. R. L. Hockey, A. W. K. Gaillard and O. Burov, Eds., IOS Press, Amsterdam, pp. 224-237, 2003.

[41] G. R. J. Hockey, P. Nickel, A. C. Roberts and M. H. Roberts, "Sensitivity of candidate markers of psychophysiological strain to cyclical changes in manual

control load during simulated process control", Applied Ergonomics, Vol. 40, No. 6, pp. 1011-1018, 2009.

[42] D. R. Royall, E. C. Lauterbach, J. L. Cummings, A. Reeve, T. A. Rummans, D. I. Kaufer, W. C. LaFrance and C. E. Coffey, "Executive control function: A review of its promise and challenges for clinical research", Journal of Neuropsychiatry & Clinical Neurosciences, Vol. 14, No. 4, pp. 377-405, 2002.

[43] T. Shallice, "The fractionation of supervisory control", in The Cognitive Neurosciences III, M. S. Gazzaniga, Ed., MIT Press, 2005, Cambridge, pp. 943-956.

[44] A. Gevins, M. E. Smith, L. McEvoy and D. Yu, "High-resolution EEG mapping of cortical activation related to working memory: effects of task difficulty, type of processing, and practice", Cerebral Cortex, Vol. 7, No. 4, pp. 374-385, 1997.

[45] A. Gevins and M. E. Smith, "Neurophysiological measures of cognitive workload during human-computer interaction", Theoretical Issues in Ergonomics Science Journal, Vol. 4, No. 1/2, pp. 113-131, 2003.

[46] P. Luu and M. I. Posner, "Anterior cingulate cortex regulation of sympathetic activity", Brain, Vol. 126, No. 10, pp. 2119-2120, 2003.

[47] M. E. Smith, A. Gevins, H. Brown, H. Karnik and R. Du, "Monitoring task loading with multivariate EEG measures during complex forms of human-computer interaction", Human Factors, Vol. 43, No. 3, pp. 366-380, 2001.

[48] ActiveTwo by Biosemi, www.biosemi.com/products.html, Nov. 2015.

[49] D. Kahneman, "Attention and Effort", Prentice-Hall, USA, 1973.

[50] D. Kahneman, "Thinking, Fast and Slow", Penguin Books, UK, 2012.

[51] E. Granholm, R. F. Asarnow, A. J. Sarkin and K. L. Dykes, "Pupillary responses index cognitive resource limitations", Psychophysiology, Vol. 33, pp. 457-461, 1996.

[52] H. Ludtke, B. Wilhelm, M. Adler, F. Schaeffel and H. Wilhelm, "Mathematical procedures in data recording and processing of pupillary fatigue waves", Vision Research, Vol. 38, pp. 2889- 2896, 1998.

[53] J. Zhai, A. Barreto, C. Chin, C. Li, "Realization of stress detection using psychophysiological signals for improvement of human-computer interactions", in Proceedings of the IEEE SoutheastCon, pp. 415-420, 2005.

[54] J. Zhai and A. Barreto, "Stress Detection in Computer Users Based on Digital Signal Processing of Noninvasive Physiological Variables", Proceedings of the 28th IEEE EMBS Annual International Conference, pp. 1355-1358, 2006.

[55] P. Ren, A. Barreto, Y. Gao and M. Adjouadi, "Affective assessment of computer users based on processing the pupil diameter signal", in 2011 Annual International Conference of the IEEE Engineering in Medicine and Biology Society, EMBC, pp. 2594-2597, 2011.

[56] F. Mokhayeri, S. Toosizadeh,M.-R. Akbarzadeh-T and F. Ghasemzadeh-R, "A Novel Method for Pupil Diameter Measurement based on Fuzzy Techniques", 2011 IEEE International Conference on Granular Computing, pp. 473-478, 2011.

[57] F. Mokhayeri, S. Toosizadeh and M-R. Akbarzadeh-T, "A Novel Approach for Pupil Diameter Measurement Based on Soft Computing Techniques", 2011 7th Iranian Machine Vision and Image Processing (MVIP), pp. 1-5, 2011.

[58] F. Mokhayeri and M.-R. Akbarzadeh-T, "Mental Stress Detection Based on Soft Computing Techniques", in 2011 IEEE International Conference on Bioinformatics and Biomedicine (BIBM), pp .430-433, 2011.

[59] F. Mokhayeri, M.-R. Akbarzadeh-T and S. Toosizadeh, "Mental stress detection using physiological signals based on soft computing techniques", in 2011 18th Iranian Conference of Biomedical Engineering (ICBME), pp. 232-237, 2011.

[60] K. Yamanaka and M. Kawakami, "Convenient Evaluation of Mental Stress With Pupil Diameter", International Journal of Occupational Safety and Ergonomics, Vol. 15, No. 4, pp. 447-450, 2009.

[61] L. A. Torres-Salomao, M. Mahfouf and E. El-Samahy, "Pupil Diameter Size Marker for Incremental Mental Stress Detection" in 2015 IEEE 17th International Conference on e-Health Networking, Applications and Services, 14-17 Oct. 2015.

[62] E. Elsamahy, M. Mahfouf, L. A. Torres-Salomao and J. Anzurez-Marin, "A New Computer Control System for Mental Stress Management using Fuzzy Logic", in 2015 IEEE Conference on Evolving and Adaptive Intelligent Systems, to be held 1-3 Dec. 2015.

[63] Gazepoint, www.gazept.com, Nov. 2015.

[64] C. Hennessey, B. Noureddin, and P. Lawrence, "A single camera eye-gaze tracking system with free head motion", in Proceedings of the 2006 symposium on Eye tracking research & applications (ETRA '06), New York, pp. 87-94, 2006.

[65] C. Hennessey and A. T. Duchowski, "An open source eye-gaze interface: expanding the adoption of eye-gaze in everyday applications", in Proceedings of

the 2010 Symposium on Eye-Tracking Research & Applications (ETRA '10), New York, pp. 81-84, 2010.

[66] P. Yuen, K. Hong, T. Chen, A. Tsitiridis, F. Kam, J. Jackman, D. James, M. Richardsen, L. Williams, W. Oxford, J. Piper, T. Francis and L. Stafford, "Emotional & physical stress detection and classification using thermal imaging technique", Crime Detection and Prevention (ICDP 2009), 3rd International Conference on, pp. 1-6, 2009.

[67] L. A. Zadeh, "The Concept of a Linguistic Variable and its Application to Approximate Reasoning-I", Information Sciences, Vol. 8, pp. 199-249, 1975.

[68] K. M. Passino and S. Yurkovich, Fuzzy Control, USA : Addison-Wesley, 1998.

[69] T. Heske and J. Neporent, Fuzzy Logic For Real World Design, San Diego, CA : Annabooks, 1996.

[70] J. Anzurez-Marin, L. A. Torres-Salomao and I. I. Lázaro-Castillo, "Fuzzy Logic Control for a Two Tanks Hydraulic System Model", in Proc. 2011 IEEE Electronics, Robotics and Automotive Mechanics Conference CERMA 2011, Cuernavaca, Mexico, 2011.

[71] R. Babuska and H. Verbruggen, "A new identification method for linguistic fuzzy models", in Proceedings of 1995 IEEE Int. Fuzzy Systems, 1995. International Joint Conference of the Fourth IEEE International Conference on Fuzzy Systems and The Second International Fuzzy Engineering Symposium, Vol. 2, pp. 905-912, 20-24 Mar 1995.

[72] R. Babuska and H. B. Verbruggen, "An Overview of Fuzzy Modelling for Control", Control Eng. Practice, Vol. 4, No. 11, pp. 1593-1606, 1996.

[73] J. M. Mendel, "Type-2 Fuzzy Sets and Systems: An Overview [corrected reprint]", in IEEE Computational Intelligence Magazine, Vol. 2, No. 2, pp. 20-29, May 2007.

[74] J. M. Mendel and R. I. B. John, "Type-2 fuzzy sets made simple", in , IEEE Transactions on Fuzzy Systems, Vol. 10, No. 2, pp. 117-127, Apr. 2002.

[75] L. A. Lucas, T. M. Centeno and M. R. Delgado, "General Type-2 Fuzzy Inference Systems: Analysis, Design and Computational Aspects", in IEEE International Fuzzy Systems Conference, pp. 1-6, 23-26 July 2007.

[76] J. M. Mendel and X. Liu, "Simplified Interval Type-2 Fuzzy Logic Systems", in IEEE Transactions on Fuzzy Systems, Vol. 21, No. 6, pp. 1056-1069, Dec. 2013.

[77] N. Sahab and H. Hagras, "Adaptive Non-singleton Type-2 Fuzzy Logic Systems: A Way Forward for Handling Numerical Uncertainties in Real World Applications", International Journal of Computers, Communications & Control, Vol. 6, No. 3, pp. 503-529, Sept. 2011.

[78] N. N. Karnik, J. M. Mendel and Qilian Liang, "Type-2 fuzzy logic systems", in , IEEE Transactions on Fuzzy Systems, Vol. 7, No. 6, pp. 643-658, Dec. 1999.

[79] T. John and S. Coupland, "Type-2 Fuzzy Logic: Challenges and Misconceptions [Discussion Forum]", in IEEE Computational Intelligence Magazine, Vol. 7, No. 3, pp. 48-52, Aug. 2012.

[80] S. Coupland and R. John, "A Fast Geometric Method for Defuzzification of Type-2 Fuzzy Sets", in IEEE Transactions on Fuzzy Systems, Vol. 16, No. 4, pp. 929-941, Aug. 2008.

[81] Qilian Liang and J. M. Mendel, "Interval type-2 fuzzy logic systems: theory and design", in IEEE Transactions on Fuzzy Systems, Vol. 8, No. 5, pp. 535-550, Oct. 2000.

[82] D. Wu and M. Nie, "Comparison and practical implementation of type-reduction algorithms for type-2 fuzzy sets and systems", in 2011 IEEE International Conference on Fuzzy Systems, pp. 2131-2138, 27-30 June 2011.

[83] L. Pack Kaelbling, M. L. Littman and A. W. Moore, "Reinforcement Learning: A Survey", Journal of Artificial Intelligence Research, Vol. 4, pp. 237-285, 1996.

[84] C.J.C.H. Watkins, "Learning from delayed rewards", PhD Thesis, University of Cambridge, England, 1989.

[85] C.-F. Juang and C.-D. Hsieh, "A Fuzzy System Constructed by Rule Generation and Iterative Linear SVR for Antecedent and Consequent Parameter Optimization", IEEE Transactions on Fuzzy Systems, Vol. 20, No. 2, pp. 372-384, April 2012.

[86] C.-F. Juang and C.-Y. Chen. "Data-Driven Interval Type-2 Neural Fuzzy System With High Learning Accuracy and Improved Model Interpretability", IEEE Transactions on Cybernetics, Vol. 43, No. 6, pp. 1781-1795, Dec. 2013.

[87] R. Qi and M. A. Brdys, "Adaptive Fuzzy Modelling and Control for Discrete-Time Nonlinear Uncertain Systems", in 2005 American Control Conference, June 2005.

[88] Y. Gao and M. J. Er., "Online adaptive fuzzy neural identification and control of a class of MIMO nonlinear systems", IEEE Transactions on Fuzzy Systems, Vol. 11 No. 4, pp. 462-477, Aug. 2003.

[89] A. Rubio-Solis and G. Panoutsos, "Interval Type-2 Radial Basis Function Neural Network: A Modelling Framework", in IEEE Transactions on Fuzzy Systems, Vol. 23, No. 2, pp. 457-473, April 2015.

[90] J.-H Lin and C. Isik, "Fuzzy modelling and control based on maximum entropy self-organizing nets and cell state mapping", in 1997 Annual Meeting of the North American Fuzzy Information Processing Society, pp. 45-50, 21-24 Sep. 1997.

[91] J. C. Dunn, "A Fuzzy Relative of the ISODATA Process and Its Use in Detecting Compact Well-Separated Clusters", Journal of Cybernetics, Vol. 3, pp. 32-57, 1973.

[92] J. C. Bezdek, R. Ehrlich and W. Full, "FCM: The fuzzy c-means clustering algorithm", Computers & Geosciences, Vol. 10, pp. 191-203, 1984.

[93] M. Delgado, A. F. Gómez-Skarmeta and F. Martin, "A fuzzy clustering-based rapid prototyping for fuzzy rule-based modelling" in , IEEE Transactions on Fuzzy Systems, Vol. 5, No. 2, pp. 223-233, May 1997.

[94] C. Hwang and F. C.-H. Rhee, "Uncertain Fuzzy Clustering: Interval Type-2 Fuzzy Approach to C-Means", IEEE Transactions on Fuzzy Systems, Vol. 15, No. 1, pp. 107-120, Feb. 2007.

[95] A. Bagherjeiran, C. F. Eick and R. Vialta, "Adaptive Clustering: Better Representatives with Reinforcement Learning". Department of Computer Science, University of Houston, Houston, USA, March 2005.

[96] J.-S. R. Jang, "ANFIS: adaptive-network-based fuzzy inference system", IEEE Transactions on Systems, Man and Cybernetics, Vol. 23, No. 3, pp. 665-685, May/Jun 1993.